
Complex plasmas: Interaction potentials and non-Hamiltonian dynamics

Roman Kompaneets



Munich 2007

Complex plasmas: Interaction potentials and non-Hamiltonian dynamics

Roman Kompaneets

Dissertation
der Fakultät für Physik
der Ludwig-Maximilians-Universität
München

vorgelegt von
Roman Kompaneets
aus Moskau

München, den 05. Juni 2007

Erstgutachter: Prof. Dr. Gregor E. Morfill

Zweitgutachter: Prof. Dr. Viatcheslav F. Mukhanov

Tag der mündlichen Prüfung: 20. Juli 2007

Contents

Abstract	ix
Abstract in German	xi
Abstract in Russian	xiii
1 Introduction	1
1.1 Complex plasmas	1
1.1.1 Experimental setups	2
1.2 Grain screening	5
1.2.1 Measurements	5
1.2.2 Theories	6
1.3 Non-Hamiltonian dynamics of grains	8
2 Cumulative thesis	13
2.1 Potential around a charged dust particle in a collisional sheath	13
2.1.1 Objective	13
2.1.2 Methods	14
2.1.3 Results	14
2.1.4 Conclusion	16
2.2 Dust-lattice waves: Role of charge variations and anisotropy of dust-dust interaction	16
2.2.1 Objective	16
2.2.2 Methods	17
2.2.3 Results	17
2.2.4 Conclusion	18

2.3	Dust clusters with non-Hamiltonian particle dynamics	19
2.3.1	Objective	19
2.3.2	Methods	19
2.3.3	Results	20
2.3.4	Conclusion	20
3	Summary and future work	23
A	Appendix: Theoretical background	27
A.1	Models of grain screening	27
A.1.1	General approach	27
A.1.2	Debye-Hückel potential	31
A.1.3	Collisionless case: Drift in the absence of field	32
A.1.4	Finite collisionality	35
A.2	Discussion of model assumptions	37
A.2.1	Ion-neutral collisions	38
A.2.2	Ion velocity distributions	40
A.2.3	Electron velocity distributions	41
A.3	Summary: Which model when?	41
	Bibliography	43
	Acknowledgments	47
	Curriculum Vitae	49
	Publication list	51
	Enclosed papers	53

List of Figures

1.1	Sketch of rf experimental setup	3
1.2	Non-reciprocal interaction between grains	9
2.1	Comparison of the proposed theory of grain screening with experiment . .	15
2.2	Calculated eigenfrequencies of 2- and 3-particle clusters	21
A.1	Equilibrium velocity distributions for the BGK collision operator	36
A.2	Ion mobility: Drift velocity vs. electric field	39

Abstract

This thesis is a cumulative dissertation that consists of three papers.

The first paper addresses the issue of screening of a charged dust particle suspended in the plasma-wall transition layer of a plasma discharge. This problem is one of the fundamental issues in the physics of complex (dusty) plasmas, because the screening of charged dust particles determines the interaction forces between them and thus governs their dynamics. The kinetic model proposed in this paper considers a point charge embedded in a weakly-ionized plasma with ion drift. The latter is considered to be due to an external electric field and assumed to be mobility-limited. Here, “mobility-limited” means that the acceleration of ions in the external field is balanced by collisions of ions with neutrals and that this balance determines the drift velocity. The embedded point charge (i.e., a charged dust particle) perturbs the ion drift, and the resulting potential distribution around the dust particle is calculated. The results are proven to be in agreement with existing measurements performed in the plasma-wall transition layer of a rf plasma discharge. One of the important applications of this work is related to the possibility of tuning the pair interaction potential between dust particles by applying an external oscillating electric field. In particular, such a tuning allows studying electrorheological properties of strongly coupled systems on all relevant time scales. First experiments of this kind have already been performed onboard the International Space Station.

The second paper deals with the dust-lattice waves — oscillations of charged dust particles forming a crystalline structure in a plasma. The role of anisotropic screening of dust particles and variations of their charges is investigated. It is well known that the mentioned effects lead to non-Hamiltonian dynamics of dust particles and, as a result, can trigger an instability of the dust-lattice waves. This instability has been already observed in experiments. The new result is that the mutual influence of particles on their charges, not considered in the analysis of the dust-lattice waves before, is shown to be capable of making a significant contribution to this instability.

The third paper examines whether a similar instability can be observed in a cluster formed by two or three charged dust particles. It is found that an instability due to the non-Hamiltonian dynamics is only possible when the interparticle separation in the cluster is such that certain cluster eigenfrequencies are sufficiently close to each other.

Zusammenfassung

Diese Dissertation ist eine kumulative Dissertation und besteht aus drei Arbeiten.

Die erste Arbeit beschäftigt sich mit der Abschirmung des in einer Plasmarandschicht zur Schwebelage gebrachten geladenen Staubteilchens. Dieses Problem ist von fundamentaler Bedeutung für die Physik der komplexen (staubigen) Plasmen, weil die Abschirmung die Form der Wechselwirkungen und somit die Dynamik der geladenen Staubteilchen bestimmt. In der Arbeit wird ein kinetisches Modell vorgeschlagen, in welchem ein Staubteilchen als eine Punktladung betrachtet wird, die sich in einem schwach ionisierten Plasma mit einer Ionendrift befindet. Es wird angenommen, dass die Ionendrift durch ein externes elektrisches Feld verursacht wird und dass diese Ionendrift der Mobilität der Ionen entspricht. Dies bedeutet, dass die Beschleunigung der Ionen im externen elektrischen Feld durch Ionen-Neutralteilchen-Stöße ausgeglichen wird und dass diese Kompensation die Geschwindigkeit der Ionendrift bestimmt. Die Punktladung (d.h. das Staubteilchen) stört diese Ionendrift, und in der vorliegenden Arbeit wird die resultierende Potentialverteilung des Staubteilchens im Plasma berechnet. Zudem wird festgestellt, dass die Resultate mit den früher in RF-Entladungen durchgeführten Experimenten konsistent sind. Die übergreifende Bedeutung dieser Untersuchung liegt in der Möglichkeit, damit durch ein externes elektrisches Wechselfeld das binäre Wechselwirkungspotential der Staubteilchen von außen zu steuern und somit z.B. elektrorheologische Eigenschaften von stark wechselwirkenden Systemen von Partikeln sichtbar zu machen und dynamisch auf allen relevanten Zeitskalen zu untersuchen. Erste Messungen dieser Art sind in Experimenten auf der Internationalen Raumstation bereits erfolgreich durchgeführt worden.

Die zweite Arbeit beschäftigt sich mit den sogenannten Staub-Gitter-Wellen (dust-lattice waves). Das sind Wellen, die durch Schwankungen der geladenen Staubteilchen, die eine Kristallstruktur im Plasma bilden, entstehen. In der vorliegenden Arbeit wird die Rolle sowohl der Anisotropie der Abschirmung der Staubteilchen als auch der Variation ihrer Ladungen untersucht. Wie bekannt führen diese Effekte zu nicht-Hamiltonischer Dynamik der Staubteilchen und können daher eine Instabilität der Staub-Gitter-Wellen auslösen. Solche Effekte sind in Experimenten bereits beobachtet worden. Das neue Ergebnis besteht darin, dass der gegenseitige Einfluss der Staubteilchen auf ihre Ladungen, ein Effekt, welcher bisher bei der Analyse der Staub-Gitter-Wellen noch nicht berücksichtigt wurde, einen wichtigen Beitrag zu dieser Instabilität leisten kann.

In der dritten Arbeit wird untersucht, ob eine ähnliche Instabilität in Partikelclustern, welche nur aus zwei oder drei Staubteilchen bestehen, beobachtet werden kann. Es wurde festgestellt, dass eine ähnliche Instabilität, die durch nicht-Hamiltonische Dynamik verursacht ist, nur dann möglich ist, wenn der Teilchenabstand so gewählt wird, dass bestimmte Eigenfrequenzen des Clusters gut miteinander übereinstimmen.

Аннотация

Настоящая диссертация является кумулятивной диссертацией и состоит из трех работ.

Первая работа посвящена экранированию заряженной пылевой частицы, левитируемой в приэлектродном слое плазменного разряда. Эта задача является одной из фундаментальных проблем физики пылевой плазмы, так как экранирование заряженных пылевых частиц определяет силы взаимодействия между ними и поэтому определяет их динамику. В статье предложена кинетическая модель, в которой рассматривается точечный заряд, помещенный в слабоионизированную плазму с ионным дрейфом. Предполагается, что ионный дрейф вызван внешним электрическим полем и соответствует мобильности ионов. Последнее означает, что подразумевается баланс между ускорением ионов во внешнем электрическом поле и столкновениями ионов с нейтралами, который и определяет скорость дрейфа. Внесенный точечный заряд (т.е., заряженная пылевая частица) возмущает дрейф ионов, и образующееся распределение потенциала вокруг пылевой частицы вычислено в настоящей работе. Результаты находятся в согласии с ранее опубликованными результатами измерений, выполненными в приэлектродном слое радиочастотного плазменного разряда. Одно из важных приложений этой работы связано с возможностью регулирования потенциала парного взаимодействия пылевых частиц посредством приложения внешнего осциллирующего электрического поля. В частности, такое регулирование позволяет изучать электрореологические свойства систем, в которых потенциальная энергия парного взаимодействия частиц превышает их кинетическую энергию. Первые эксперименты такого типа уже были проведены на борту Международной Космической Станции.

Предметом исследования второй работы являются так называемые пылекристаллические волны – колебания заряженных пылевых частиц, образующих кристаллическую структуру в плазме. Исследована роль как анизотропии экранирования пылевых частиц, так и вариаций их зарядов. Как известно, эти эффекты приводят к негамильтоновой динамике пылевых частиц и поэтому могут вызвать неустойчивость пылекристаллических волн, которая уже была обнаружена в экспериментах. Новый результат заключается в том, что взаимное влияние пылевых частиц на их заряды, которое ранее не учитывалось при анализе пылекристаллических волн, может обеспечить значительный вклад в эту неустойчивость.

В третьей работе исследовано, может ли подобная неустойчивость наблюдаться в кластере, состоящем из двух или трех пылевых частиц. Получено, что подобная неустойчивость из-за негамильтоновой динамики может возникнуть только тогда, когда расстояние между пылевыми частицами близко к резонансному значению, при котором определенные собственные частоты кластера совпадают.

Chapter 1

Introduction

The present cumulative thesis deals with the field of complex (dusty) plasmas and addresses one of the fundamental issues in this field — screening/interaction of charged dust particles levitated in the (pre)sheath region [plasma-wall transition layer] of a plasma discharge. In addition, instabilities of dust plasma crystals and clusters, due to non-reciprocal interaction forces between dust particles and variations of their charges, are investigated as well. These instabilities highlight non-Hamiltonian dynamics of charged dust particles in a plasma.

This chapter provides an introduction to the papers enclosed to the present thesis. In this chapter, very specific details and formulas are avoided. In the next chapter, it is explained what is done in the papers enclosed. A theoretical background necessary for a detailed reading of the papers is placed in Appendix A.

1.1 Complex plasmas

Complex (dusty) plasma is a plasma where a third charged species — the charged dust particles — is present (see, e.g., reviews [1,2,3,4]). The dust particles in complex plasmas are electrically charged by collection of plasma electrons and ions as well as by photoemission or secondary electron emission. In laboratory and industrial plasmas usually the collection processes dominate and the particles acquire a high negative charge. (A typical dust grain of a few μm in diameter in a typical glow discharge will have an equilibrium negative charge of $\sim 10^4$ electrons). Complex plasmas are ubiquitous in technological applications (e.g., in microchip production, in plasma deposition techniques) as well as in astrophysical situations (e.g., formation of stars and planetary systems, planetary rings and comet tails,

interstellar dust clouds, dust in the Earth’s magnetosphere and ionosphere). Moreover, an important feature of complex plasmas is the introduction of strongly coupled phenomena into the plasma. Here, “strongly coupled” means that the interaction energy of dust particles exceeds their thermal kinetic energy. This includes observations of both liquid-like and solid-like states in complex plasmas as well as phase transitions. The solid-like, crystalline state — so-called “plasma (dust) crystal” — represents a two or three-dimensional lattice structure formed by the dust particles. The fact that dynamic processes in systems of dust particles become visible on the kinetic level makes the field of complex plasmas of interest to neighboring disciplines such as condensed matter or material science. The field of complex plasmas is relatively new (active investigation began in 1994 when the dust crystals were obtained in the laboratory conditions) and rapidly evolving (approx. 200 publications per year).

1.1.1 Experimental setups

Many experiments in the field of complex plasmas are performed in radio-frequency (rf) discharges. The so-called Gaseous Electronic Conference (GEC) cell [5] is frequently used, with the electrode diameter of 10–15 cm and electrode separation of 2–4 cm (see Fig. 1.1). The electrodes are placed in a vacuum chamber. Usually, the lower electrode is connected to a rf generator (at frequency 13.56 MHz) via a blocking capacitor and a matching network, whereas the upper electrode is grounded. The chamber is filled by a noble gas, most frequently argon, at the room temperature and pressure of 0.5–100 Pa. Typically, the peak-to-peak voltage applied to the powered electrode is 50–500 V.

Under these conditions, probe measurements performed near the horizontal midplane of the discharge yield the plasma density of the order of 10^8 – 10^9 cm⁻³ (i.e., the ionization fraction is usually of the order of 10^{-6} – 10^{-7}) and the electron temperature of a few eV. Because of the extremely small ionization fraction, ions collide with neutrals much more frequently than with each other or electrons. For this reason, there exists a certain region near the midplane of the discharge — called here the “bulk region”, or “bulk” — where ions are in/near thermal equilibrium with neutrals. The rf frequency appears to be much larger than the ion plasma frequency and much less than the electron plasma frequency. Therefore, while electrons respond to the rf electric field, ions respond to the time-averaged field only. Because in the bulk region the electrons have larger velocities than ions and the

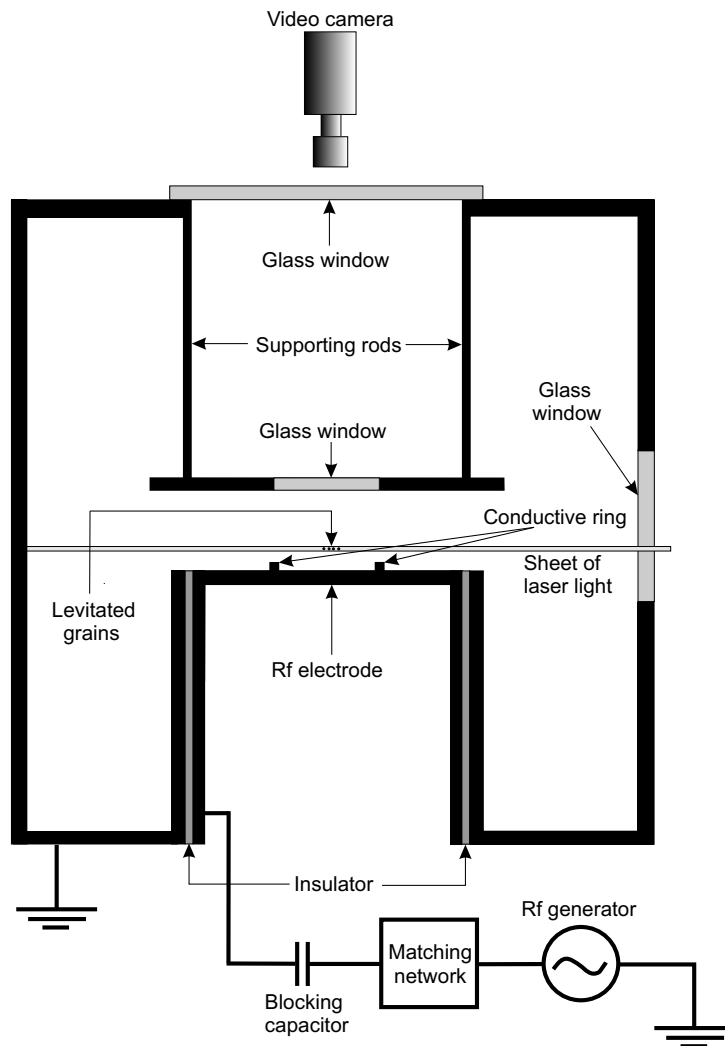


Figure 1.1: Principal scheme of rf experimental setup.

time-averaged current through the discharge should be zero due to the blocking capacitor, there appears a significant time-averaged electric field near the electrodes: This field repels electrons from the electrodes and attracts ions to the electrodes from the bulk region, thus maintaining the balance between the ion and electron fluxes on either of the electrodes. Because of some geometric asymmetry of the discharge, the powered electrode usually acquires a negative time-averaged self-bias potential of 20–40% of the peak-to-peak voltage at the powered electrode.

Then, dust particles — melamine-formaldehyde, silica, or even metallic grains, typically of a few μm in diameter — are introduced into the discharge. The grains collect free

ions and electrons from the plasma and thus instantaneously acquire equilibrium negative charges determined by the balance of the ion and electron fluxes on the grain surface. Because of the inhomogeneity of the discharge, these fluxes depend on the exact position of the grain in the discharge. Therefore, the grain charge exhibits adjustments as the grain moves through the discharge.

Since the grains are charged, the electric field force acts on them, in addition to gravity. Because of their large mass, grains (and even ions, as stated above) respond to the time-averaged electric field only. The time-averaged electric field is zero somewhere near the horizontal midplane of the discharge and increases towards either of the electrodes (see, e.g., simulations of Ref. [6]). Given the fact that the time-averaged electric field is directed towards the electrode approached, the grain levitation is only possible near the lower electrode. If the grains are not too heavy, an equilibrium levitation position exists. The equilibrium position is stable with respect to vertical oscillations, because the time-averaged electric field increases as the electrode approached. However, a horizontal confinement may be necessary, otherwise the particles may escape from the space between the electrodes. Because of the mutual electrostatic repulsion of particles, inducing a horizontal confinement may be particularly important when many particles should be levitated simultaneously. A horizontal confinement can be easily induced, for example, by placing a conductive ring on the lower electrode or, alternatively, by machining a cavity in the lower electrode. The particles are usually illuminated by a laser beam which is transformed into a sheet of $\sim 100 \mu\text{m}$ thick. The light scattered by the particles is recorded by a video camera with a resolution sufficient to resolve individual grains.

The described experimental setup allows studying a variety of phenomena, ranging from manipulations of a single dust particle as a fine probe in the plasma-wall transition layer [7], to observations of wave propagation in dust crystals [8] and phase transitions [9]. In many cases, a single horizontal layer with a crystalline structure is formed by the dust particles (two-dimensional dust crystal), with the interparticle separation of 0.1–1 mm [10, 11] and reciprocal time scale of dust dynamics (e.g., the Einstein frequency) of 10–100 s⁻¹. Processes occurring on these temporal scales can be easily resolved by an appropriate video camera.

It is necessary to note that not all experiments in the field of complex plasmas are performed using the setup described above. In fact, there have been experiments in direct current (dc) discharges [12] and under microgravity conditions [13], as well.

1.2 Grain screening

The interaction between charged grains is not simply a Coulomb interaction. In fact, the dust particles are not in vacuum — they are in the background plasma which modifies/screens the Coulomb field of a dust particle. Here, there are two important things to realize: (i) In the plasma-wall transition layer the kinetic energies of ions and electrons are usually high enough so that grains induce *weak* perturbations of the ion and electron densities (i.e., the region of nonlinear screening around a grain is usually much smaller than the characteristic screening length), and therefore the perturbations induced by different grains can be considered independently and then linearly summarized, (ii) the grain masses are high enough so that the time scale of dust dynamics and plasma time scales are far separated (i.e., the plasma quasistatically reacts to the motion of grains), and the characteristic grain velocities are negligible as compared to the characteristic ion and electron velocities. For all these reasons, the dynamics of grains can be described by a certain *pair* interaction potential determined by the distribution of the electrostatic potential around a single stationary dust particle in a plasma, and the force on the first grain from the second one is the product of the charge of the first grain and the gradient of the potential induced by the second grain in the plasma. (However, the summation of these pair interaction forces is only valid when the amount of dust is not large enough to give rise to collective effects [14]).

Many phenomena in complex plasmas strongly depend on this pair interaction law. For example, attractive forces between grains may give rise to spontaneous formation of dust “molecules” comprising of a few particles [15]. Not yet observed critical point and gas to fluid transitions are believed to be only possible in the presence of attractive forces between grains [16]. Non-reciprocal interaction forces (*actio* \neq *reactio*) lead to non-Hamiltonian dynamics of dust grains, as will be discussed in Subsection 1.3. Hence, the problem of screening/interaction of grains [especially in the plasma-wall transition layer where they are usually levitated] is one of the fundamental issues in the physics of complex plasmas.

1.2.1 Measurements

Up to now, the most precise measurements of the inter-grain interaction forces in the typical setup described in Subsection 1.1.1 were performed by Konopka *et al.* [17, 18].

During the first step of the experiment, a single particle was levitated. The horizontal motion of the particle was activated by a horizontal electric probe introduced into the discharge chamber. An analysis of the recorded particle trajectory in the horizontal plane allowed to determine the horizontal confinement potential. During the second step, two particles identical to that levitated before were levitated simultaneously. The particles aligned themselves horizontally (i.e., perpendicular to the ion drift), approximately in the same horizontal plane as a single particle was levitated before. Now, the electric probe was used to activate a simultaneous horizontal motion of the two particles. During their motion, the particles almost did not deviate from the initial horizontal plane. Analysis of their trajectories in the horizontal plane allowed to reconstruct the energy of the “horizontal interaction” between particles as a function of distance between them, since the horizontal confinement potential was determined during the first step of the experiment. Within the experimental uncertainties and considered range of distances between the particles, no deviation from the Debye-Hückel (Yukawa) screening potential, $\phi = (Q/r) \exp(-r/\lambda)$, was found. (Here, r is the distance from the particle, Q is the particle charge, λ is the screening length characterizing the Debye-Hückel potential).

Also, there have been some “indirect” measurements of the interaction forces. For example, the analysis of the measured frequencies of particle oscillations in different clusters formed by a few particles aligned horizontally could not reveal deviations from the Debye-Hückel potential, as well [19, 20].

The aforementioned experiments dealt with the particles aligned horizontally. At the same time, there have been experiments with two particles levitated at different heights because of their different sizes/masses [21, 22]. In spite of large experimental uncertainties, these experiments revealed that the interaction forces are non-reciprocal (i.e., *actio* \neq *reactio*). In particular, the lower particle strongly tended to occupy the position below the upper particle, whereas the upper particle almost did not “feel” the lower one.

1.2.2 Theories

The electric field which levitates the charged grains against gravity causes ions to drift towards the electrode and thus makes their distribution highly anisotropic: In many cases, the drift velocity in the region of grain levitation is believed to be much larger than the thermal velocity of neutrals. In this case, the classical Debye-Hückel screening is irrelevant

for the description of the ion contribution to grain screening.

The problem of the electron contribution to the grain screening is even more complicated, because electrons respond to the rf electric field, as stated above. Simulations [6,23] and recent spectroscopic measurements [24] suggest that in the sheath region the electrons may have quite different velocity distributions during different phases of the rf period and that these distributions may be quite different from Maxwellian.

Unfortunately, there have been no convincing measurements of plasma parameters in the region of grain levitation. In particular, the ratio of the mean kinetic energy of ions to the mean kinetic energy of electrons and the shapes of the ion and electron velocity distributions are not known.

As a consequence, there have been many grain screening theories [25,26,27,28,29,30,31,32,33,34] based on quite different assumptions. Not surprisingly, the results given by different models are different. Some models yield a series of potential minima and maxima below the grain — the so-called “oscillatory wake potential” [25,26,27,28,29,30]. Some models give that two like-charged grains aligned perpendicular to the ion drift can attract each other electrostatically [31]. A review of different models is given in Appendix A.

It is not surprising that the simplest conception which is in agreement with existing experimental data has gained popularity. According to this conception, ions have too large drift kinetic energy to participate in screening. Thus, the primary contribution to the grain screening is attributed to electrons [1,2,35,36]. Any effects related to either the time variations of the electron velocity distribution or possible anisotropy of the latter are neglected. Thus, the grain potential is assumed to be of the Debye-Hückel form with the local electron Debye length. (At the same time, this Debye-Hückel potential is believed to be somewhat disturbed below the grain because of the focusing of the ion drift [26,30]. This serves as an explanation why non-reciprocal forces were observed in some experiments).

As a consequence, many phenomena in complex plasmas have been theoretically studied by assuming the Debye-Hückel interaction potential. In this manner, waves in dust crystals [37], waves in dust fluids [38], phase transitions [39], and dust viscosity [40] have been investigated. Apparently, the most frequently cited evidence for the justification of the applicability of the Debye-Hückel interaction potential is the aforementioned experiment by Konopka *et al.* [17,18].

However, the arguments for the aforementioned conception are not convincing enough. First of all, measurements of Konopka *et al.* [17,18] were performed in a limited range of

distances between grains, 0.5–2 mm, while the deduced screening length was ~ 0.5 mm which is comparable with the distance range itself. Given the fact of marked experimental uncertainties, one could argue that other theories might be not in contradiction with the results of these measurements, as well. In this regard, a *quantitative* comparison of other models with this experiment could be very helpful. Furthermore, there are some evidences which suggest that the grain screening in the plasma-wall transition layer under typical conditions could be primarily due to ions and not electrons. The first evidence comes from the fact that, in the experiment by Konopka *et al.* [17, 18], the deduced screening length (*in the plasma-wall transition layer*) turned out to be about, or in some cases *smaller* than the electron Debye length *measured in the bulk* [18]. If the screening of grains was primarily due to electrons, the deduced screening length would be in contrast always significantly *larger* than the electron Debye length measured in the bulk, because the electron density decreases and the mean kinetic energy of electrons increases as the electrode approached [6]. The second evidence is related to the value of the grain charge deduced in the experiment [17, 18]. This value allows to find the electric field levitating the grains against gravity. The obtained value of the electric field, in turn, allows to obtain an estimate for the ion drift kinetic energy in the region of grain levitation, by assuming a mobility-limited drift. (The assumption of the mobility-limited drift gives an upper estimate of the ion drift kinetic energy). This upper estimate appears to be somewhat smaller than the mean electron kinetic energy measured in the bulk. This suggests that the mean kinetic energy of ions in the region of grain levitation is smaller than that of electrons and, hence, ions — not electrons — should play the primary role in grain screening, at least under conditions of the experiment [17, 18].

1.3 Non-Hamiltonian dynamics of grains

The interaction forces between grains were experimentally shown to be non-reciprocal (i.e., *actio* \neq *reactio*) [21, 22]. Of course, the non-reciprocity of the interaction forces between grains does not imply a violation of the third Newton’s law itself. In the presence of the ion drift, the screening cloud around a grain is not spherically symmetric: An excess of the positive charge — the so-called wake — is accumulated behind the grain due to ion focusing (see Fig. 1.2). These plasma wakes behind grains act as a third body and lead to non-reciprocal interaction forces between grains.

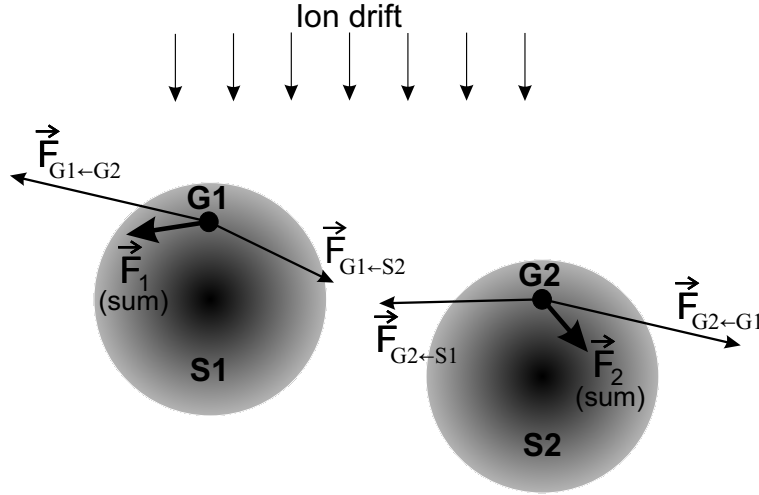


Figure 1.2: Illustration of non-reciprocal interaction forces between grains G1 and G2. S1, S2 — screening clouds around grains G1 and G2, respectively. $\mathbf{F}_{G1←G2}$ — direct Coulomb force exerted on the grain G1 by the grain G2. $\mathbf{F}_{G1←S2}$ — sum of the Coulomb forces exerted on the grain G1 by the charges of the screening cloud S2. The vector sum of $\mathbf{F}_{G1←G2}$ and $\mathbf{F}_{G1←S2}$ is denoted as \mathbf{F}_1 . The forces exerted on the grain G2 due to the presence of the grain G1 are denoted in a similar manner.

Non-reciprocal interaction forces $\mathbf{F}_1 \neq -\mathbf{F}_2$ between two particles can be regarded as if a certain “external” force $(\mathbf{F}_1 + \mathbf{F}_2)/2$ would act on each of the two particles, in addition to reciprocal forces $\pm(\mathbf{F}_1 - \mathbf{F}_2)/2$. This “external” force $(\mathbf{F}_1 + \mathbf{F}_2)/2$ depends on the relative positions of the two particles with respect to each other. If two particles return to their initial positions after some motion, the work done by this force during this motion is generally non-zero and, hence, energy is not conserved in this system. The physical reason for the energy nonconservation is that such systems of grains are not closed systems because of the presence of the plasma.

There is another effect — variations of grain charges — which also leads to the energy non-conservation. As stated above, the grain charge is determined by the balance of the ion and electron fluxes on the grain surface. Because of the discharge inhomogeneity, the grain charge is a function of the exact position of the grain in the discharge [1]. Furthermore, the ion and electrons fluxes on the grain surface and, hence, the grain charge can be influenced by other grains [41]. Because of the charge variations, the interaction forces between the grains are not simply functions of the relative coordinates of the grains with respect to each

other, but rather the interaction forces are functions of the absolute positions of the grains in the discharge. In this case, if the particles return to their initial positions after some motion, the work done by the interaction forces during this motion is generally non-zero, even in the case when the interaction forces are reciprocal [42]. The latter fact can be easily realized when one considers two particles interacting via the Coulomb forces, with the particle's charges being a function of the height. In this case, the work done by the interaction forces during, e.g., the following motion is obviously non-zero: (i) Initially, the two particles are at the same height and infinitely far away from each other, then (ii) the particles are approached to each other up to a certain distance, remaining at the same height as initially, then (iii) the particles are simultaneously shifted to a certain new height, and, finally, (iv) they are removed to infinite separation from each other, remaining at the same height as at the end of the vertical shift.

Finally, there is a third factor — variations of grain screening — which also leads to the energy nonconservation. Because of the discharge inhomogeneity, the grain screening depends on the exact position of the grain in the discharge. This dependence leads to the energy nonconservation in a similar manner as the grain charge variations.

Realistically, all of the three factors — non-reciprocal forces, charge variations, and screening variations — are present simultaneously. These factors and the associated effects should not be considered independently; in fact, some interesting effects are only possible in the *simultaneous* presence of some of the three aforementioned factors [43].

However small the charge/screening variations and non-reciprocity of the interaction forces are, they lead to the energy non-conservation, and such systems of charged dust particles in a plasma cannot be described in terms of the Hamiltonian dynamics [1]. The non-Hamiltonian dynamics of dust grains makes a complex plasma a convenient model to study non-Hamiltonian dynamical systems which are of fundamental physical interest [44, 45] and have a long history in mechanics.

The non-Hamiltonian dynamics of grains was demonstrated in the experiment reported by Ivlev *et al.* [11]. In this experiment, a horizontal crystalline monolayer (i.e., a two-dimensional dust crystal) was formed by the grains in a horizontal confinement potential. Then, additional grains were gradually injected and the interparticle distance in the monolayer decreased accordingly. When the interparticle distance became less than a certain threshold, the crystal spontaneously “melted” — the amplitudes of the vertical and horizontal vibrations of the particles drastically increased and became comparable with the

interparticle distance. However, it was possible to return the system to a stable crystalline monolayer by increasing the gas pressure. If the gas pressure was sufficiently high, the system never melted. In the latter case, when the interparticle distance became less than a certain threshold, the monolayer transformed into a bi-layer system. To explain the melting, Ivlev *et al.* [11] theoretically demonstrated that the non-reciprocity of the interaction forces can trigger an instability of the monolayer. This instability represents a growth over time of otherwise stable particle oscillations in a dust lattice and is only possible when the dust-neutral friction is sufficiently small. The latter fact explains why no melting was observed at high pressures. Lately, Yaroshenko *et al.* [43] pointed out that the presence of the vertical gradient of the grain charge might significantly contribute to this instability.

Chapter 2

Cumulative thesis

The results of this cumulative thesis are published in three papers enclosed to this thesis:

- R. Kompaneets, U. Konopka, A. V. Ivlev, V. Tsytovich, and G. Morfill, Potential around a charged dust particle in a collisional sheath, *Phys. Plasmas* **14**, 052108 (2007).
- R. Kompaneets, A. V. Ivlev, V. Tsytovich, and G. Morfill, Dust-lattice waves: Role of charge variations and anisotropy of dust-dust interaction, *Phys. Plasmas* **12**, 062107 (2005).
- R. Kompaneets, S. V. Vladimirov, A. V. Ivlev, V. Tsytovich, and G. Morfill, Dust clusters with non-Hamiltonian particle dynamics, *Phys. Plasmas* **13**, 072104 (2006).

The objectives, methods, results and conclusions of the papers listed above are summarized below. The full list of publications, including those with results not included to this thesis, is given separately (see Contents).

2.1 Potential around a charged dust particle in a collisional sheath

2.1.1 Objective

The objective is to test the hypothesis that the grain screening in the plasma-wall transition layer under typical conditions might be primarily due to ions and not electrons. For this

purpose, the corresponding model of the grain screening is developed and quantitatively compared with the experiment of Konopka *et al.* [17, 18].

2.1.2 Methods

As a basis of the proposed model, a recent kinetic model [32, 33] is taken. The model [32, 33] assumes a mobility-limited ion drift in a homogeneous external electric field. Here, “mobility-limited” means that the acceleration of ions in this external electric field is balanced by collisions with neutrals and that this balance determines the drift velocity. A charged grain treated as a non-absorbing point charge is considered to perturb this balance. No assumption is made about the ratio of the effective length of grain screening to the ion-neutral collision length. Therefore, the ion drift perturbed by the grain is *not* assumed to be mobility-limited.

With respect to the model [32, 33], a further improvement has been made in the present work: While the model [32, 33] assumes a velocity-independent ion-neutral collision frequency, the present work deals with the realistic case of velocity-independent cross-section [46]. Also, in the present work, the electron density is considered to be not perturbed by the grain and thus the screening is attributed to ions only. [The (time-averaged) electron density is assumed to be equal to the (unperturbed by the grain) ion density, so that the proposed model is relevant to the so-called presheath — that part of the plasma-wall transition layer where the plasma is still (almost) quasineutral]. Further, the velocity of the ion drift is assumed to be much larger than the thermal velocity of neutrals, and for this reason the thermal motion of neutrals is completely excluded from the consideration. The assumptions made allow to express the result — the potential distribution in plasma around the grain — via definite integrals. The obtained expression is quantitatively compared with the experiment of Konopka *et al.* [17, 18].

2.1.3 Results

The model is found to be in a very good agreement with the experimental data. The normalized squared deviation from the data is approximately the same as that given by the Debye-Hückel potential (see Fig. 2.1a, b). However, outside the distance range where the measurements [17, 18] were performed, the Debye-Hückel fit and the fit by the proposed model dramatically deviate from each other (see Fig. 2.1c). For the given experimental

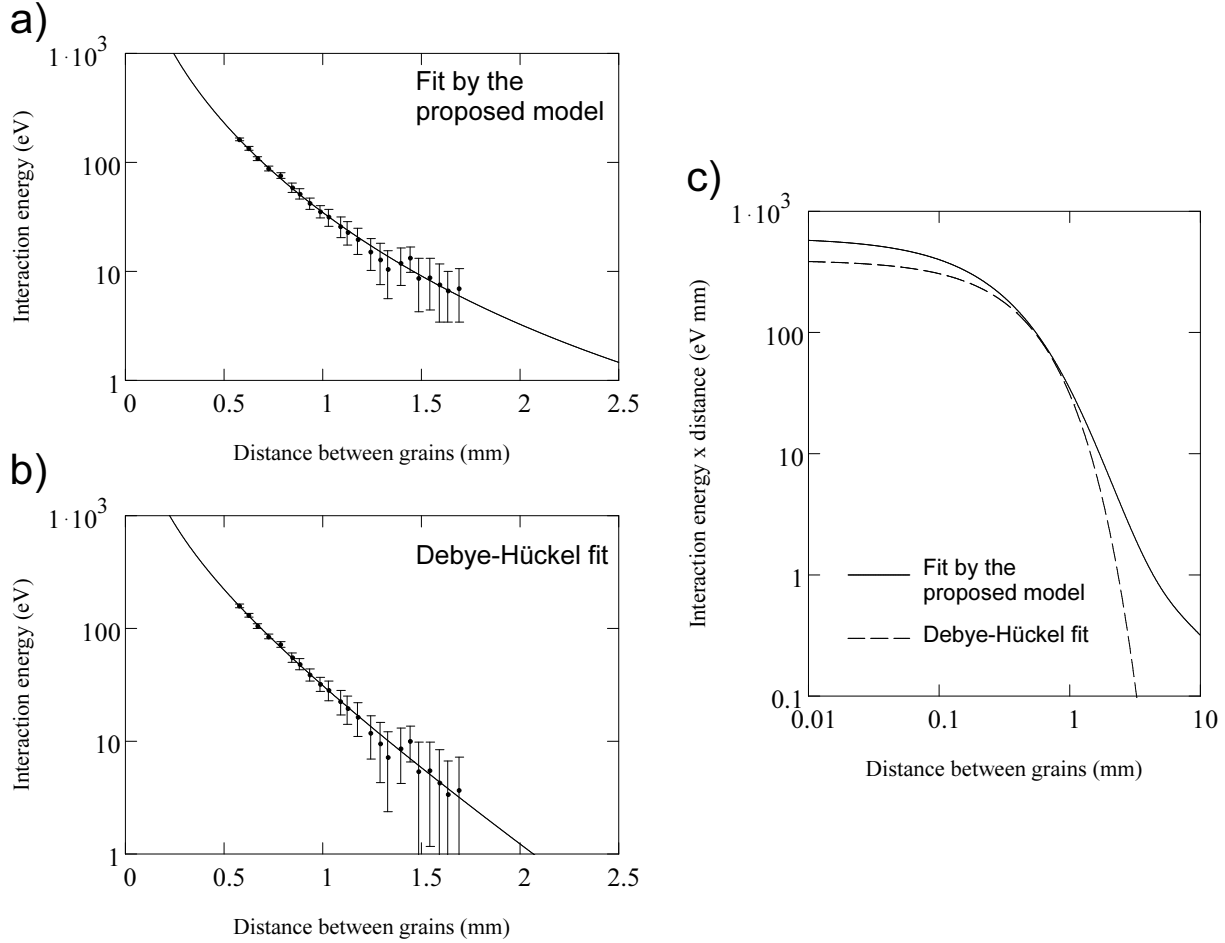


Figure 2.1: Comparison of experiment by Konopka *et al.* [17,18] with the proposed model of grain screening and the Debye-Hückel potential. a, b) Vertical axis is the interaction energy relative to infinite separation. Since the interaction energy was measured not relative to infinite separation, an unknown constant (offset) should be added to the measured energies as one of the fit parameters. The value of this offset is found to be not the same for both fits. The experimental data are shown with this offset added. c) Comparison of the fits (shown in a and b) with each other. Vertical axis is the interaction energy relative to infinite separation, multiplied by the distance between grains. (Unscreened Coulomb interaction would be a straight horizontal line).

conditions [17, 18], one of the model assumptions — unperturbed drift being mobility-limited — is found to be at the edge of applicability because of the inhomogeneity of the vertical electric field. (The inhomogeneity length of the vertical electric field is estimated from the measured frequency of vertical oscillations of a single particle and is found to be about the ion-neutral collision length). All other model assumptions, including the assumption that the ion drift velocity is much larger than the thermal velocity of neutrals, are found to be well justified, based on the parameter values deduced from the fit.

2.1.4 Conclusion

The results demonstrate that the experiment [17, 18] *cannot* be used as justification of either the applicability of the Debye-Hückel potential or the dominant role of electrons in grain screening. Therefore, more experiments are necessary to unravel the issue. Because of the all-importance of this problem to the field of complex plasmas, such experiments are currently being planned at the institution of this author [47].

2.2 Dust-lattice waves: Role of charge variations and anisotropy of dust-dust interaction

2.2.1 Objective

The objective is to investigate theoretically whether the mutual influence of particles on their charges could significantly contribute to the monolayer instability observed in the experiment reported by Ivlev *et al.* [11]. In the original paper by Ivlev *et al.* [11], the instability was explained by only the non-reciprocity of the interaction forces, whereas Yaroshenko *et al.* [43] pointed out that the simultaneous presence of the vertical gradient of the grain charge might significantly increase the effect. Thus, the objective of the present paper is to additionally include the charge variations due to change in the distances between the particles and thus obtain the “whole picture”.

2.2.2 Methods

Similar to papers by Ivlev *et al.* [11] and Yaroshenko *et al.* [43], the so-called chain model is employed. The chain model considers an infinite horizontal chain of particles, instead of a two-dimensional crystal structure. In the chain model, the particles are only allowed to move in the longitudinal and vertical directions. Each particle is assumed to interact with the neighboring particles only; the forces from the more distant particles are neglected. In the present work, the grain screening potential is assumed to be an arbitrary function of the relative coordinates of the observer with respect to the grain, which allows accounting for the non-reciprocity of the interaction forces. The vertical gradient of the grain charge is included as well. Concerning the mutual influence of the grains on their charges, the grain charge is assumed to be influenced by the neighboring particles only. The “horizontal” gradient of the grain charge, i.e., the derivative of the grain charge with respect to the inter-particle separation in the chain, is considered as a free parameter.

In the framework of this model, the dispersion relation of the dust-lattice waves (i.e., oscillations of dust particles in the dust lattice) is obtained and analyzed. Then, a numerical example with realistic parameter values is presented. In this numerical example, the interaction potential is assumed to be the sum of the Debye-Hückel potential and an additional dipole-like term which introduces the non-reciprocity of the interaction forces. As discussed above, the applicability of the Debye-Hückel potential is not well justified and the grain potential may be of other form. Nevertheless, a numerical example with the Debye-Hückel potential and dipole term is useful to illustrate the general expressions obtained.

2.2.3 Results

The parameter responsible for the instability — coefficient of coupling between the longitudinal and vertical transverse modes — is found to be the sum of four important terms, each caused by a different physical mechanism. Of these four terms, the first two were considered earlier by Ivlev *et al.* [11] and Yaroshenko *et al.* [43], respectively. The two remaining terms are new and are only possible in the presence of the “horizontal” gradient of the grain charge.

Under typical conditions, the “horizontal” gradient of the grain charge is believed to be significantly less than the vertical one. Probably for this reason the “horizontal” gradient

of the grain charge was not accounted for before in the analysis of the dust-lattice waves. The present study shows that, to compare the effects caused by the vertical and “horizontal” gradients of the grain charge, one should compare not the gradients themselves, but rather one should compare the product of the vertical gradient of the grain charge and the horizontal inter-grain repulsion force with the product of the “horizontal” gradient of the grain charge and the vertical electric field force levitating the grains against gravity. Usually, the vertical electric field force is much larger than the horizontal inter-grain interaction forces. Therefore, the “horizontal” gradient of the grain charge may be important even when it is less than the vertical one.

Furthermore, the presence of the “horizontal” gradient of the grain charge gives rise to a new effect: When the vertical and “horizontal” gradients of the grain charge are present simultaneously, the instability due to the non-Hamiltonian dynamics can be triggered even when the interaction forces are reciprocal.

The instability is triggered when all of the following conditions are satisfied:

- The branches of the longitudinal and vertical transverse modes should intersect with each other [in the (ω, k) -plane]. From the practical standpoint, this condition implies that the interparticle distance in the monolayer should be less than a certain threshold.
- The coefficient of coupling between the longitudinal and vertical transverse modes, which is determined by the charge gradients and the “degree of non-reciprocity” of the interaction forces, should be of the proper sign.
- The dust-neutral friction should not suppress the instability. Therefore, the gas pressure should be not too high.

2.2.4 Conclusion

It is found that the mutual influence of particles on their charges might significantly contribute to the monolayer instability observed in the experiment reported by Ivlev *et al.* [11].

2.3 Dust clusters with non-Hamiltonian particle dynamics

2.3.1 Objective

The objective is to theoretically investigate whether a system of a few dust particles can exhibit something similar to the monolayer instability reported by Ivlev *et al.* [11]. Can the non-Hamiltonian dynamics of dust particles trigger an instability of 2- or 3-particle clusters aligned perpendicular to the ion drift? Observation of such instability could not only clearly demonstrate the non-Hamiltonian dynamics of dust particles but also might provide important information about non-reciprocal interaction forces and/or charge variations.

2.3.2 Methods

Expressions for eigenfrequencies of 2- and 3-particle clusters aligned horizontally (i.e., perpendicular to the ion drift) are obtained. The clusters are considered to be horizontally confined by a parabolic potential, so that the interparticle separation is determined by the balance of the horizontal confinement and mutual repulsion of particles. In the 3-particle cluster, the particles are considered to form an equilateral triangle — as observed in experiments [19, 20] — and not a string. The grain screening potential is assumed to be an arbitrary function of both the relative position of the observer with respect to the grain and vertical position of the grain itself. This allows accounting for both the screening variations and the non-reciprocity of the interaction forces. The vertical gradient of the grain charge is included as well. However, the “horizontal” gradient of the grain charge is not included, in order not to make the analysis too complicated.

The derived expressions are analyzed to assess the possibility of an instability. Then, a numerical example with realistic parameter values is presented. In this numerical example, the interaction potential is assumed to be the sum of the Debye-Hückel interaction potential and an additional dipole-like term which introduces the non-reciprocity of the interaction forces.

2.3.3 Results

It is found that an instability due to the non-Hamiltonian dynamics of dust grains can indeed be triggered, similar to a monolayer: The non-Hamiltonian dynamics of grains can cause a gradual growth over time of otherwise stable oscillations of grains in a cluster. The instability is triggered when all of the following conditions are satisfied:

- Two certain cluster eigenfrequencies should be sufficiently close to each other. From the practical standpoint, this implies that the horizontal confinement should be varied during experiment until the interparticle distance becomes close to the resonance value.
- The “coupling coefficient” (between those modes whose eigenfrequencies are close to each other, according to the preceding condition) determined by the charge gradient, screening variations, and “degree of non-reciprocity” of the interaction forces should be of the proper sign.
- The dust-neutral friction should not suppress the instability. Therefore, the gas pressure should be not too high.

As compared with the instability condition for a monolayer [11, 43], the instability condition for a cluster is somewhat similar. However, there is one important difference. In the case of a cluster, the interparticle distance should be adjusted to a certain resonance value. In the case of a monolayer, the interparticle distance should be simply less than a certain threshold.

A numerical example is shown in Fig. 2.2.

2.3.4 Conclusion

The instability is found to be theoretically possible, but hardly “realizable” in experiments. The main difficulty is related to the necessity of the adjustment of the interparticle distance to a certain resonance value.

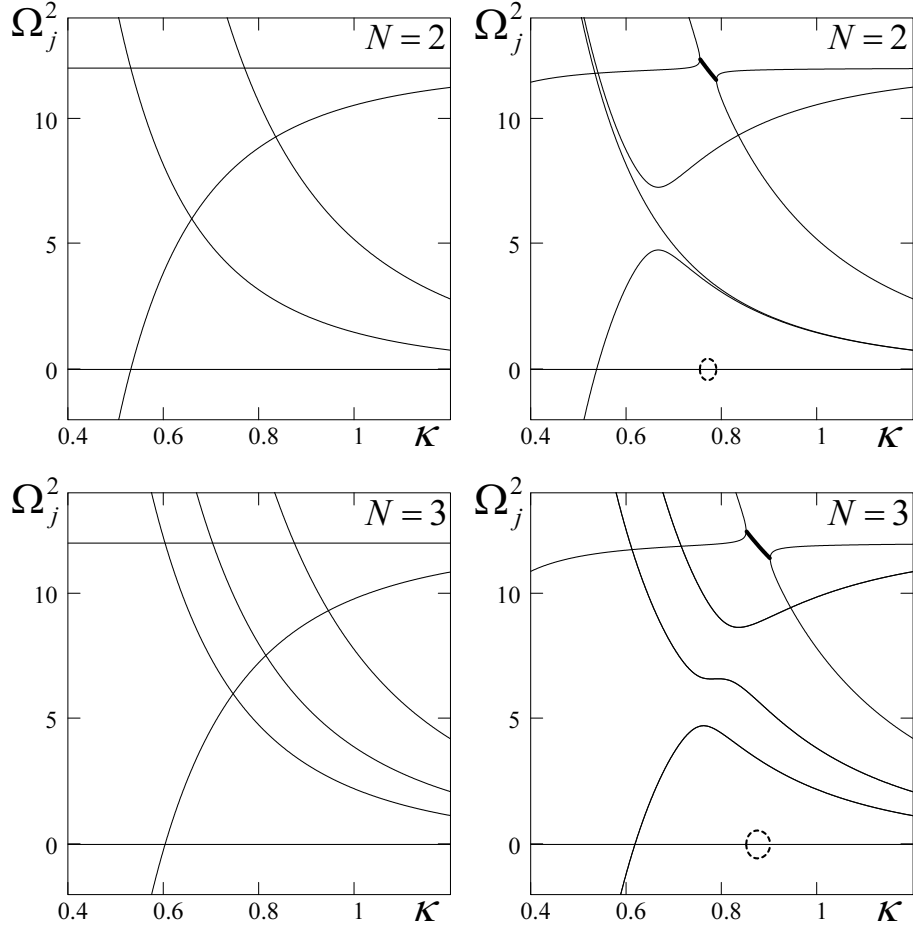


Figure 2.2: The calculated squared eigenfrequencies of $N = 2$ and $N = 3$ clusters in a parabolic horizontal confinement potential. The two left graphs show the case of the Debye-Hückel screening potential. The case shown in the two right graphs additionally includes (1) a (particle-wake) dipole term in the grain screening potential, which is responsible for the non-reciprocal interaction, and (2) vertical gradients of (a) the screening length, (b) particle charge, and (c) horizontal confinement potential. The vertical axis shows the squared eigenfrequencies normalized by $Q^2/(M\lambda^3)$, the horizontal axis is the interparticle distance in the cluster, normalized by λ . (Here Q is the equilibrium particle charge, M is the grain mass, and λ is the screening length characterizing the Debye-Hückel potential). All the parameter values are taken as measured and/or estimated in experimental works by Konopka *et al.* [17, 18]. In all graphs, the imaginary parts of all squared frequencies are zero except the imaginary parts shown by the dash lines (the corresponding real parts are shown by the thick lines).

Chapter 3

Summary and future work

The first paper enclosed to this thesis deals with one of the fundamental issues in the physics of complex plasmas — screening/interaction of charged grains suspended in the plasma-wall transition layer. In the complex plasma community, there exists a strong belief that, under typical conditions, the pair interaction potential is of the Debye-Hückel form and is determined by electrons. In part, this belief is based on direct measurements by Konopka *et al.* [17, 18] who did not find noticeable deviations of the measured potential from the Debye-Hückel form. In the present work, attention is drawn to some evidences against this belief and it is suggested that the grain screening might be primarily due to ions and not electrons. The present work proposes a kinetic model for the grain screening, attributing screening to ions only. The proposed model is proven to be in full agreement with the mentioned experiment by Konopka *et al.* [17, 18]. At the same time, the proposed model suggests significant deviations from the Debye-Hückel potential outside the range of distances where the measurements [17, 18] were performed. Therefore, given the all-importance of the problem for the field of complex plasmas, further research is necessary to clarify the issue. This research includes but is not limited to:

- *Computation and numerical analysis of the dispersion relation for the ion-acoustic waves in the framework of the proposed kinetic model.* It is necessary to assess and prove the stability of the ion drift in a homogeneous external electric field, which is assumed by the model. Moreover, the ion-acoustic modes in the presence of the ion drift are of general importance for the physics of plasmas.

- *Measurements of the intergrain interaction energy in a broader range of distances* may help to clarify the issue, since the grain screening potential given by the proposed model and the Debye-Hückel potential dramatically deviate from each other outside the distance range where the measurements [17, 18] were performed.
- *Development of a model which combines both modeling of the plasma-wall transition layer and grain screening in the plasma-wall transition layer* would ideally be necessary, because such approach would allow accounting for the inhomogeneity of the electric field and plasma parameters in the plasma-wall transition layer.
- *Extension of the proposed model of grain screening to the case of a finite ratio of the ion drift velocity to the thermal velocity of neutrals* is important for microgravity experiments.

One of the important applications of this work is related to the possibility of tuning the pair interaction potential by applying external fields [48]. The possibility to obtain and tune an attraction between particles provides a very convenient tool to study electrorheological properties of strongly coupled systems. With respect to “usual” electrorheological fluids, complex plasmas have an important advantage: The particle motion in complex plasmas is not strongly affected by the neutral gas friction, while the dynamical processes in “usual” electrorheological fluids are strongly damped by the background fluid and thus cannot be observed on their “original” time scales.

First experiments devoted to the study of electrorheological properties of complex plasmas were performed under microgravity conditions onboard the International Space Station in January 2007 [49]. In these experiments, a linearly oscillating electric field was applied to cause oscillations of the ion drift, with the frequency being in between the inverse ion plasma and grain dynamics time scales. The interaction forces between grains under such conditions are reciprocal, because non-reciprocal forces are averaged out due to oscillations of the ion drift, and thus the non-Hamiltonian dynamical effects due to non-reciprocity of the interaction forces are excluded. When the amplitude of the applied field exceeded a certain threshold, the particles exhibited a phase transition: They arranged themselves into strings aligned along the direction of oscillations of the ion drift. This suggests that the (averaged over oscillations of the ion drift) interaction potential had an attractive part in the direction of oscillations of the ion drift.

Non-Hamiltonian dynamics of dust particles, considered in the second and third papers enclosed to this thesis, is closely connected with the issue of the intergrain interaction considered in the first paper. In particular, the proposed model of grain screening gives a certain expression for the effective particle-wake dipole moment (see enclosed papers for details). This effective particle-wake dipole moment is responsible for the non-reciprocity of the interaction forces and leads to non-Hamiltonian dynamics of dust particles. However, not only the non-reciprocity of the interaction forces can lead to non-Hamiltonian dynamics of dust particles. Charge and screening variations, each taken alone, lead to non-Hamiltonian dynamics, as well. One of the results obtained in the second paper is that all these three factors should not be considered separately, because the combination of these factors gives rise to some new important effects.

As shown in the second and third papers enclosed, the non-Hamiltonian dynamics of grains can trigger instabilities, both for monolayers and finite clusters. Such instabilities are critical phenomena (i.e., they are either present or absent for given conditions) and can be easily visualized. Therefore, they may be used for plasma diagnostics in the plasma-wall transition layer.

Appendix A

Appendix: Theoretical background

This Appendix addresses the specific details of the main topic of this cumulative thesis — grain screening in a plasma with ion drift — and is organized in the following way. First, various theoretical models of grain screening are reviewed. Then, the applicability of the models is assessed by discussing both the properties of the ion-neutral collisions and existing measurements of ion and electron velocity distributions in the plasma-wall transition layer.

A.1 Models of grain screening

A.1.1 General approach

Almost all existing models of grain screening assume an infinite homogeneous plasma with ion drift. Although plasma discharges are not homogeneous, this approach may be justified when the plasma parameters do not change significantly on the characteristic length of grain screening.

A derivation of the potential distribution around a grain generally involves the following three steps:

1. Formulation of kinetic equations for the distribution functions of plasma species.
2. Setting of the boundary conditions far from the grain.
3. Solution.

These steps are separately discussed below.

Kinetic equation

For ions, the steady-state kinetic equation [50] is

$$\mathbf{v} \frac{\partial f}{\partial \mathbf{r}} + \frac{e\mathbf{E}}{m} \frac{\partial f}{\partial \mathbf{v}} = \text{St}[f], \quad (\text{A.1})$$

where $f = f(\mathbf{r}, \mathbf{v})$ is the ion velocity distribution function, $\mathbf{E} = \mathbf{E}(\mathbf{r})$ is the electric field, $e > 0$ is the elementary charge (all ions are assumed to be singly ionized), m is the ion mass, $\text{St}[f]$ is the collision operator describing the ion-neutral collisions. (The ion-ion and ion-electron collisions, ionization, and absorption of ions on the grain are usually neglected and thus are not included in the collision operator). For typical conditions, only binary ion-neutral collisions should be taken into account. The velocity distribution of neutrals (present in the collision operator) is assumed to be homogeneous Maxwellian with constant temperature and density. The exact form of the collision operator is determined by the expression for the differential cross-section. Such a collision operator has the following properties:

- the collision operator conserves the number of ions, i.e.,

$$\int \text{St}[f(\mathbf{r}, \mathbf{v})] d\mathbf{v} = 0, \quad (\text{A.2})$$

- the collision operator is linear, i.e.,

$$\text{St}[\alpha f + \beta g] = \alpha \text{St}[f] + \beta \text{St}[g] \quad (\text{A.3})$$

where $f, g = f, g(\mathbf{r}, \mathbf{v})$ and $\alpha, \beta = \alpha, \beta(\mathbf{r})$,

- the collision operator yields zero for a Maxwellian velocity distribution of ions if the temperature of this Maxwellian distribution is equal to the temperature of neutrals.

Some models employ the hydrodynamic (fluid) equations instead of the kinetic equation (A.1). In fact, the hydrodynamic equations — the continuity and momentum equations — are derived from the kinetic equation under the assumption that the ion velocity distribution $f(\mathbf{r}, \mathbf{v})$ is shifted Maxwellian, with the temperature and drift velocity dependent on spatial coordinates [50]. This assumption is indeed applicable when the ion-ion collisions are frequent enough to “maxwellize” the ion velocity distribution. But this is not the case in typical complex plasmas experiments, because in these experiments ions collide with

neutrals much more frequently than with each other, and, as a consequence, the velocity distributions of ions in electric fields are generally not shifted Maxwellian. For this reason, fluid models of grain screening will not be discussed here, although they are sometimes used in literature without any justification (e.g., see Refs. [51,52]).

Concerning electrons, some models assume that the (time-averaged) electron density is not perturbed at all by the grain [33]. However, the majority of models assume the Boltzmann response [25, 26, 27, 28, 29, 30, 31, 32, 34],

$$n_e = n_{e,0} \exp\left(\frac{e\phi}{T_e}\right), \quad (\text{A.4})$$

where $n_e = n_e(\mathbf{r})$ is the (time-averaged) electron density, $n_{e,0}$ is the (time-averaged) electron density far from the grain, $\phi = \phi(\mathbf{r})$ is the (time-averaged) potential induced by the grain, and T_e is the (effective) electron temperature. As will be discussed in Subsection A.2.3, such approach is not well justified for grain screening in the plasma-wall transition layer, and, strictly speaking, the time-dependent kinetic equation for the electron velocity distribution function is necessary if the electron response should be taken into account.

The kinetic equations are closed by the Poisson equation,

$$\frac{\partial \mathbf{E}}{\partial \mathbf{r}} = 4\pi(n - n_e)e + 4\pi Q\delta(\mathbf{r}), \quad (\text{A.5})$$

where $n = n(\mathbf{r}) = \int f(\mathbf{v}, \mathbf{r}) d\mathbf{v}$ is the ion density, Q is the grain charge, $\delta(\mathbf{r})$ is the delta-function. The delta-function approximation is well justified by the fact that the grain size is typically two orders of magnitude smaller than the effective length of grain screening.

Boundary conditions far from the grain

Far from the grain (i.e., for $\mathbf{r} \rightarrow \infty$), a spatially homogeneous ion distribution $f_0 = f_0(\mathbf{v})$ and a spatially homogeneous electric field \mathbf{E}_0 are usually assumed, as stated above. According to Eq. (A.1), the distribution f_0 is given by

$$\frac{e\mathbf{E}_0}{m} \frac{df_0}{d\mathbf{v}} = \text{St}[f_0]. \quad (\text{A.6})$$

The solution of Eq. (A.6) depends on the exact form of the collision operator and is generally not of the shifted Maxwellian form. Further, the plasma is assumed to be quasineutral far from the grain [$n_0 = n_{e,0}$ where $n_0 = \int f_0(\mathbf{v}) d\mathbf{v}$ is the ion density far from the grain], otherwise the Poisson equation (A.5) is not satisfied.

The question generally arises as to whether the state far from the grain, defined above, is stable with respect to the ion-acoustic waves. The question requires a derivation of the corresponding dispersion relation [50]. The answer may depend on parameter values and the exact form of the collision operator. The analysis of the dispersion relation usually can be only performed numerically and sometimes yields infinite number of solutions/modes (e.g., the higher-order Landau modes [53,54]), which makes it difficult to assess the stability. Because of the difficulty of proving the stability, it might be acceptable not to perform the stability analysis when no instability mechanism is expected a priori.

Solution

Solution of the kinetic equations with the boundary conditions discussed above gives the grain potential $\phi = \phi(\mathbf{r})$ defined as

$$-\frac{\partial\phi}{\partial\mathbf{r}} = \mathbf{E} - \mathbf{E}_0, \quad \phi|_{\mathbf{r}\rightarrow\infty} = 0. \quad (\text{A.7})$$

Usually, the so-called linear approximation is used, i.e., the so-called linearized grain potential is found. The linearized grain potential is the first term in the expansion of the grain potential $\phi(\mathbf{r})$ in a series of the grain charge Q . This approach is justified when the region of nonlinear screening around the grain is small enough. Further, the notation ϕ will be understood as the linearized grain potential.

The linear approximation significantly simplifies the solution which can now be performed in the following way. The Fourier transforms are considered:

$$\phi(\mathbf{r}) = \int \phi_{\mathbf{F}}(\mathbf{k}) \exp(i\mathbf{k}\mathbf{r}) d\mathbf{k}, \quad (\text{A.8})$$

$$f(\mathbf{r}, \mathbf{v}) = f_0(\mathbf{v}) + \int f_{1,\mathbf{F}}(\mathbf{k}, \mathbf{v}) \exp(i\mathbf{k}\mathbf{r}) d\mathbf{k}. \quad (\text{A.9})$$

Substitution of Eqs. (A.8) and (A.9) to Eq. (A.1) and subsequent linearization give

$$i\mathbf{k}\mathbf{v}f_{1,\mathbf{F}} + \frac{e\mathbf{E}_0}{m} \frac{\partial f_{1,\mathbf{F}}}{\partial\mathbf{v}} - \frac{i\mathbf{k}e\phi_{\mathbf{F}}}{m} \frac{df_0}{d\mathbf{v}} = \text{St}[f_{1,\mathbf{F}}]. \quad (\text{A.10})$$

Then, $f_{1,\mathbf{F}}(\mathbf{k}, \mathbf{v})$ should be expressed via \mathbf{k} , \mathbf{v} , and $\phi_{\mathbf{F}}(\mathbf{k})$, by solving Eq. (A.10) with the boundary condition $f_{1,\mathbf{F}}(\mathbf{k}, \mathbf{v})|_{\mathbf{v}\rightarrow\infty} = 0$. Then, the static ion susceptibility $\chi(\mathbf{k})$ should be calculated according to

$$\chi(\mathbf{k}) = -\frac{4\pi e n_{1,\mathbf{F}}(\mathbf{k})}{|\mathbf{k}|^2 \phi_{\mathbf{F}}(\mathbf{k})} \quad (\text{A.11})$$

where

$$n_{1,F}(\mathbf{k}) = \int f_{1,F}(\mathbf{k}, \mathbf{v}) d\mathbf{v}. \quad (\text{A.12})$$

Using the Fourier transform of the delta-function

$$\delta(\mathbf{r}) = \frac{1}{(2\pi)^3} \int \exp(i\mathbf{k}\mathbf{r}) d\mathbf{k} \quad (\text{A.13})$$

and assuming that the electron density is not perturbed by the grain, one can substitute Eqs. (A.8), (A.9), (A.11), (A.12), and (A.13) to the Poisson equation (A.5) and thus obtain

$$\phi_F(\mathbf{k}) = \frac{Q}{2\pi^2} \frac{1}{|\mathbf{k}|^2 [1 + \chi(\mathbf{k})]}. \quad (\text{A.14})$$

Therefore, the grain potential is given by

$$\phi(\mathbf{r}) = \frac{Q}{2\pi^2} \int \frac{\exp(i\mathbf{k}\mathbf{r})}{|\mathbf{k}|^2 [1 + \chi(\mathbf{k})]} d\mathbf{k}. \quad (\text{A.15})$$

Including the electron Boltzmann response [Eq. (A.4)] results in adding the electron susceptibility $\chi_e(\mathbf{k}) = (\lambda_{De}|\mathbf{k}|)^{-2}$ to the ion susceptibility $\chi(\mathbf{k})$ in the denominator in Eq. (A.15). Here $\lambda_{De} = [T_e/(4\pi n_{e,0}e^2)]^{1/2}$ is the electron Debye length.

A.1.2 Debye-Hückel potential

This Subsection deals with the case where (i) the electric field is absent ($\mathbf{E}_0 = \mathbf{0}$) and (ii) the (unperturbed by the grain) velocity distribution of ions is Maxwellian,

$$f_0(\mathbf{v}) = n_0 \Phi_M(\mathbf{v}, T), \quad (\text{A.16})$$

where

$$\Phi_M(\mathbf{v}, T) = \left(\frac{m}{2\pi T}\right)^{3/2} \exp\left(-\frac{m|\mathbf{v}|^2}{2T}\right) \quad (\text{A.17})$$

is the Maxwellian distribution normalized by the ion density, T is the temperature characterizing the Maxwellian distribution. In Eq. (A.16), the temperature T is considered to be equal to the neutral temperature, so that $\text{St}[f_0] = 0$ and, hence, condition (A.6) is satisfied. In this case, the solution of Eq. (A.10) is

$$f_{1,F}(\mathbf{v}) = -\frac{e\phi_F}{T} n_0 \Phi_M(\mathbf{v}, T), \quad (\text{A.18})$$

irrespective of the exact form of the collision operator. [This is because the equality $\text{St}[f_{1,F}] = 0$ takes place. This equality is proven by the linearity (A.3) of the collision

operator and the fact that f_0 (A.16) and $f_{1,F}$ (A.18) have the same velocity dependence]. Therefore, the ion susceptibility (A.11) is

$$\chi(\mathbf{k}) = \frac{1}{\lambda_D^2 |\mathbf{k}|^2} \quad (\text{A.19})$$

where

$$\lambda_D = \sqrt{\frac{T}{4\pi n_0 e^2}} \quad (\text{A.20})$$

is the ion Debye length (radius). For the susceptibility (A.19), the integration in Eq. (A.15) can be performed analytically and yields

$$\phi = \frac{Q}{|\mathbf{r}|} \exp\left(-\frac{|\mathbf{r}|}{\lambda_D}\right). \quad (\text{A.21})$$

This is the classical Debye-Hückel potential [50]. If the Boltzmann electron response is included, then the result (A.21) will be changed as follows: The λ_D will be replaced by $\lambda_D \lambda_{De} / \sqrt{\lambda_D^2 + \lambda_{De}^2}$.

A.1.3 Collisionless case: Drift in the absence of field

This Subsection deals with the case where (i) the external electric field is absent/neglected ($\mathbf{E}_0 = \mathbf{0}$), (ii) the collision operator term in Eq. (A.1) is absent/neglected, and (iii) the unperturbed velocity distribution of ions f_0 is anisotropic (in the direction of the ion drift). In this case, the solution of Eq. (A.10) takes the form

$$f_{1,F} = \frac{e\phi_F}{m} \mathbf{k} \frac{df_0}{d\mathbf{v}} \frac{1}{\mathbf{k}\mathbf{v} - i0}, \quad (\text{A.22})$$

which gives the ion susceptibility (A.11) to be

$$\chi(\mathbf{k}) = -\frac{4\pi e^2}{m|\mathbf{k}|^2} \int \mathbf{k} \frac{df_0}{d\mathbf{v}} \frac{d\mathbf{v}}{\mathbf{k}\mathbf{v} - i0}. \quad (\text{A.23})$$

The term $-i0$ is included to avoid the singularity. The inclusion of this term can be “justified”, e.g., by accounting for an infinitely small collision operator term $\text{St}[f_{1,F}]$ which is then replaced by $-0 \cdot f_{1,F}$ [50].

Existing calculations of the potential (A.15) for the susceptibility (A.23) are discussed below.

Isotropic distribution

If the distribution f_0 is isotropic (i.e, f_0 depends only on $|\mathbf{v}|$), then the ion susceptibility (A.23) is

$$\chi(\mathbf{k}) = \frac{(4\pi)^2 e^2}{m|\mathbf{k}|^2} \int_0^\infty f_0(\mathbf{v}) d|\mathbf{v}|. \quad (\text{A.24})$$

The susceptibility (A.24) is of the same form as (A.19), with the only difference that the λ_D^2 is replaced by $m/[(4\pi)^2 e^2 \int_0^\infty f_0(\mathbf{v}) d|\mathbf{v}|]$. Therefore, the grain potential $\phi(\mathbf{r})$ is again of the Debye-Hückel form. This example demonstrates that the Debye-Hückel potential is possible not only for the Maxwellian velocity distribution.

Potential at large distances: General statement for anisotropic distribution

Montgomery *et al.* [55] investigated the asymptotic behavior of the potential (A.15) at large distances, for the susceptibility (A.23). They found that the potential generally falls off as the inverse third power of the distance $|\mathbf{r}|$, i.e.,

$$\phi(\mathbf{r}) = \frac{Q}{|\mathbf{r}|^3} F(\theta) + o\left(\frac{1}{|\mathbf{r}|^3}\right), \quad \mathbf{r} \rightarrow \infty, \quad (\text{A.25})$$

where θ is the angle between \mathbf{r} and the direction of the ion drift. Montgomery *et al.* expressed $F(\theta)$ via definite integrals which contain f_0 .

Eq. (A.25) demonstrates that the Debye-Hückel screening is violated in anisotropic plasmas.

Shifted Maxwellian distribution

If the distribution f_0 is shifted Maxwellian,

$$f_0(\mathbf{v}) = n_0 \Phi_M(\mathbf{v} - \mathbf{u}, T), \quad (\text{A.26})$$

where \mathbf{u} is the ion drift velocity, T is the temperature characterizing this shifted Maxwellian distribution, then the ion susceptibility (A.23) is

$$\chi(\mathbf{k}) = \frac{1}{\lambda_D^2 |\mathbf{k}|^2} \frac{1}{\sqrt{2\pi}} \int_{-\infty}^{\infty} \frac{t}{t + \mathbf{k}\mathbf{u}/(|\mathbf{k}|v_T) - i0} \exp\left(-\frac{t^2}{2}\right) dt, \quad (\text{A.27})$$

where $\lambda_D = \sqrt{T/(4\pi n_0 e^2)}$ is the ion Debye radius corresponding to the temperature T , $v_T = \sqrt{T/m}$ is the “thermal” velocity.

Weakly shifted Maxwellian distribution. Assuming that the susceptibility is given by Eq. (A.27), Cooper [56] derived the expansion of the potential (A.15) in a series of \mathbf{u} , up to the $|\mathbf{u}|^2$ -term inclusive. In particular, he found that the function $F(\theta)$ [see Eq. (A.25)] was

$$F(\theta) = \lambda_D^2 \left[-\sqrt{\frac{8}{\pi}} \frac{|\mathbf{u}|}{v_T} \cos \theta - \left(\frac{\pi}{2} - 1 \right) \frac{|\mathbf{u}|^2}{v_T^2} (1 - 3 \cos^2 \theta) \right] + o(|\mathbf{u}|^2), \quad \mathbf{u} \rightarrow \mathbf{0}. \quad (\text{A.28})$$

Eq. (A.28) implies that two like-charged grains aligned perpendicular to the ion drift will attract each other electrostatically if the distance between the particles is large enough. Eq. (A.28) also implies that the interaction forces between particles aligned perpendicular to the drift have non-zero components in the direction of the ion drift. The latter fact demonstrates that the interaction forces are not reciprocal.

Strongly shifted Maxwellian distribution. In the case $T \rightarrow 0$ (i.e., when the distribution f_0 is a shifted delta-function), the ion susceptibility (A.27) is

$$\chi(\mathbf{k}) = -\frac{4\pi n_0 e^2}{m} \frac{1}{(\mathbf{k}\mathbf{u} - i0)^2}. \quad (\text{A.29})$$

There have been many calculations of the potential (A.15) for the susceptibility (A.29), in most cases with the Boltzmann electron response included [25,26,27,28]. These calculations demonstrate that a series of potential minima and maxima can be formed “behind” the grain.

General case. Peter [57] calculated the potential (A.15) for the susceptibility (A.27) for $|\mathbf{u}| = v_T\sqrt{2}, 3v_T\sqrt{2}, 7v_T\sqrt{2}, 15v_T\sqrt{2}$. His graph for $|\mathbf{u}| = 3v_T\sqrt{2}$ demonstrates a series of at least 11 potential extrema “behind” the test particle. The possibility of attraction between like-charged particles aligned perpendicular to the drift is evident in his graphs obtained for $|\mathbf{u}| = v_T\sqrt{2}$ and $|\mathbf{u}| = 3v_T\sqrt{2}$.

Lampe *et al.* [30] performed calculations with the Boltzmann electron response included. For the considered parameter regime ($T_e = 15T, 0.25 < |\mathbf{u}|/\sqrt{T_e/m} < 1.5$), the potential upstream and to the side was found to be close to the Debye-Hückel potential, at least up to several screening lengths. In figures presented by Lampe *et al.*, at least one potential extremum “behind” the grain was always evident. No evidence of attraction forces between like-charged grains aligned perpendicular to the drift was demonstrated.

Benkadda *et al.* [31] also performed calculations with the Boltzmann electron response included. They assumed a shifted Maxwellian distribution with different upstream, down-

stream, and perpendicular temperatures and demonstrated the possibility of attraction between like-charged grains aligned perpendicular to the drift.

A.1.4 Finite collisionality

To consider the case of finite collisionality, one needs to choose a certain collision operator in Eq. (A.1). The only collision operator employed so far to calculate the grain potential is the so-called BGK (Bhatnagar-Gross-Krook) collision operator. In the following, existing calculations performed by using the BGK collision operator are discussed.

BGK collision operator

The BGK collision operator is based on two assumptions:

- Only the charge exchange collisions are taken into account.
- The collision frequency is velocity independent.

The applicability of the two listed assumptions will be discussed in Subsection A.2.1.

The BGK collision operator has the following form:

$$\text{St}[f(\mathbf{r}, \mathbf{v})] = -\nu f(\mathbf{r}, \mathbf{v}) + \nu \Phi_{\text{M}}(\mathbf{v}, T_n) \int f(\mathbf{r}, \mathbf{v}') d\mathbf{v}', \quad (\text{A.30})$$

where ν is the collision frequency, T_n is the neutral temperature.

For the BGK collision operator (A.30), Eq. (A.6) gives the unperturbed velocity distribution of ions f_0 in the form [32]

$$f_0(\mathbf{v}) = n_0 \int_0^\infty \Phi_{\text{M}}\left(\mathbf{v} - \frac{e\mathbf{E}_0 t}{m\nu}, T_n\right) e^{-t} dt. \quad (\text{A.31})$$

Therefore, the ion velocity distribution is a *superposition* of shifted Maxwellian distributions with exponential weights. Integration in Eq. (A.31) yields [58]

$$f_0(\mathbf{v}) = \frac{n_0}{(2\pi v_{T_n}^2)^{3/2}} \sqrt{\frac{\pi}{2}} \frac{v_{T_n}}{u} \exp\left(-\frac{v_\perp^2}{2v_{T_n}^2} + \frac{v_{T_n}^2}{2u^2} - \frac{v_\parallel}{u}\right) \left[1 + \text{erf}\left(\frac{v_\parallel u - v_{T_n}^2}{v_{T_n} u \sqrt{2}}\right)\right], \quad (\text{A.32})$$

where $v_{T_n} = \sqrt{T_n/m}$ is the thermal velocity of neutrals, v_\parallel and v_\perp are respectively the longitudinal and perpendicular components of the velocity \mathbf{v} with respect to the direction of the ion drift (i.e., with respect to \mathbf{E}_0), $u = e|\mathbf{E}_0|/(m\nu)$, and $\text{erf}(x) = (2/\sqrt{\pi}) \int_0^x \exp(-t^2) dt$

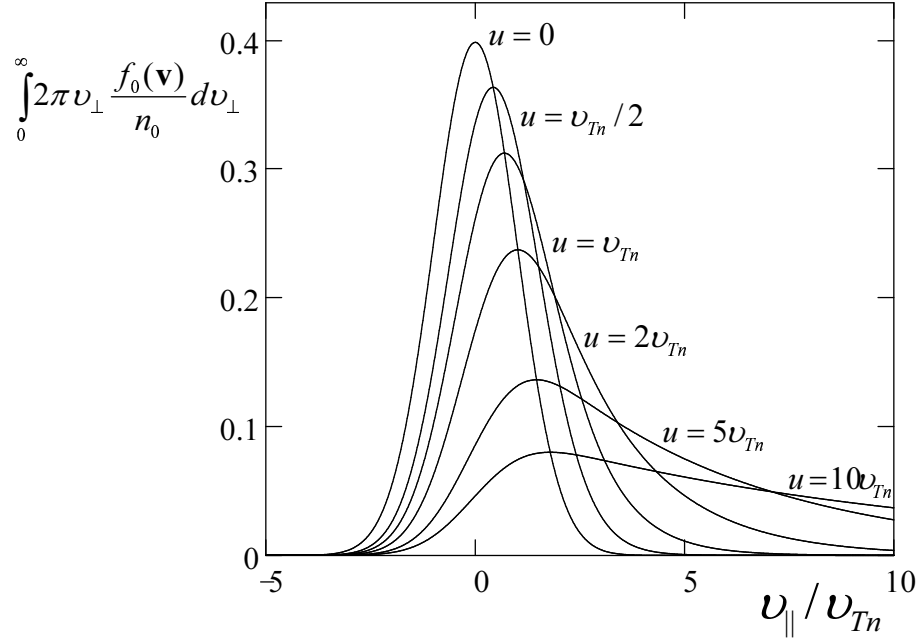


Figure A.1: Longitudinal velocity distributions of ions in homogeneous electric fields, calculated by using the BGK ion-neutral collision operator. Vertical axis is the ion velocity distribution normalized by the ion density and integrated over the velocity components perpendicular to the direction of the electric field. Horizontal axis is the longitudinal velocity normalized by the thermal velocity of neutrals. Different distributions shown correspond to different electric fields. The drift velocities u corresponding to these electric fields are indicated in units of the thermal velocity of neutrals v_{Tn} .

is the error function. The mean velocity $\int \mathbf{v} f_0(\mathbf{v}) d\mathbf{v}/n_0$ appears to be equal to u [58] and, hence, proportional to the applied electric field \mathbf{E}_0 .

Fig. A.1 shows the distribution function (A.32) for different u/v_{Tn} . It can be seen that the shape of the distribution function (A.32) is different from the shape of a shifted Maxwellian distribution, particularly when the ratio u/v_{Tn} is large.

The ion susceptibility (A.11) takes the form [33, 32]

$$\chi(\mathbf{k}) = \frac{4\pi n_0 e^2}{m\nu^2} \frac{B(\mathbf{k})}{1 - A(\mathbf{k})}, \quad (\text{A.33})$$

where

$$A(\mathbf{k}) = \int_0^\infty \exp[-\Psi(\mathbf{k}, \eta)] d\eta, \quad (\text{A.34})$$

$$B(\mathbf{k}) = \int_0^\infty \frac{\eta \exp[-\Psi(\mathbf{k}, \eta)]}{1 + ik_{\parallel} u \eta / \nu} d\eta, \quad (\text{A.35})$$

$$\Psi(\mathbf{k}, \eta) = \eta + \frac{1}{2} \left[\frac{ik_{\parallel} u}{\nu} + \left(\frac{|\mathbf{k}| v_{Tn}}{\nu} \right)^2 \right] \eta^2, \quad (\text{A.36})$$

k_{\parallel} is the longitudinal component of the wave number \mathbf{k} [i.e., $k_{\parallel} = \mathbf{k} \mathbf{E}_0 / |\mathbf{E}_0|$].

Schweigert *et al.* [34] calculated the potential (A.15) for the susceptibility (A.33), with the Boltzmann electron response included. In the graphs presented by them, an extremum of the potential downstream the grain is sometimes quite evident, whereas no evidence of possibility of attraction between like-charged grains aligned perpendicular to the ion drift can be seen.

If one considers the limit $|\mathbf{E}_0|, \nu \rightarrow 0$, $u \equiv e|\mathbf{E}_0|/(m\nu) \rightarrow \text{const}$ (i.e., ‘‘collisionless’’ limit with finite drift velocity) and *then* the limit $\mathbf{r} \rightarrow \infty$, one obtains [59]

$$\phi(\mathbf{r}) = \frac{Q}{|\mathbf{r}|^3} F_{\text{BGK}}(\theta) + o\left(\frac{1}{|\mathbf{r}|^3}\right), \quad \mathbf{r} \rightarrow \infty. \quad (\text{A.37})$$

In the limit of small drift velocities u , the function F_{BGK} is [59]

$$F_{\text{BGK}}(\theta) = \lambda_{D,Tn}^2 \left[-\sqrt{\frac{8}{\pi}} \frac{u}{v_{Tn}} \cos \theta + \left(2 - \frac{\pi}{2}\right) \frac{u^2}{v_{Tn}^2} (1 - 3 \cos^2 \theta) \right] + o(u^2), \quad u \rightarrow 0, \quad (\text{A.38})$$

where $\lambda_{D,Tn} = \sqrt{T_n / (4\pi n_0 e^2)}$. Eqs. (A.37) and (A.38) demonstrate that attraction forces between like-charged grains aligned perpendicular to the drift are impossible in the limit considered. This is in contrast to the case of shifted Maxwellian distribution [see Eqs. (A.25) and (A.28)]. The reason for the difference is related to the fact that the distribution (A.32) is different from a shifted Maxwellian distribution (A.26).

A.2 Discussion of model assumptions

As discussed above, there have been various models of grain screening with different assumptions. The present Section addresses the applicability of the assumptions of the models.

A.2.1 Ion-neutral collisions

The exact form of the collision operator is determined by the assumptions about microscopic description of the ion-neutral collisions. Therefore, to construct the correct ion-neutral collision operator, one should understand the physics of the ion-neutral collisions. The present Subsection addresses this issue.

There are three important processes contributing to the ion-neutral collisions [60]:

- *Polarization scattering.* The physics of the polarization scattering is related to the electrostatic interaction between an ion and the dipole moment induced on a neutral by the electric field of the ion. The corresponding transport cross-section is [60]

$$\sigma_p = 2\pi \sqrt{\frac{\alpha e^2}{\epsilon}}, \quad (\text{A.39})$$

where ϵ is the incident kinetic energy, α is the polarizability of the neutral. For argon, the polarizability is $\alpha \approx 11a_0^3$ where $a_0 = 0.529 \times 10^{-8}$ cm is the Bohr radius [60]. Because of the dependence $\sigma_p \propto 1/\sqrt{\epsilon}$, the polarization scattering dominates over other processes at small kinetic energies (e.g., for energies corresponding to the room temperature).

- *Charge exchange.* A charge exchange is not a true collision. Rather, it is a quantum-mechanical process of resonance tunneling of a single electron from a neutral to an ion. The result of this process is a new ion moving with the incident (i.e., before the “collision”) neutral velocity and a new neutral moving with the incident ion velocity. For argon and incident kinetic energies of $10^{-1} - 10$ eV, the charge exchange cross section is $\sim 5 \times 10^{-15}$ cm² and is almost velocity-independent [61]. (The theoretical approach yields a weak logarithmic dependence [60]). The corresponding transport cross-section is two times larger [60] and, therefore, is $\sim 10^{-14}$ cm². The comparison of the latter value with the cross-section (A.39) gives that the charge exchange dominates over polarization scattering when incident kinetic energies ϵ are larger than ~ 0.1 eV.
- *Gas-kinetic collisions.* The physics of the gas-kinetic collisions is the same as that of the neutral-neutral collisions (i.e., it is related to the short-range repulsion forces). The gas kinetic collisions can be well modeled by a hard sphere interaction. The

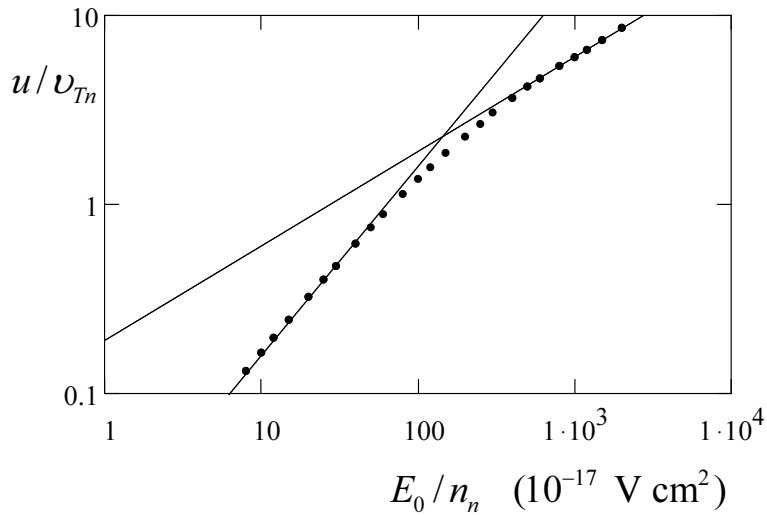


Figure A.2: Measured dependence of the ion drift velocity on the applied electric field. Vertical axis is the ratio of the drift velocity u to the thermal velocity of neutrals v_{Tn} . Horizontal axis is the ratio of the applied electric field E_0 to the neutral density n_n . The shown experimental data are taken from Ref. [62]. The measurements were performed in argon at $T_n = 300$ K. The straight lines illustrate that $u/v_{Tn} \propto E_0/n_n$ and $u/v_{Tn} \propto \sqrt{E_0/n_n}$ for small and large u/v_{Tn} , respectively.

gas-kinetic cross-section (almost) does not depend on the velocity, similar to charge-exchange collisions. For argon, the gas-kinetic cross-section is $\approx 4 \cdot 10^{-15}$ cm² [60]. (In the framework of the hard sphere model, the transport cross section is exactly equal to the collision cross section). Therefore, for argon, the gas-kinetic collisions are always somewhat less frequent than the charge-exchange collisions (see also Fig. 2.13 of Ref. [60]).

One should keep in mind that collisions of “mixed” types may occur. That is, an ion and a neutral interacting with each other due to polarization may exhibit a gas kinetic collision accompanied by the charge transfer.

From what is stated above it follows that the BGK collision operator is generally not applicable. This is particularly evident when one analyzes the dependence of the ion drift velocity u on the electric field E_0 . As stated above, the BGK collision operator implies a linear dependence ($u \propto E_0$). At the same time, measurements [62, 46] performed at the room temperature demonstrate that $u \propto \sqrt{E_0}$ at large drift velocities (see Fig.

A.2). Nevertheless, the BGK collision operator is believed to provide (qualitatively) correct results for the grain screening at small drift velocities [63].

A.2.2 Ion velocity distributions

This Subsection discusses measurements of ion velocity distributions in electric fields under conditions when the drift velocity exceeds the thermal velocity of neutrals.

Zeuner and Meichsner [64] performed measurements of the ion velocity distributions by sampling ions through an aperture in the grounded electrode of a rf discharge. They demonstrated that the shape of the ion velocity distribution is different in two limiting cases.

- The first limiting case occurs when the gas pressure is small enough and/or the rf power is large enough so that the ion motion near the electrode is *inertia-limited* (ballistic). In this limiting case, in the measured velocity distribution the mean velocity of ions was much larger than the dispersion of velocities. Therefore, the frequently used assumption that the (unperturbed by the grain) ion velocity distribution is a shifted delta-function (or shifted Maxwellian) is reasonable in this case.
- The second limiting case occurs when the gas pressure is large enough and/or the rf power is small enough so that the ion motion near the electrode is *mobility-limited*. In this limiting case, the shape of the measured velocity distribution was quite different from the shape of a shifted Maxwellian distribution. In particular, the velocity corresponding to the maximum of the velocity distribution function was much less than the mean velocity. Note that the distribution (A.32) has the same property for $u \gg v_{Tn}$ (see Fig. A.1).

Similar observations were made by Olthoff *et al.* [65].

Rao *et al.* [66] performed precise measurements of the ion velocity distributions in the case of mobility-limited drift. They found the longitudinal velocity distribution to be well described by

$$\int_0^{\infty} 2\pi v_{\perp} f_0(\mathbf{v}) dv_{\perp} = \text{const} \times \exp\left(-\frac{\sigma n_n m v_{\parallel}^2}{2eE_0}\right), \quad v_{\parallel} > 0, \quad (\text{A.40})$$

whereas almost no ions were present for $v_{\parallel} < 0$. Here σ is a constant which was interpreted by Rao *et al.* to be the charge exchange cross section, n_n is the neutral density. Eq.

(A.40) shows the inapplicability of the distribution (A.32). Indeed, in the limit $u \gg v_{Tn}$ (i.e., $v_{Tn} \rightarrow 0$ at constant u), the distribution (A.32) integrated over velocity components perpendicular to the direction of the electric field is

$$\int_0^{\infty} 2\pi v_{\perp} f_0(\mathbf{v}) dv_{\perp} = \frac{n_0}{u} \exp\left(-\frac{v_{\parallel}}{u}\right), \quad v_{\parallel} > 0, \quad (\text{A.41})$$

whereas $f_0 = 0$ for $v_{\parallel} < 0$. The distribution (A.41) is different from the measured distribution (A.40). The reason for the difference is that the BGK collision operator implies a velocity-independent collision frequency.

A.2.3 Electron velocity distributions

By performing probe measurements, Godyak and Piejak [67] demonstrated that the velocity distribution of electrons can be not Maxwellian but rather bi-Maxwellian, even in the bulk region.

Surendra and Graves [6] performed particle-in-cell-simulations of a rf discharge. They found that, in the sheath region, the electron density can significantly vary during the rf period. They also found that the mean kinetic energy of electrons significantly increases as either of the electrodes approached.

Recently, Gans *et al.* [24] performed spectroscopic measurements of phase-resolved electron kinetic energy distributions in the sheath region. The fit by a shifted Maxwellian distribution to the experimental data obtained 1–4 mm in front of the powered electrode during the field-reversal phase yielded the temperature of a few eV and drift kinetic energy (i.e., the shift) of 10–20 eV. Similar results were obtained in simulations by Vender and Boswell [23]. They obtained that the direction of the shift (towards or outwards the electrode) depends on the phase of the rf period.

To conclude, the behavior of electrons in the sheath region of a rf discharge may be rather complicated, since electrons respond to the rf electric field. This questions the applicability of the assumption of the Boltzmann electron response [Eq. (A.4)].

A.3 Summary: Which model when?

Three limiting regimes of screening of a grain levitated in the plasma-wall transition layer are generally possible:

1. When the local electron Debye length is *less* than the effective length of grain screening due to ions (the simplest estimate for the latter is $[\varepsilon_i/(4\pi n_i e^2)]^{1/2}$ where ε_i is the local mean kinetic energy of ions and n_i is the local ion density), then the screening should be primarily due to electrons. In this case, the grain screening potential is of the Debye-Hückel form with the local electron Debye length. However, the Debye-Hückel potential may be violated because of the anisotropy and time variations of the velocity distribution of electrons, since electrons respond to the rf electric field.
2. When the local electron Debye length is *greater* than the effective length of grain screening due to ions, then the screening should be primarily due to ions. Here, two limiting regimes are possible:
 - (a) When the ion-neutral collisions are rare enough, the ion motion in the region of grain levitation is ballistic. In this case, the theories discussed in Subsection A.1.3 should be relevant.
 - (b) When the ion-neutral collisions are frequent enough so that the inhomogeneity length of the vertical electric field in the region of grain levitation is larger than the ion-neutral collision length, the (unperturbed by the grain) ion motion is mobility-limited. In this case, a theory similar to the BGK model is required, but (especially in the case of large ion drift velocity) with assumption of velocity-independent cross section, instead of the assumption of velocity-independent collision frequency. Such a theory is proposed in the first paper enclosed to this thesis.

Bibliography

- [1] V. E. Fortov, A. V. Ivlev, S. A. Khrapak, A. G. Khrapak, and G. E. Morfill, *Phys. Rep.* **421**, 1 (2005).
- [2] V. E. Fortov, A. G. Khrapak, S. A. Khrapak, V. I. Molotkov, and O. F. Petrov, *Phys. Usp.* **47**, 447 (2004).
- [3] A. Piel and A. Melzer, *Plasma Phys. Control. Fusion* **44**, R1 (2002).
- [4] S. V. Vladimirov and K. Ostrikov, *Phys. Rep.* **393**, 175 (2004).
- [5] P. J. Hargis et al., *Rev. Sci. Instrum.* **65**, 140 (1994).
- [6] M. Surendra and D. B. Graves, *IEEE Trans. Plasma Sci.* **19**, 144 (1991).
- [7] A. A. Samarian and B. W. James, *Plasma Phys. Control. Fusion* **47**, B629 (2005).
- [8] S. Zhdanov, S. Nunomura, D. Samsonov, and G. Morfill, *Phys. Rev. E* **68**, 035401 (2003).
- [9] G. E. Morfill, H. M. Thomas, U. Konopka, and M. Zuzic, *Phys. Plasmas* **6**, 1769 (1999).
- [10] H. Thomas et al., *Phys. Rev. Lett.* **73**, 652 (1994).
- [11] A. V. Ivlev, U. Konopka, G. Morfill, and G. Joyce, *Phys. Rev. E* **68**, 026405 (2003).
- [12] V. I. Molotkov et al., *High Temp.* **42**, 827 (2004).
- [13] G. E. Morfill et al., *Phys. Rev. Lett.* **83**, 1598 (1999).
- [14] V. N. Tsytovich, G. E. Morfill, and H. Thomas, *Plasma Phys. Rep.* **28**, 623 (2002).

-
- [15] V. N. Tsytovich, *Phys. Usp.* **40**, 53 (1997).
- [16] S. A. Khrapak et al., *Phys. Rev. Lett.* **96**, 015001 (2006).
- [17] U. Konopka, G. E. Morfill, and L. Ratke, *Phys. Rev. Lett.* **84**, 891 (2000).
- [18] U. Konopka, PhD thesis, Ruhr-Universität Bochum.
- [19] A. Melzer, M. Klindworth, and A. Piel, *Phys. Rev. Lett.* **87**, 115002 (2001).
- [20] T. E. Sheridan, M. R. Katschke, and K. D. Wells, *Rev. Sci. Instr.* **78**, 023502 (2007).
- [21] G. A. Hebner, M. E. Riley, and B. M. Marder, *Phys. Rev. E* **68**, 016403 (2003).
- [22] A. Melzer, V. A. Schweigert, and A. Piel, *Phys. Rev. Lett.* **83**, 3194 (1999).
- [23] D. Vender and R. W. Boswell, *J. Vac. Sci. Technol. A* **10**, 1331 (1992).
- [24] T. Gans, V. S. von der Gathen, and H. F. Döbele, *Europhys. Lett.* **66**, 232 (2004).
- [25] S. V. Vladimirov and O. Ishihara, *Phys. Plasmas* **3**, 444 (1996).
- [26] S. V. Vladimirov and M. Nambu, *Phys. Rev. E* **52**, R2172 (1995).
- [27] O. Ishihara and S. V. Vladimirov, *Phys. Plasmas* **4**, 69 (1997).
- [28] D. Winske, W. Daughton, D. S. Lemons, and M. S. Murillo, *Phys. Plasmas* **7**, 2320 (2000).
- [29] G. Lapenta, *Phys. Rev. E* **62**, 1175 (2000).
- [30] M. Lampe, G. Joyce, G. Ganguli, and V. Gavrishchaka, *Phys. Plasmas* **7**, 3851 (2000).
- [31] S. Benkadda, V. N. Tsytovich, and S. V. Vladimirov, *Phys. Rev. E* **60**, 4708 (1999).
- [32] A. V. Ivlev, S. K. Zhdanov, S. A. Khrapak, and G. E. Morfill, *Phys. Rev. E* **71**, 016405 (2005).
- [33] V. A. Schweigert, *Plasma Phys. Rep.* **27**, 997 (2001).
- [34] I. V. Schweigert, V. A. Schweigert, and F. M. Peeters, *Phys. Plasmas* **12**, 113501 (2005).

-
- [35] T. Nitter, *Plasma Sources Sci. Technol.* **5**, 93 (1996).
- [36] S. A. Khrapak et al., *Phys. Plasmas* **10**, 4579 (2003).
- [37] X. Wang, A. Bhattacharjee, and S. Hu, *Phys. Rev. Lett.* **86**, 2569 (2001).
- [38] H. Ohta and S. Hamaguchi, *Phys. Rev. Lett.* **84**, 6026 (2000).
- [39] S. Hamaguchi, R. T. Farouki, and D. H. E. Dubin, *Phys. Rev. E* **56**, 4671 (1997).
- [40] G. Salin and J.-M. Caillol, *Phys. Plasmas* **10**, 1220 (2003).
- [41] S. V. Vladimirov, S. A. Maiorov, and N. F. Cramer, *Phys. Rev. E* **67**, 016407 (2003).
- [42] S. K. Zhdanov, A. V. Ivlev, and G. E. Morfill, *Phys. Plasmas* **12**, 072312 (2005).
- [43] V. V. Yaroshenko, A. V. Ivlev, and G. E. Morfill, *Phys. Rev. E* **71**, 046405 (2005).
- [44] M. E. Tuckerman, C. J. Mundy, and G. J. Martyna, *Europhys. Lett.* **45**, 149 (1999).
- [45] M. E. Tuckerman, Y. Liu, G. Ciccotti, and G. J. Martyna, *J. Chem. Phys.* **115**, 1678 (2001).
- [46] J. A. Hornbeck, *Phys. Rev.* **84**, 615 (1951).
- [47] U. Konopka, private communications (2007).
- [48] G. E. Morfill et al., Tunable interparticle interaction in complex plasmas, in preparation.
- [49] A. V. Ivlev et al., String fluid in electrorheological complex plasmas, in preparation.
- [50] E. M. Lifshitz and L. P. Pitaevskii, *Physical Kinetics*, Pergamon, Oxford, 1981.
- [51] F. Melandso and J. Goree, *Phys. Rev. E* **52**, 5312 (1995).
- [52] L.-J. Hou, Y.-N. Wang, and Z. L. Miskovic, *Phys. Rev. E* **68**, 016410 (2003).
- [53] J. Denavit, *Phys. Fluids* **8**, 471 (1965).
- [54] H. Ferfler and T. Simonen, *Phys. Fluids* **12**, 269 (1969).
- [55] D. Montgomery, G. Joyce, and R. Sugihara, *Plasma Phys.* **10**, 681 (1968).

- [56] G. Cooper, *Phys. Fluids* **12**, 2707 (1969).
- [57] T. Peter, *J. Plasma Phys.* **44**, 269 (1990).
- [58] H. Sugawara, H. Tagashira, and Y. Sakai, *J. Phys. D* **29**, 1168 (1996).
- [59] R. Kompaneets et al., Charge screening in anisotropic plasmas, unpublished.
- [60] Y. P. Raizer, *Fizika gazovogo razryada (Gas discharge physics)*, Nauka, Moscow, 1987.
- [61] A. V. Phelps, *J. Appl. Phys.* **76**, 747 (1994).
- [62] H. W. Ellis, R. Y. Pai, E. W. McDaniel, E. A. Mason, and L. A. Viehland, *Atom. Data Nucl. Data Tabl.* **17**, 178 (1976).
- [63] A. V. Ivlev, private communications (2007).
- [64] M. Zeuner and J. Meichsner, *Vacuum* **46**, 151 (1995).
- [65] J. K. Olthoff, R. J. V. Brunt, S. B. Radovanov, J. A. Rees, and R. Surowiec, *J. Appl. Phys.* **75**, 115 (1994).
- [66] M. V. V. S. Rao, R. J. V. Brunt, and J. K. Olthoff, *Phys. Rev. E* **54**, 5641 (1996).
- [67] V. A. Godyak and R. B. Piejak, *Appl. Phys. Lett.* **63**, 3137 (1993).

Acknowledgments

The author is very grateful to

- Prof. Dr. Dr. h. c. Gregor Morfill for his supervision and the opportunity to perform the research at the Max-Planck-Institute for Extraterrestrial Physics,
- Dr. Alexei Ivlev for his guidance, help, and teaching,
- Prof. Dr. Vadim Tsytovich for his help,
- Dr. Uwe Konopka, Prof. Dr. Sergey Vladimirov, Dr. Sergey Khrapak, Dr. Vladimir Nosenko, Dr. Boris Klumov, Dr. Svetlana Ratynskaia, and Dr. Mikhail Pustynnik for helpful discussions.

The author thankfully acknowledges the financial support from

- German Academic Exchange Service [Deutscher Akademischer Austauschdienst (DAAD), Scholarship A/04/00273, October 2004 – July 2005, October 2005 – July 2006, October 2006 – July 2007),
- Max-Planck Institute for Extraterrestrial Physics [Max-Planck-Institut für extraterrestrische Physik, Garching (Germany), Promotionsstipendium, August 2005 – September 2005, August 2006 – September 2006).

Curriculum Vitae

Roman Kompaneets

Date and place of birth June 03, 1980, Moscow, U.S.S.R. (now Russia)

School education

1987 – 1994

Moscow School 948

1994 – 1997

Moscow Physics Mathematics Lyceum 1523

1997 School leaving certificate with silver medal
(average note 4.94)

University education

1997 – 2003

Moscow Institute of Physics and Technology
(State University), undergraduate student

2001 Bachelor's degree in applied mathematics and physics,
honors diploma (average note 5.00 — best possible),
degree work “The two-dimensional structure of thin
accretion disks”, supervisor Prof. Dr. Vasily Beskin,
chair of problems of physics and astrophysics

2003 Master's degree in applied mathematics and physics,
honors diploma (average note 5.00 — best possible),
degree work “Weakly nonlinear solitons in complex
plasmas and collective interaction of dust particles”,
supervisor Prof. Dr. Vadim Tsytovich, chair of
problems of physics and astrophysics

2003 – 2006

Moscow Institute of Physics and Technology
(State University), PhD student, theoretical physics,
supervisor Prof. Dr. Vadim Tsytovich, chair of problems
of physics and astrophysics

2004 – 2005

Ludwig Maximilians University of Munich, program student,
physics

2005 – present

Ludwig Maximilians University of Munich, PhD student,
physics, supervisor Prof. Dr. Dr. h. c. Gregor Morfill

Publication list

Publications in refereed journals:

1. R. Kompaneets, U. Konopka, A. V. Ivlev, V. Tsytovich, and G. Morfill, Potential around a charged dust particle in a collisional sheath, *Phys. Plasmas* **14**, 052108 (2007).
2. A. V. Ivlev, V. Steinberg, R. Kompaneets, H. Höfner, I. Sidorenko, and G. E. Morfill, Non-Newtonian viscosity of complex-plasma fluids, *Phys. Rev. Lett.* **98**, 145003 (2007).
3. S. Ratynskaia, R. Kompaneets, A. V. Ivlev, C. Knappek, and G. E. Morfill, Transport in strongly coupled two-dimensional complex plasmas: Role of the interaction potential, *Phys. Plasmas* **14**, 010702 (2007).
4. R. Kompaneets, S. V. Vladimirov, A. V. Ivlev, V. Tsytovich, and G. Morfill, Dust clusters with non-Hamiltonian particle dynamics, *Phys. Plasmas* **13**, 072104 (2006).
5. V. Tsytovich, R. Kompaneets, U. de Angelis, and C. Castaldo, Collective grain interactions for constant ionization source, *Contrib. Plasma Phys.* **46**, 280 (2006).
6. V. N. Tsytovich and R. Kompaneets, Collective grain interactions II. Non-linear collective drag force, *Contrib. Plasma Phys.* **45**, 544 (2005).
7. R. Kompaneets, A. V. Ivlev, V. Tsytovich, and G. Morfill, Dust-lattice waves: Role of charge variations and anisotropy of dust-dust interaction, *Phys. Plasmas* **12**, 062107 (2005).
8. R. Kompaneetz and V. Tsytovich, Collective electrostatic interaction of particles in a complex plasma with ion flow, *Contrib. Plasma Phys.* **45**, 130 (2005).
9. R. Kompaneetz, V. Tsytovich, and G. Morfill, Weak dust ion-acoustic and dust-acoustic solitons with absorption of ions, ionization, and ion drag, *IEEE Trans. Plasma Sci.* **32**, 561 (2004).
10. V. S. Beskin, R. Yu. Kompaneetz, and A. D. Tchekhovskoy, The two-dimensional structure of thin accretion disks, *Astron. Lett.* **28**, 543 (2002).

Enclosed papers

The three papers this cumulative dissertation consists of are enclosed below.

Copyright notice

Reprinted with permission from

- R. Kompaneets, U. Konopka, A. V. Ivlev, V. Tsytovich, and G. Morfill, Potential around a charged dust particle in a collisional sheath, *Physics of Plasmas*, Volume 14, Issue 5, Article 052108, 2007.
- R. Kompaneets, A. V. Ivlev, V. Tsytovich, and G. Morfill, Dust-lattice waves: Role of charge variations and anisotropy of dust-dust interaction, *Physics of Plasmas*, Volume 12, Issue 6, Article 062107, 2005.
- R. Kompaneets, S. V. Vladimirov, A. V. Ivlev, V. Tsytovich, and G. Morfill, Dust clusters with non-Hamiltonian particle dynamics, *Physics of Plasmas*, Volume 13, Issue 7, Article 072104, 2006.

Copyright 2005, 2006, 2007, American Institute of Physics.

Potential around a charged dust particle in a collisional sheath

R. Kompaneets^{a)}

Max-Planck-Institut für Extraterrestrische Physik, 85748 Garching, Germany
Moscow Institute of Physics and Technology, 141700 Dolgoprudny, Russia

U. Konopka and A. V. Ivlev

Max-Planck-Institut für Extraterrestrische Physik, 85748 Garching, Germany

V. Tsytovich

General Physics Institute of the Russian Academy of Sciences, 117942 Moscow, Russia

G. Morfill

Max-Planck-Institut für Extraterrestrische Physik, 85748 Garching, Germany

(Received 15 February 2007; accepted 22 March 2007; published online 16 May 2007)

By employing a self-consistent kinetic approach, an analytical expression is derived for the potential of a test charge in a weakly ionized plasma with ion drift. The drift is assumed to be due to an external electric field, with the velocity being mobility-limited and much larger than the thermal velocity of neutrals. The derived expression is proven to be in excellent agreement with the measurements by Konopka *et al.* [Phys. Rev. Lett. **84**, 891 (2000)] performed in the sheath region of a rf discharge. © 2007 American Institute of Physics. [DOI: 10.1063/1.2730498]

I. INTRODUCTION

Many experiments in the field of complex (dusty) plasmas are performed in weakly ionized low-pressure radiofrequency (rf) discharges (gas pressure 1–10 Pa, gas temperature 300 K, frequency 13.56 MHz, and ionization fraction 10^{-6} – 10^{-7} ; see Refs. 1 and 2). Microparticles (grains of a few μm in diameter) embedded in a plasma acquire large negative charges ($\sim 10^4 e$) determined by the balance of collecting free ions and electrons. Under gravity conditions, charged microparticles levitate in the sheath region near the lower electrode, where the vertical electric field is sufficient to compensate for gravity. This electric field causes ions to drift toward the electrode and makes their velocity distribution highly anisotropic. The determination of the (electrostatic) interaction of grains in such conditions is one of the fundamental issues in the physics of complex plasmas.

The issue is complicated by the fact that the values of many relevant parameters in the region of grain levitation are not well known. In particular, one of the most important parameters is the ratio of the ion and electron local effective Debye lengths, $\sqrt{(\varepsilon_i/\varepsilon_e)(n_e/n_i)}$, where $\varepsilon_{i,e}$ and $n_{i,e}$ are the local mean kinetic energies and densities, respectively. This parameter is believed to determine the relative contribution of ions and electrons to grain screening.^{3,4} In the quasineutral bulk plasma, where ions are in equilibrium with neutrals and the electron temperature is usually of a few eV, we have $\varepsilon_i/\varepsilon_e \sim 10^{-2}$. Hence, grain screening in the bulk plasma is mostly due to ions. Mean kinetic energy of ions increases towards the electrode and can exceed the bulk electron temperature.⁵ On the other hand, the ratio n_e/n_i decreases.^{6,7} Moreover, the mean kinetic energy of electrons ε_e can dramatically increase because of their response to the time variations of the electric field,^{6–8} as the time variations of the

electric field can be particularly high in the sheath region.^{6–8} (Usually, the discharge frequency is less than the electron plasma frequency but greater than the ion plasma frequency, so that electrons respond to the time variations of the electric field and ions do not.⁷) The resulting dependence of the parameter $\sqrt{(\varepsilon_i/\varepsilon_e)(n_e/n_i)}$ on the distance from the electrode and, in particular, its value at the grain levitation height are not known.

Nevertheless, the screening is often attributed to electrons rather than to ions,^{1,2,4,9} with the resulting interaction potential being the Yukawa (Debye-Hückel) potential with the local electron Debye length (except for the wake region downstream).^{10,11} Apparently, the most frequently cited “evidence” for the Yukawa interaction is the experiment by Konopka *et al.*,^{12,13} who did not find deviations from the Yukawa interaction by analyzing trajectories of two interacting particles levitated at the same height from the electrode.

However, no *quantitative* comparison of the aforementioned experiment^{12,13} with other models has been performed to exclude other possibilities. Moreover, the screening length deduced in the experiment^{12,13} turned out to be about, or in some cases *smaller* than, the electron Debye length measured in the bulk;¹³ if the screening would be primarily due to electrons, the former should always be *larger* than the latter. Furthermore, the grain charge deduced in the experiment^{12,13} allows us to find the electric field, supporting the grains against gravity; this, in turn, allows us to obtain an upper (i.e., mobility-limited) estimate for the ion drift kinetic energy. The latter appears to be somewhat smaller than the mean kinetic energy of electrons measured in the bulk. This suggests that the screening could be primarily due to ions and not electrons.

If ions indeed play the primary role in grain screening, then an essential question is as follows: Is the ion drift in the region of particle levitation inertia- or mobility-limited? In the former case, the assumption that the ion velocity distri-

^{a)}Electronic mail: komp@mpe.mpg.de

bution is a shifted delta function (or shifted Maxwellian) is reasonable,⁵ which is usually employed in models for grain screening.^{10,11,14–18} However, in many experiments the ion drift in the region of grain levitation is rather mobility-limited. This coupled with the dominating role of the charge-exchange collisions¹⁹ can make the ion velocity distribution quite different from the shifted delta-function/Maxwellian form^{5,20–22} and change the ion response function dramatically,^{21,22} which should lead to a principally different grain screening. The model of Refs. 21 and 22 calculates the ion response function for the case of velocity-independent collision frequency, whereas no model has been suggested for the realistic case of a velocity-independent cross section.²³

II. OBJECTIVE

The objective of the present paper is to derive an expression for grain screening in the sheath region with mobility-limited ion drift, attributing screening to ions only, and to compare the derived expression with the experiment.^{12,13}

III. METHODS: MODEL AND EXPERIMENT

A. Model assumptions

Our model is based on the following assumptions:

- (i) Only the charge-exchange collisions are taken into account, i.e., gas-kinetic and polarization collisions are neglected.
- (ii) The ion-neutral cross section is velocity-independent.
- (iii) Without the grain, a mobility-limited ion drift in a homogeneous electric field is assumed (i.e., the balance between acceleration in the electric field and collisions with neutrals is assumed); note that the time-averaged electric field is considered, as ions are assumed not to respond to the time variations of the electric field.
- (iv) The ion drift velocity substantially exceeds the thermal velocity of neutrals (therefore, we consider the velocity distribution of neutrals to be the delta function).
- (v) Grain is considered to be a nonabsorbing point charge.
- (vi) The nonlinear screening region near the grain is negligibly small (therefore we employ the linear-response formalism).
- (vii) The electron response is negligible.

Note that *no assumption* is made about the ratio of the ion-neutral “mean” free path to the effective length of grain screening. Therefore, the ion drift perturbed by the grain is *not* assumed to be mobility-limited.

B. Model equations

We consider a point test charge Q immersed in a weakly ionized plasma and located in the origin of Cartesian coordinates. Far from the test charge, the electric field is E_0 and directed along the z axis.

For ions, we use the steady-state kinetic equation

$$\mathbf{v} \cdot \frac{\partial f}{\partial \mathbf{r}} + \frac{e\mathbf{E}}{m} \cdot \frac{\partial f}{\partial \mathbf{v}} = -v\ell^{-1}f + \delta(\mathbf{v}) \int v' \ell^{-1} f(\mathbf{r}, \mathbf{v}') d\mathbf{v}', \quad (1)$$

where $f=f(\mathbf{r}, \mathbf{v})$ is the ion distribution function, $e>0$ is the elementary charge, m is the ion/neutral mass, $\mathbf{E}=\mathbf{E}(\mathbf{r})$ is the electric field, $\ell=(\sigma n_n)^{-1}$ is the ion-neutral “mean” free path, σ is the ion-neutral cross section assumed to be velocity-independent, n_n is the neutral density, and $\delta(\mathbf{v})$ is the delta function.

Kinetic equation (1) is coupled with the Poisson equation,

$$\frac{\partial \mathbf{E}}{\partial \mathbf{r}} = 4\pi(n - n_e)e + 4\pi Q\delta(\mathbf{r}), \quad (2)$$

where $n=n(\mathbf{r})=\int f(\mathbf{r}, \mathbf{v})d\mathbf{v}$ is the ion density, n_e is the electron density, which is assumed to be homogeneous and not influenced by the test charge, and $\delta(\mathbf{r})$ is the delta function.

Far from the test charge (i.e., for $\mathbf{r} \rightarrow \infty$), we assume a spatially homogeneous ion distribution $f_0=f_0(\mathbf{v})$ and a spatially homogeneous electric field \mathbf{E}_0 directed along the z axis. The distribution f_0 is derived from Eq. (1) to be

$$f_0 = n_0 \sqrt{\frac{2m}{\pi T_{\parallel}}} \exp\left(-\frac{mv_z^2}{2T_{\parallel}}\right) \delta(v_x) \delta(v_y), \quad v_z > 0, \quad (3)$$

whereas for $v_z < 0$ we have $f_0=0$. Here $T_{\parallel}=eE_0\ell$ is the field-induced “temperature” characterizing such *half-Maxwellian* distribution, and $n_0=\int f_0(\mathbf{v})d\mathbf{v}$ is the ion density far from the test charge. (Note that similar distributions were directly measured in experiments^{5,24} and obtained in simulations.²⁰) Also, as follows from Eq. (2), there should be $n_0=n_e$.

We are interested in the test charge potential $\phi=\phi(\mathbf{r})$. Mathematically, it is defined by

$$-\frac{\partial \phi}{\partial \mathbf{r}} = \mathbf{E} - \mathbf{E}_0, \quad \phi|_{\mathbf{r} \rightarrow \infty} = 0. \quad (4)$$

In the present work, we consider the linearized test charge potential only. The linearized test charge potential is defined as the first term in expansion of the test charge potential in a series of Q . Further, the notation ϕ will be understood as the linearized test charge potential.

The described model mathematically defines the linearized test charge potential ϕ as a function of spatial coordinates and the following parameters: (i) charge Q , (ii) “field-induced” ion Debye length $\lambda=[eE_0\ell/(4\pi n_0 e^2)]^{1/2}$, and (iii) ion-neutral “mean” free path ℓ ; no other parameters are required.

C. Experimental data

Although measurements^{12,13} were performed for different gases, gas pressures, rf peak-to-peak voltages, and grain sizes (see Ref. 13), we only consider the measurements performed in argon at 2.7 Pa, rf peak-to-peak voltage 145 V, particle diameter 8.9 μm , and particle material density 1510 kg/m^3 . (Analysis of other measurements gives similar results.) The gas temperature was $T_n=293$ K and the discharge frequency was 13.56 MHz.

TABLE I. Experimentally measured interaction energy between two particles (levitated at the same height from the lower electrode) as a function of distance between them. The table shows *not* the interaction energy relative to infinite separation: To get the latter, a certain unknown constant (offset) should be added to the given values of the energy.

Distance (mm)	Energy (eV)
0.5777	157.6±5.6
0.6254	129.9±5.1
0.6709	104.5±4.7
0.7261	83.8±4.3
0.7865	71.6±4.1
0.8471	54.8±5.3
0.8850	47.6±5.4
0.9357	38.5±5.1
0.9882	31.7±4.6
1.0310	28.0±5.6
1.0905	22.2±5.5
1.1280	19.3±5.6
1.1788	16.1±5.3
1.2436	11.6±4.9
1.2930	9.3±5.2
1.3312	7.0±4.8
1.3966	8.4±4.4
1.4435	9.8±3.5
1.4864	5.2±4.4
1.5429	5.3±4.3
1.5932	4.1±4.1
1.6357	3.2±3.2
1.6911	3.5±3.5

The interaction energy between two particles (levitated at the same height from the lower electrode) was measured as a function of distance between them (see Table I). Note that the interaction energy was measured *not* relative to infinite separation (see caption to Table I).

D. Fitting procedure

To fit the experimental data by our model, we first determine the ion-neutral “mean” free path $\ell = (n_n \sigma)^{-1}$. We determine σ as follows: Eq. (3) gives the ion drift velocity $|\int \mathbf{v} f_0(\mathbf{v}) d\mathbf{v}|/n_0$ in the form $\sqrt{2eI/(\pi m \sigma)} \times \sqrt{E_0/n_n}$, and we require that the proportionality coefficient between the ion drift velocity and $\sqrt{E_0/n_n}$ should be the same as that measured experimentally for argon in Ref. 23. This gives $\sigma \approx 6.5 \times 10^{-15} \text{ cm}^2$ and, hence, the ion-neutral “mean” free path $\ell \approx 2.3 \text{ mm}$.

Having the “mean” free path defined, the linearized potential ϕ contains two unknown parameters: the particle charge Q and “field-induced” ion Debye length λ . Therefore, the fit to the experimental data has three degrees of freedom: Q , λ , and the offset ΔW (to be added to the measured interaction energies given in Table I). We find the best fit by minimizing the normalized squared deviation,

$$\chi^2 = \frac{1}{N - \nu} \sum_{i=1}^N \frac{1}{\sigma_i^2} [W_i + \Delta W - W_{\text{th}}(r_i, Q, \lambda)]^2, \quad (5)$$

where W_i is the measured interaction energy at distance r_i , σ_i is the error for W_i [Table I provides the data in the format $(r_i, W_i \pm \sigma_i)$], $W_{\text{th}}(r_i, Q, \lambda)$ is the interaction energy (relative to infinite separation) given by our theory ($W_{\text{th}} = Q\phi$, where ϕ is calculated for $|\mathbf{r}| = r_i$ and \mathbf{r} directed perpendicular to the z axis, i.e., perpendicular to the ion drift), $\nu = 3$ is the number of the degrees of freedom, and $N = 23$ is the number of experimental points.

By employing an analogous procedure, we also fit the experimental data by the Yukawa interaction potential, $W_Y(r_i, Q_Y, \lambda_Y) = (Q_Y^2/r_i) \exp(-r_i/\lambda_Y)$. The latter fit has three degrees of freedom as well: Q_Y , λ_Y , and the offset ΔW_Y to be added to the measured interaction energies.

IV. RESULTS

A. Theoretical expression

Our model gives the following analytical expression for the linearized test charge potential:

$$\phi(r_{\perp}, z) = \frac{2Q}{\pi \ell} \text{Re} \int_0^{\infty} dt \frac{\exp[it(z/\ell)]}{1 + (\ell/\lambda)^2 Y(t)} \times K_0 \left(\frac{r_{\perp}}{\ell} \sqrt{t^2 + (\ell/\lambda)^2 X(t)} \right). \quad (6)$$

Here r_{\perp} is the distance from the test charge in the plane perpendicular to the ion drift, and z is the distance along the drift. Further, K_0 is the zero-order modified Bessel function of the second kind.²⁵ Equation (6) is expressed in terms of two functions,

$$X(t) = 1 - \sqrt{1 + it},$$

$$Y(t) = \frac{2\sqrt{1 + it}}{it} \int_0^1 \frac{d\alpha}{[1 + it(1 - \alpha^2)]^2} - \frac{1}{it(1 + it)}. \quad (7)$$

In Eqs. (6) and (7), the square root with positive real part is to be taken. The mathematical derivation of Eq. (6) is given in the Appendix.

B. Comparison with experiment

Results of the comparison with experiment are shown in Fig. 1.

Both the fit by Eq. (6) and the fit by the Yukawa potential describe very well the experimental data. The normalized squared deviations appear to be approximately the same for both fits: $\chi^2 \approx 0.160$ and $\chi^2 \approx 0.143$ for Eq. (6) and the Yukawa potential, respectively. Such small values of χ^2 (relative to unity) can be explained by possible overestimation of errors.

However, outside the distance range where the measurements were performed, the fit by Eq. (6) and the Yukawa fit behave very differently (see Fig. 2). At large distances, Eq. (6) has power scaling ($\phi \propto r_{\perp}^{-3}$) and, hence, falls off much

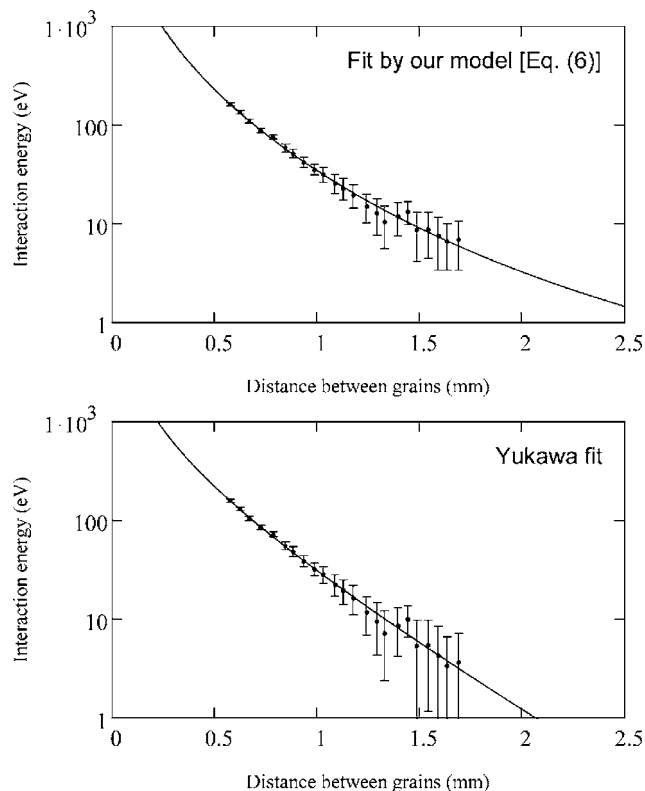


FIG. 1. Comparison of experiment with our theoretical expression [Eq. (6)] and Yukawa potential. Vertical axis is the interaction energy relative to infinite separation. The horizontal axis is the distance between the charged grains. Since the interaction energy was measured not relative to infinite separation, an unknown constant (offset) to be added to the measured energies is one of the fit parameters. The value of this offset is found to be not the same for both fits. The experimental data are shown with this offset added. Fit by Eq. (6) yields the grain charge $Q \approx -2.05 \times 10^4 e$, “field-induced” ion Debye length $\lambda \approx 0.62$ mm, and the offset $\Delta W \approx 3.4$ eV (to be added to the energies given in Table 1). Yukawa fit yields the grain charge $Q_Y \approx -1.66 \times 10^4 e$, screening length $\lambda_Y \approx 0.39$ mm, and the offset $\Delta W_Y \approx 0.16$ eV.

slower than the Yukawa potential. At small distances, the difference between the fits is significant as well (approximately a factor of 2).

V. DISCUSSION

A. Determination of local plasma parameters

By fitting the measured interaction energy with our theory, one can determine not only the particle charge Q but also some information about the local plasma parameters. Namely, based on the value of the “field-induced” Debye length λ , one can obtain the ratio of the electric field to the ion density (since $\lambda = [eE_0\ell / (4\pi n_0 e^2)]^{1/2}$). Further information about plasma parameters can be obtained by considering the balance of vertical forces acting on the grains. For example, if we neglect the ion drag force^{1,2} and simply use $-QE_0 = Mg$, where $M \approx 5.6 \times 10^{-10}$ g is the particle mass, we obtain the electric field $E_0 \approx 17$ V/cm, field-induced “temperature” of ions $T_{||} = eE_0\ell \approx 3.8$ eV, and the ion density $n_0 \approx 5.5 \times 10^8$ cm⁻³. The deduced ion density appears to be about the plasma density measured in the midplane of the discharge, 6×10^8 cm⁻³ $\pm 50\%$.¹³ The ion densities in the

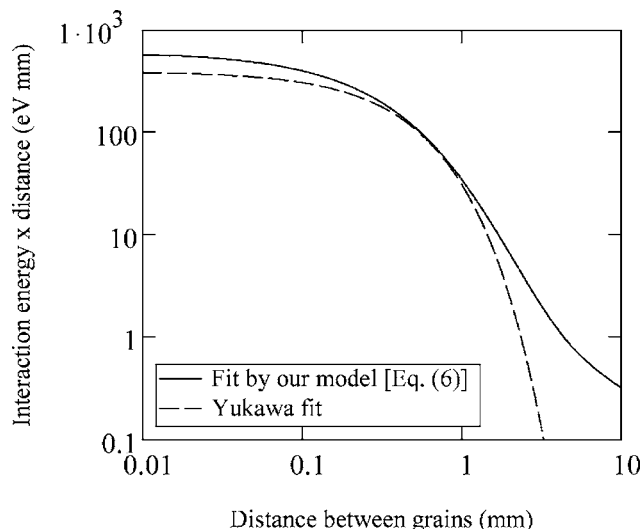


FIG. 2. Comparison of the fit by our theoretical expression [Eq. (6)] with the Yukawa fit. The vertical axis is the interaction energy relative to infinite separation, multiplied by the distance between grains. The horizontal axis is the distance between grains. (Unscreened Coulomb interaction would be a straight horizontal line.) Parameters of both fits are given in the caption to Fig. 1.

midplane and at the particle levitation height could indeed be close to each other or at least be of the same order, as the particles were levitated at the height ≈ 8.5 mm (relative to the lower electrode) and the electrode separation was only 30 mm.

The question about the accuracy of the deduced values of Q and λ is essential. To estimate the accuracy, we find numerically the region [in $(Q, \lambda, \Delta W)$ space] where the χ^2 exceeds the aforementioned value 0.160 no more than by a factor of 2. Projections of this region to the Q and the λ axis determine the uncertainties of Q and λ , respectively. These uncertainties appear to be about $\pm 20\%$.

B. Check of the model assumptions

Let us now consider all the assumptions listed in Sec. III A. Assumptions (i) and (ii) are justified by available experimental data.^{19,23} The validity of all other assumptions is the question of particular experimental conditions. In the following, we check the model assumptions for the considered experimental conditions.^{12,13} Concerning assumption (iii), the inhomogeneity length of the electric field, $L_E = E/E'$, can be found by $L_E = g/\omega_v^2$, where $\omega_v/(2\pi) \approx 15$ Hz is the measured resonance frequency of vertical oscillations of a single particle¹³ and g is the acceleration of gravity. (Here, charge variations^{1,2} are neglected.) This gives $L_E \approx 1$ mm, which is somewhat greater than the observed screening scale, ~ 0.5 mm, but somewhat smaller than the ion-neutral “mean” free path, $\ell \approx 2.3$ mm. The latter fact suggests that the conditions of this particular experiment^{12,13} are at the edge of applicability of the mobility-limited drift assumption. Further, assumption (iv) is justified by the fact that the ratio of the ion drift velocity $\sqrt{2eE_0\ell / (\pi m)}$ to the thermal velocity of neutrals $\sqrt{T_n/m}$ is ≈ 9.8 , based on the parameter values deduced from the fit. Assumptions (v) and (vi) are

justified by the fact that both the absorption impact parameter $\min(a, \sqrt{|Q|ea/T_{\parallel}})$ (see Refs. 1 and 2) and the Coulomb radius $|Q|e/T_{\parallel}$ are of the same order as the particle radius a , which is two orders of magnitude smaller than the observed screening scale, ~ 0.5 mm. Concerning assumption (vii), the electron temperature in the midplane of the discharge was measured to be 2.2 eV,^{12,13} which corresponds to the mean kinetic energy of $3/2 \times 2.2$ eV = 3.3 eV. As mentioned in the Introduction, the mean kinetic energy of electrons in the region of particle levitation can be even larger. At the same time, our fit yields the mean kinetic energy of ions (in the region of particle levitation) to be $T_{\parallel}/2 \approx 1.9$ eV. Also, the Poisson equation $E/L_E = 4\pi(n_i - n_e)e$ coupled with the found values of L_E , n_i ($\equiv n_0$), and E ($\equiv E_0$) gives $n_e/n_i \approx 0.85$. This supports the idea that the screening should be primarily due to ions and not electrons.

To conclude, the experiment^{12,13} corresponds to the edge of applicability of the mobility-limited drift assumption [i.e., assumption (iii)], whereas all other assumptions are more or less well justified. Thus, the experimental conditions^{12,13} are not best suitable to check our theory, yet they provide excellent agreement between experimental results and our model within experimental uncertainties.

C. Potential at large distances

One can easily derive from Eq. (6) the asymptotic behavior of the potential at large distances: We introduce the distance r from the test charge and angle θ with respect to the ion drift direction via $r_{\perp} = r \sin \theta$ and $z = r \cos \theta$. Using the integral representation $K_0(x) = \int_0^{\infty} \exp(-x \cosh \xi) d\xi$ valid for $\text{Re}(x) > 0$ (see Ref. 25) and employing new variable of integration $\tilde{t} = tr$, we expand the integrand in a series of $1/r$. Then we can perform integration over \tilde{t} and ξ analytically, which gives the asymptotic potential,

$$\phi = -\frac{Q\lambda^2 \cos \theta}{\ell r^2} \left(\frac{2}{1 + \cos^2 \theta} \right)^{3/2} + O\left(\frac{1}{r^3}\right). \quad (8)$$

Thus, at large distances the test charge produces a dipole-like field, with the dipole moment $|Q|\lambda^2/\ell$. For a negatively charged grain ($Q < 0$), this dipole moment is directed along the ion drift. Note the difference from the pure dipole field, due to the additional anisotropic factor $[2/(1 + \cos^2 \theta)]^{3/2}$.

It is well known that, in a collisionless plasma with arbitrary anisotropic ion velocity distribution, the potential of a non-absorbing point charge at large distances generally has the $1/r^3$ dependence.²⁶ Hence, the collisions included in our model are essential in the formation of the $1/r^2$ potential derived above. This conclusion is supported by the results of Stenflo *et al.*,²⁷ who considered a slowly moving non-absorbing point charge in an isotropic collisional plasma and obtained an inverse squared dependence as well.

Unscreened dipole potentials have already been used as model interaction potentials to investigate instabilities of dust-lattice waves^{28,29} and modes of finite clusters.³⁰ Our expression (8) not only justifies such unscreened dipole potentials but also provides the value of the corresponding dipole moment.

D. Applicability of Eq. (6)

The range of applicability of Eq. (6) is restricted by the assumptions listed in Sec. III A. In particular, the ion drift should be mobility-limited and, simultaneously, the drift velocity should be much greater than the thermal velocity of neutrals. Measurements⁵ clearly demonstrate that the two latter conditions can indeed be satisfied simultaneously with a good margin, allowing for a certain range of applicability of our model.

Although the present paper is rather devoted to charge screening in rf discharges, the obtained expression (6) can be applied to direct-current (dc) discharges as well. (Again, all the assumptions listed in Sec. III A should be checked for particular experimental conditions.) Measurements³¹ performed in a dc discharge demonstrate that all our assumptions can be satisfied even in weakly collisional discharges: In a weakly collisional discharge, there exists the so-called presheath where the ion drift is mobility-limited, with the drift kinetic energy being in between the neutral and electron temperatures.

Our model assumes a spatially homogeneous electric field. Realistically, inhomogeneity is always present in the sheath region. The question naturally arises as to what is the characteristic inhomogeneity scale of the electric field, $L_E = E/E'$, at which our result (6) is no longer valid. The inhomogeneity may also restrict the range of distances from the grain where the derived potential (6) is valid. We emphasize that L_E should be at least greater than ℓ , otherwise the drift is not mobility-limited, leading to a quite different ion velocity distribution, which, in turn, should lead to a principally different grain screening.

Strictly speaking, the model assumption of a homogeneous electric field implies a quasineutral plasma. Indeed, the inhomogeneity length of the electric field is connected with the degree of plasma quasineutrality via the Poisson equation, $E/L_E = 4\pi(n_i - n_e)e$, which gives $L_E = (\lambda^2/\ell)n_i/(n_i - n_e)$. (Here, we omit the subscript "0" used throughout the paper for E_0 and n_0 and assume $n_i > n_e$.) The aforementioned condition of the drift being mobility-limited, $L_E \gg \ell$, takes the form

$$\left(\frac{\lambda}{\ell}\right)^2 \frac{n_i}{n_i - n_e} \gg 1. \quad (9)$$

For a quasineutral plasma region ($n_i - n_e \ll n_i$), condition (9) is satisfied for a wide range of values of the ratio λ/ℓ . For an essentially nonquasineutral plasma region ($n_i - n_e \sim n_i$), e.g., deep in the sheath, condition (9) is only satisfied when $(\lambda/\ell)^2 \gg 1$. This should be taken into account by possible applications of our model.

E. Stability

The question arises as to whether and when the equilibrium given by Eq. (3) is stable (with respect to ion-acoustic waves). (If it is not, then our approach is not justified.) To answer the question, a derivation of the corresponding dispersion relation (within the model considered) is necessary. A derivation of the dispersion relation and subsequent stability analysis is much more difficult than the derivation of the

static potential (6). Note that the classical situation of the two-stream instability—one-component collisionless plasma with the velocity distribution being a sum of an otherwise stable distribution and an additional term representing a beam³²—is different from our case of collisional plasma with the half-Maxwellian velocity distribution (3) formed by the balance of acceleration in the electric field and collisions with neutrals. Another case of the two-stream instability—ions and electrons flowing with respect to each other³²—is irrelevant as well, because, in our model, electron response is neglected. Therefore, we see no physical reason for instability and so an investigation of the dispersion relation is beyond the scope of the present paper.

VI. CONCLUSION

Our model attributes grain screening to ions only. Assuming a mobility-limited ion drift with velocity much larger than the thermal velocity of neutrals, we derived an analytical expression for grain screening (6), which appeared to be generally not of the Yukawa (Debye-Hückel) form. Both our expression (6) and the Yukawa potential are in excellent agreement with the experiment.^{12,13} At the same time, our expression (6) strongly suggests that measurements performed in a broader range of distances should reveal significant deviations from the Yukawa potential. Hence, the experiment of Refs. 12 and 13 *cannot* be used as justification for either the Yukawa potential or the dominant role of electrons in grain screening, and more experiments are necessary to resolve the issue.

ACKNOWLEDGMENT

R.K. acknowledges the Deutscher Akademischer Austauschdienst (DAAD) for financial and organizational support (scholarship A/04/00273).

APPENDIX: DERIVATION OF EQ. (6)

The linearized potential of the point test charge Q has the form

$$\phi(r_{\perp}, z) = \frac{Q}{\pi} \int_{-\infty}^{\infty} dk_{\parallel} \int_0^{\infty} k_{\perp} dk_{\perp} \frac{J_0(k_{\perp} r_{\perp}) \exp(ik_{\parallel} z)}{(k_{\parallel}^2 + k_{\perp}^2) [1 + \chi_i(k_{\parallel}, k_{\perp})]}, \quad (\text{A1})$$

where J_0 is the zero-order Bessel function of the first kind, and $\chi_i(k_{\parallel}, k_{\perp})$ is the ion susceptibility for the wave vector whose components along and perpendicular to the ion drift are k_{\parallel} and k_{\perp} , respectively.

To derive the ion susceptibility χ_i from Eqs. (1) and (3), we consider a perturbation of the potential in the form $\phi_1 \exp(ik_{\perp} x + ik_{\parallel} z)$ with $\phi_1 = \text{const}$ and find the resulting linear perturbation of the distribution function, $f(\mathbf{r}, \mathbf{v}) - f_0(\mathbf{v}) = f_1(\mathbf{v}) \exp(ik_{\perp} x + ik_{\parallel} z)$. Substituting in Eq. (1), we obtain

$$(ik_{\perp} v_x + ik_{\parallel} v_z + \ell^{-1} v) f_1 + \frac{eE_0}{m} \frac{\partial f_1}{\partial v_z} = \frac{ie\phi_1}{m} \left(k_{\perp} \frac{\partial f_0}{\partial v_x} + k_{\parallel} \frac{\partial f_0}{\partial v_z} \right) + \ell^{-1} \delta(\mathbf{v}) \int f_1(\mathbf{v}') v' d\mathbf{v}'. \quad (\text{A2})$$

Then, substitution $f_1(\mathbf{v}) = A(\mathbf{v}) \exp[-m\Psi(\mathbf{v})/(2T_{\parallel})]$, with $\Psi(\mathbf{v}) = (k_{\parallel} v_z + 2k_{\perp} v_x) i \ell v_z + v v_z + \frac{1}{2}(v^2 - v_z^2) \ln(v + v_z)$, reduces Eq. (A2) to the equation

$$\frac{eE_0}{m} \frac{\partial A}{\partial v_z} = (\dots) \exp\left(\frac{m\Psi}{2T_{\parallel}}\right), \quad (\text{A3})$$

where (\dots) denotes the right-hand side of Eq. (A2). Direct integration of Eq. (A3) with the boundary condition $f_1|_{v \rightarrow \infty} = 0$ gives $A(\mathbf{v}) = 0$ for $v_z < 0$ and $A(\mathbf{v}) = \delta(v_x) \cdot \delta(v_z) \cdot [\alpha(v_z) + (m/T_{\parallel}) J + \dots] + \delta(v_y) \cdot \delta'(v_x) \cdot [\beta(v_z) + \gamma(v_z) \cdot v_x + \dots]$ for $v_z > 0$, respectively, where $\delta'(v_x)$ is the derivative of the delta-function, functions $\alpha(v_z)$ and $\gamma(v_z)$ can be expressed through elementary functions, function $\beta(v_z)$ can be expressed through the Fresnel sine and cosine integrals or, alternatively, through the error function of complex argument,²⁵ J is the integral standing in the right-hand side of Eq. (A2) [$J = \int f_1(\mathbf{v}') v' d\mathbf{v}'$], and the ellipsis denotes the higher-order terms with respect to v_x , which are not important for subsequent calculations because these terms are multiplied either by $\delta(v_x)$ or $\delta'(v_x)$. Now, substitution $f_1(\mathbf{v}) = A(\mathbf{v}) \exp[-m\Psi(\mathbf{v})/(2T_{\parallel})]$ [with $A(\mathbf{v})$ determined above] to $J = \int f_1(\mathbf{v}') v' d\mathbf{v}'$ gives the value of J [here, the formula $\int_{-\infty}^{\infty} \delta'(t) \cdot g(t) dt = -g'(0)$ is useful], which completes the solution of Eq. (A2). Using the definition $\chi_i = -[4\pi e / (k_{\parallel}^2 + k_{\perp}^2)] \int f_1(\mathbf{v}) d\mathbf{v} / \phi_1$, we finally derive the ion susceptibility,

$$\chi_i(k_{\parallel}, k_{\perp}) = \frac{1}{(k_{\parallel}^2 + k_{\perp}^2) \lambda^2} [X(k_{\parallel} \ell) + k_{\perp}^2 \ell^2 Y(k_{\parallel} \ell)], \quad (\text{A4})$$

where functions X and Y are defined by Eq. (7).

For the susceptibility (A4), the integration over k_{\perp} in Eq. (A1) can be performed analytically,²⁵ which gives the final expression (6).

¹V. E. Fortov, A. G. Khrapak, S. A. Khrapak, V. I. Molotkov, and O. F. Petrov, Phys. Usp. **47**, 447 (2004).

²V. E. Fortov, A. V. Ivlev, S. A. Khrapak, A. G. Khrapak, and G. E. Morfill, Phys. Rep. **421**, 1 (2005).

³A. Piel and A. Melzer, Plasma Phys. Controlled Fusion **44**, R1 (2002).

⁴S. A. Khrapak, A. V. Ivlev, G. E. Morfill, H. M. Thomas, S. K. Zhdanov, U. Konopka, M. H. Thoma, and R. A. Quinn, Phys. Plasmas **10**, 4579 (2003).

⁵M. Zeuner and J. Meichsner, Vacuum **46**, 151 (1995).

⁶M. Surendra and D. B. Graves, IEEE Trans. Plasma Sci. **19**, 144 (1991).

⁷D. Vender and R. W. Boswell, J. Vac. Sci. Technol. A **10**, 1331 (1992).

⁸T. Gans, V. Schulz-von der Gathen, and H. F. Döbele, Europhys. Lett. **66**, 232 (2004).

⁹T. Nitter, Plasma Sources Sci. Technol. **5**, 93 (1996).

¹⁰S. V. Vladimirov and M. Nambu, Phys. Rev. E **52**, R2172 (1995).

¹¹M. Lampe, G. Joyce, G. Ganguli, and V. Gavrishchaka, Phys. Plasmas **7**, 3851 (2000).

¹²U. Konopka, G. E. Morfill, and L. Ratke, Phys. Rev. Lett. **84**, 891 (2000).

¹³U. Konopka, Ph.D. thesis, Ruhr-Universität Bochum (2000).

¹⁴S. V. Vladimirov and O. Ishihara, Phys. Plasmas **3**, 444 (1996).

¹⁵O. Ishihara and S. V. Vladimirov, Phys. Plasmas **4**, 69 (1997).

¹⁶S. Benkadda, V. N. Tsytovich, and S. V. Vladimirov, Phys. Rev. E **60**, 4708 (1999).

¹⁷G. Lapenta, Phys. Rev. E **62**, 1175 (2000).

- ¹⁸D. Winske, W. Daughton, D. S. Lemons, and M. S. Murillo, *Phys. Plasmas* **7**, 2320 (2000).
- ¹⁹Yu. P. Raizer, *Gas Discharge Physics* (Springer-Verlag, Berlin, 1991), pp. 23–27.
- ²⁰S. A. Maiorov, *Plasma Phys. Rep.* **32**, 737 (2006).
- ²¹V. A. Schweigert, *Plasma Phys. Rep.* **27**, 997 (2001).
- ²²A. V. Ivlev, S. K. Zhdanov, S. A. Khrapak, and G. E. Morfill, *Phys. Rev. E* **71**, 016405 (2005).
- ²³J. A. Hornbeck, *Phys. Rev.* **84**, 615 (1951).
- ²⁴M. V. S. Rao, R. J. Van Brunt, and J. K. Olthoff, *Phys. Rev. E* **54**, 5641 (1996).
- ²⁵M. Abramowitz and I. A. Stegun, *Handbook of Mathematical Functions* (Dover, New York, 1972), formulas 9.6.24, 7.3.1, 7.3.2, 7.1.1, 11.4.44.
- ²⁶D. Montgomery, G. Joyce, and R. Sugihara, *Plasma Phys.* **10**, 681 (1968).
- ²⁷L. Stenflo, M. Y. Yu, and P. K. Shukla, *Phys. Fluids* **16**, 450 (1973).
- ²⁸R. Kompaneets, A. V. Ivlev, V. Tsytovich, and G. Morfill, *Phys. Plasmas* **12**, 062107 (2005).
- ²⁹V. V. Yaroshenko, H. M. Thomas, and G. E. Morfill, *New J. Phys.* **8**, 54 (2006).
- ³⁰R. Kompaneets, S. V. Vladimirov, A. V. Ivlev, V. Tsytovich, and G. Morfill, *Phys. Plasmas* **13**, 072104 (2006).
- ³¹L. Oksuz and N. Hershkowitz, *Plasma Sources Sci. Technol.* **14**, 201 (2005).
- ³²E. M. Lifshitz and L. P. Pitaevskii, *Physical Kinetics* (Pergamon, Oxford, 1981), pp. 265–268.

Dust-lattice waves: Role of charge variations and anisotropy of dust-dust interaction

R. Kompaneets,^{a)} A. V. Ivlev, V. Tsytovich,^{b)} and G. Morfill

Max-Planck-Institut für extraterrestrische Physik, Giessenbachstraße, 85748 Garching, Germany

(Received 17 February 2005; accepted 15 April 2005; published online 27 May 2005)

Dust-lattice waves are studied in the framework of the one-dimensional particle string model. The dust-dust interaction potential is assumed to have an arbitrary dependence on the vertical and horizontal coordinates, which allows to take into account the wake field effects. Both the vertical and horizontal charge variations are also included into the model. The model yields the coupling between the vertical and horizontal (longitudinal) modes: the coupling coefficient is the sum of six terms, each caused by a different physical mechanism. It is shown that the coupling can trigger the resonance oscillatory instability, which has been already observed in experiments. It is also shown that a nonoscillatory instability can appear at small wave numbers due to the coupling.

© 2005 American Institute of Physics. [DOI: 10.1063/1.1926650]

I. INTRODUCTION

Dust-lattice waves represent the oscillations of charged dust particles forming crystalline structures in a plasma. There has been a number of experiments on dust-lattice waves in two-dimensional (2D) dust crystals in rf discharge plasmas (see Refs. 1–5). In these experiments, a horizontal layer with crystalline structure was formed by negatively charged dust particles in the sheath at the lower electrode, where the electrostatic force compensated for gravity. In addition, there have been experiments on dust-lattice waves in 1D dust crystals [see Refs. 6 and 7 (rf and dc discharges, respectively)], where the horizontal confinement was used to form a particle chain.

In the laboratory experiments, the motion of individual dust particles can be easily observed, which makes the dust crystal a convenient model to study the fundamental physical processes such as propagation of waves in crystals and phase transitions. On the other hand, the system of charged dust particles in a plasma has some important features distinguishing it from many other physical systems. The first important feature is that the dust-dust interaction is anisotropic. The strong electric field supporting the particles against gravity causes ion streaming (usually, the ion flow speed is believed to be superthermal), which leads to the anisotropy of the electrostatic potential induced by a dust particle: an excess of the positive charge is accumulated “behind” the negatively charged dust particle due to ion focusing (see numerical simulations,^{8,9} theoretical studies,^{10–12} and experiments^{13,14}). It is important to note that the energy of particles interacting via such a potential is not conserved.⁵ The second important feature which results in the energy nonconservation is that the charge of dust particles is not constant: the charge is given by the balance of ion and elec-

tron fluxes on the particle surface (some models for dust charging are discussed in Refs. 15 and 16). Because of the inhomogeneity of the electric field of the sheath, the ion flow speed depends on the height, and, hence, the charge depends on the height as well. In addition, the ion and electron fluxes on the particle surface can be influenced by neighboring dust particles, which also leads to dust charge variations. All these features may induce new physical effects unusual for Coulomb or Debye–Hückel (Yukawa) systems often used as a model to study processes in dusty plasmas.

In Ref. 17, it is shown that the anisotropy of the dust-dust interaction leads to the coupling between the vertical and horizontal (longitudinal) modes, which can cause the resonance oscillatory instability near the intersection point of the modes. In Ref. 18, another mechanism of the coupling is found. The latter is related to the simultaneous presence of the anisotropy of the dust-dust interaction and dust charge variations due to vertical displacements. The contribution of the mechanism of Ref. 18 to the coupling coefficient is proportional to the product of the particle-wake dipole moment and the charge gradient in the vertical direction, while the contribution of the mechanism of Ref. 17 is quadratic with respect to the particle-wake dipole moment.

In the present paper, we use the 1D particle string model with interaction between neighboring particles (as in Refs. 17 and 18) and include into the model not only the anisotropy of the dust-dust interaction and dust charge variations due to vertical displacements but also dust charge variations due to change in the distance between particles. We show that the resulting coupling coefficient is the sum of six terms (including the two terms investigated before in Refs. 17 and 18, respectively). All the six terms correspond to different physical mechanisms of the coupling. Under typical laboratory conditions, two of four new terms can be comparable with the two previously investigated terms, while two remaining terms are relatively small. We also investigate the instabilities that can be caused by the coupling.

^{a)}Also at Moscow Institute of Physics and Technology, Institutsky pereulok 9, Dolgoprudny, 141700 Moskovskaya oblast, Russia. Electronic mail: komp@mpe.mpg.de

^{b)}Also at General Physics Institute of the Russian Academy of Sciences, Vavilova 38, 117942 Moscow, Russia.

II. THEORY

A. Model description

We consider an infinite string of dust particles with equilibrium charge $(-Q) < 0$ and equilibrium separation L . The equilibrium positions of dust particles are on the horizontal x axis. The z axis is directed vertically downward. We consider the motion of particles to be in the xz plane. The forces acting on the dust particles are the gravity force, the force of the electric field of the sheath, the dust-dust interaction, and the dust-neutral friction. In the xz plane, the electric field of the sheath is directed vertically downward and depends only on the coordinate z : $E = E(z)$. As for the dust-dust interaction, we consider only interaction with neighboring dust particles and apply the following model: each dust particle induces the electrostatic potential given by

$$\phi_n(x, z) = (-Q_n)f(|x - x_n|, z - z_n), \quad (1)$$

where $(-Q_n) < 0$ is the momentary value of the charge of the n th particle, x_n and z_n are the coordinates of the n th particle, $f(|x - x_n|, z - z_n)$ is some function of the specified arguments. We use a power series expansion of this function near $|x - x_n| = L, z - z_n = 0$:

$$\begin{aligned} f(|x - x_n|, z - z_n) = & f_0 + (|x - x_n| - L)f_x + (z - z_n)f_z + \frac{1}{2}(|x \\ & - x_n| - L)^2 f_{xx} + \frac{1}{2}(z - z_n)^2 f_{zz} + (|x - x_n| \\ & - L)(z - z_n)f_{xz} + \dots \end{aligned} \quad (2)$$

Concerning the dust charge variations, we apply the following model: the linear perturbations of the dust charge are given by

$$\delta Q_n = (\delta x_{n+1} - \delta x_{n-1})Q_x + (\delta z_n)Q_z, \quad (3)$$

where the symbol δ is used to designate the deviations from the equilibrium values: $\delta Q_n = Q_n - Q$ is the perturbation of the absolute value of the n th particle charge, $\delta x_n = x_n - nL$ is the perturbation of the x coordinate of the n th particle, $\delta z_n = z_n$.

Note that we do not include explicitly the ion drag force into the model. If we include the ion drag force $Q_n^2 f_{dr}(z)$ in the downward z direction, the linear perturbation of the total vertical force from the sheath will be given by $\delta[Q_n E(z) - Q_n^2 f_{dr}(z)] = Q[dE(z)/dz|_{z=0} - Q df_{dr}(z)/dz|_{z=0}]\delta z + [E(0) - 2Q f_{dr}(0)]\delta Q_n$. Therefore, including the ion drag force is equivalent to replacing the values of $E(0)$ and $dE(z)/dz|_{z=0}$ by the corresponding effective values.

Also note that, in our model, the force balance in the equilibrium reads as follows: the gravity is compensated by the electric field of the sheath and the vertical components of the forces from the two neighboring dust particles,

$$Mg = QE(0) + 2Q^2 f_z, \quad (4)$$

where M is the dust mass, g is the gravity constant.

B. Dimensionless parameters

To normalize distances, we use some arbitrary length λ . This length λ can be associated, for example, with the Debye radius or the length of the dust-dust interaction. The set of our dimensionless parameters is as follows:

$$\begin{aligned} e_0 = E(0)\frac{\lambda^2}{Q}, \quad e_1 = \left. \frac{dE(z)}{dz} \right|_{z=0} \frac{\lambda^3}{Q}, \\ \kappa = \frac{L}{\lambda}, \quad q_x = \frac{Q_x \lambda}{Q}, \quad q_z = \frac{Q_z \lambda}{Q}, \end{aligned} \quad (5)$$

$$\sigma_x = f_x \lambda^2, \quad \sigma_z = f_z \lambda^2,$$

$$\sigma_{xx} = f_{xx} \lambda^3, \quad \sigma_{zz} = f_{zz} \lambda^3, \quad \sigma_{xz} = f_{xz} \lambda^3.$$

C. Dispersion relation

The linearized equations take the following form:

$$\begin{aligned} \frac{d^2(\delta \tilde{x}_n)}{dt^2} = & -\gamma \frac{d(\delta \tilde{x}_n)}{dt} + (\delta \tilde{x}_{n+1} - 2\delta \tilde{x}_n + \delta \tilde{x}_{n-1})\sigma_{xx} \\ & - (\delta \tilde{z}_{n+1} - \delta \tilde{z}_{n-1})\sigma_{xz} + (\delta \tilde{q}_{n+1} - \delta \tilde{q}_{n-1})\sigma_x, \end{aligned} \quad (6)$$

$$\begin{aligned} \frac{d^2(\delta \tilde{z}_n)}{dt^2} = & -\gamma \frac{d(\delta \tilde{z}_n)}{dt} + (\delta \tilde{z}_{n+1} - 2\delta \tilde{z}_n + \delta \tilde{z}_{n-1})\sigma_{zz} - (\delta \tilde{x}_{n+1} \\ & - \delta \tilde{x}_{n-1})\sigma_{xz} - (\delta \tilde{q}_{n+1} + 2\delta \tilde{q}_n + \delta \tilde{q}_{n-1})\sigma_z \\ & - (\delta \tilde{q}_n)e_0 - (\delta \tilde{z}_n)e_1, \end{aligned} \quad (7)$$

$$\delta \tilde{q}_n = (\delta \tilde{x}_{n+1} - \delta \tilde{x}_{n-1})q_x + (\delta \tilde{z}_n)q_z, \quad (8)$$

where $\delta \tilde{q}_n = \delta Q_n / Q$, $\delta \tilde{x}_n = \delta x_n / \lambda$, $\delta \tilde{z}_n = \delta z_n / \lambda$, the time t is normalized by $\lambda^{3/2} \sqrt{M/Q}$, the dimensionless parameter $\gamma > 0$ describes the dust-neutral friction. Assuming the perturbations are proportional to $\exp(ikn\kappa - i\omega t)$, we obtain the dispersion relation

$$[\omega^2 + i\gamma\omega - \Omega_h^2(k)][\omega^2 + i\gamma\omega - \Omega_v^2(k)] = U_c(k), \quad (9)$$

where

$$\Omega_h^2(k) = 4[\sigma_{xx} \sin^2(k\kappa/2) + \sigma_x q_x \sin^2(k\kappa)], \quad (10)$$

$$\Omega_v^2(k) = e_1 + e_0 q_z + 4\sigma_{zz} \sin^2(k\kappa/2) + 4\sigma_z q_z \cos^2(k\kappa/2), \quad (11)$$

$$\begin{aligned} U_c(k) = & 4 \sin^2(k\kappa) [-\sigma_{xz}^2 + \sigma_{xz} \sigma_x q_x - \sigma_{xz} q_x e_0 + \sigma_x q_x q_z e_0 \\ & - 4\sigma_{xz} \sigma_z q_x \cos^2(k\kappa/2) + 4\sigma_x \sigma_z q_x q_z \cos^2(k\kappa/2)]. \end{aligned} \quad (12)$$

Discussion. We have two modes [characterized by $\Omega_h(k)$ and $\Omega_v(k)$] damped by the dust-neutral friction and coupled with each other through the coupling coefficient $U_c(k)$. The frequencies $\Omega_h(k)$ and $\Omega_v(k)$ are respectively the horizontal and vertical frequencies in the following sense. If we assume that the particles can move only along the x axis (i.e., we use $\delta z_n \equiv 0$ instead of considering forces in the vertical direction), $\Omega_h(k)$ will be the frequency of these horizontal oscillations. Analogously, if we assume that the particles can move only vertically (i.e., we use $\delta x_n \equiv 0$), the frequency of these vertical oscillations will be $\Omega_v(k)$.

For the reader's convenience, we mention what signs of the dimensionless parameters [Eq. (5)] are believed to be relevant to the laboratory experiments. The parameters e_0

and e_1 are naturally positive. It means that the electric field is directed downward and decreases with the height. The parameters $\sigma_x, \sigma_z, \sigma_{xx}, \sigma_{zz}, \sigma_{xz}$: (i) $\sigma_x < 0$ (the horizontal component of the interaction force is repulsive), (ii) $\sigma_{xx} > 0$ (the horizontal repulsion force decreases with the distance at horizontal displacements), (iii) $\sigma_z < 0$ (the vertical component of the dust-dust interaction force in the equilibrium is directed downward, because an excess of the positive charge is accumulated “below” the particle), (iv) $\sigma_{xz} > 0$ (the absolute value of this vertical component decreases with the interparticle distance at horizontal displacements), and (v) $\sigma_{zz} < 0$ (as for spherically symmetric repulsion). The parameters q_x and q_z can be of any sign.

Concerning the horizontal frequency $\Omega_h(k)$ [Eq. (10)], the first term in Eq. (10) is simply the dust-dust interaction without dust charge variations, while the second term is responsible for the horizontal dust charge variations.

As for the vertical frequency $\Omega_v(k)$ [Eq. (11)], the terms $e_1 + e_0 q_z$ describe the vertical oscillations of a single dust particle with dust charge variations. The term $4\sigma_{zz} \sin^2(k\kappa/2)$ is simply the dust-dust interaction without dust charge variations. The last term in Eq. (11) combines the effects of the vertical dust charge variations and the presence of the vertical dust-dust interaction forces in the equilibrium.

Now we discuss the coupling coefficient $U_c(k)$ [Eq. (12)]. From the physical point of view, the coupling means that the horizontal motion of particles influences the vertical motion, and, simultaneously, the vertical motion influences the horizontal motion—a feedback takes place. All the six terms of expression (12) represent different physical mechanisms of the feedback.

(i) The first coupling term $-\sigma_{xz}^2$ is considered in Ref. 17 and is related only to the anisotropy of the dust-dust interaction. The wake “behind” one particle induces the vertical force on another particle. When the horizontal distance between the particles changes, the vertical force changes as well. The influence of the vertical motion on the horizontal

motion is similar: when one particle is shifted vertically with respect to another particle, it implies a variation of the horizontal force from the wake of the latter particle.

(ii) The physics of the second coupling term $\sigma_{xz}\sigma_x q_z$ is considered in Ref. 18 and is as follows: while the influence of the horizontal motion on the vertical motion is related to the anisotropy of the dust-dust interaction (as in the first term), the influence of the vertical motion on the horizontal motion is related to the dust charge variations due to vertical displacements: when two particles are shifted in the vertical direction, the charges of the particles change, and, therefore, the horizontal repulsion forces between the two particles are changed as well.

(iii) The third coupling term $-\sigma_{xz} q_x e_0$ is similar to the preceding one. Now the horizontal dust charge variations cause the influence of the horizontal motion on the vertical motion (the vertical force of the electric field of the sheath is perturbed by the horizontal charge variations), while the influence of the vertical motion on the horizontal motion is due to the anisotropy of the dust-dust interaction (as in the first term).

(iv) The physics of the fourth coupling term $\sigma_x q_x q_z e_0$ combines the influence of the horizontal and vertical motion on each other due to charge variations only.

(v) The fifth and sixth terms are much less than the third and fourth terms, respectively, if $e_0 \gg |\sigma_z|$ (i.e., the force of the electric field of the sheath is much greater than the vertical component of the dust-dust interaction force in the equilibrium).

D. Stability analysis

In this section, we perform the stability analysis of the dispersion relation (9) with any arbitrary real functions $\Omega_h^2(k), \Omega_v^2(k), U_c(k)$ [e.g., $\Omega_h^2(k), \Omega_v^2(k)$ can be negative, and $U_c(k)$ can be large]. We use only $\gamma > 0$. All the four solutions of the dispersion relation (9) can be written in the following form:

$$\omega = -\frac{i\gamma}{2} \pm \sqrt{-\left(\frac{\gamma}{2}\right)^2 + \frac{1}{2}[\Omega_v^2(k) + \Omega_h^2(k) \pm \sqrt{[\Omega_v^2(k) - \Omega_h^2(k)]^2 + 4U_c(k)}}]} \quad (13)$$

The instability conditions for a given k are as follows.

(i) When $[\Omega_v^2(k) - \Omega_h^2(k)]^2 + 4U_c(k) < 0$, we have oscillatory instability if

$$|[\Omega_v^2(k) - \Omega_h^2(k)]^2 + 4U_c(k)| > 2\gamma^2[\Omega_v^2(k) + \Omega_h^2(k)], \quad (14)$$

otherwise the system is stable;

(ii) When $[\Omega_v^2(k) - \Omega_h^2(k)]^2 + 4U_c(k) > 0$, we have nonoscillatory instability if any of the following is satisfied:

$$\Omega_h^2(k) + \Omega_v^2(k) < 0, \quad (15)$$

$$\Omega_h^2(k)\Omega_v^2(k) < U_c(k), \quad (16)$$

otherwise the system is stable.

Discussion. We suppose that, for a given k , Ω_h^2 and Ω_v^2 are positive. In the case of no coupling and no friction, the eigenfrequencies of the system coincide with the horizontal Ω_h and vertical Ω_v frequencies. With increasing of the absolute value of the coupling coefficient U_c , the eigenfrequencies change as follows: in the case of positive coupling coefficient ($U_c > 0$), the lower eigenfrequency decreases, while the upper eigenfrequency increases (the eigenfrequencies become further removed from each other); in the case of nega-

tive coupling coefficient ($U_c < 0$), the lower eigenfrequency increases, while the upper eigenfrequency decreases (the eigenfrequencies become closer). Moreover, at some value of the negative coupling coefficient [this value is given by $(\Omega_v^2 - \Omega_h^2)^2 + 4U_c = 0$], the eigenfrequencies become equal to each other. Further increasing of the absolute value of the negative coupling coefficient trigger the resonance instability—imaginary parts of the eigenfrequencies appear and are of opposite signs, while the real parts remain equal to each other. Concerning the case of the positive coupling coefficient, the lower eigenfrequency becomes equal to zero at $U_c = \Omega_h^2 \Omega_v^2$. At further increasing of the positive coupling coefficient, the nonoscillatory instability of the lower eigenfrequency appears. From the physical point of view, the positive feedback becomes sufficient to overcome the restoring forces, which implies that the initial particle configuration is no longer a ground state.

In the case of the presence of the friction, the condition for the resonance oscillatory instability also requires that the friction should be small enough [condition (14)]. On the other hand, the presence of the friction does not affect the condition for the nonoscillatory instability [Eq. (16)].

For a system with weak coupling, the resonance oscillatory instability can occur only in the case of crossing of the horizontal $\Omega_h(k)$ and vertical $\Omega_v(k)$ frequencies at some k . The instability condition is

$$U_c(k_{\text{cross}}) < 0, \quad |U_c(k_{\text{cross}})| > \gamma^2 \Omega_{\text{cross}}^2, \quad (17)$$

where $(k_{\text{cross}}, \Omega_{\text{cross}})$ is the crossing point. In this case, the oscillatory instability occurs in a small interval of wave numbers near the crossing point.

E. Oscillatory instability [Eq. (14)]

In this section, we consider the following case: the anisotropy of the dust-dust interaction and the horizontal dust charge variations are small corrections to the simplest model where (i) the dust-dust interaction is described by the Debye–Hückel (Yukawa) potential, (ii) the dust charge depends on the coordinate z and is not influenced by the neighboring particles. We choose the length λ used to normalize distances in Eq. (5) to be the screening length. For the screened Coulomb interaction $\phi_n(\mathbf{r}) = (-Q_n) \exp(-|\mathbf{r} - \mathbf{r}_n|/\lambda)/|\mathbf{r} - \mathbf{r}_n|$ (where \mathbf{r}_n is the current position of the n th particle), we have

$$\sigma_{xx} = \frac{\kappa^2 + 2\kappa + 2}{\kappa^3} \exp(-\kappa), \quad (18)$$

$$\sigma_{zz} = -\frac{\kappa + 1}{\kappa^3} \exp(-\kappa). \quad (19)$$

Thus, the horizontal and vertical modes are approximately given respectively by $\Omega_h^2(k) = 4\sigma_{xx} \sin^2(k\kappa/2)$ and $\Omega_v^2(k) = e_1 + e_0 q_z + 4\sigma_{zz} \sin^2(k\kappa/2)$, where σ_{xx} and σ_{zz} are given respectively by Eqs. (18) and (19). For large κ , the vertical frequency is greater than the horizontal frequency at any k . If we inject new particles to the system in order to decrease the interparticle distance, the following physics takes place. The horizontal and vertical frequencies become equal to each

other at the boundary of the first Brillouin zone ($k\kappa = \pi$). The corresponding value of the parameter κ is given by

$$e_1 + e_0 q_z = 4 \frac{\kappa^2 + 3\kappa + 3}{\kappa^3} \exp(-\kappa). \quad (20)$$

Note that the coupling coefficient $U_c(k)$ is equal to zero at the boundary of the first Brillouin zone [see Eq. (12)]. Further decreasing of the interparticle distance leads to the following: the crossing point k_{cross} becomes situated before the boundary of the first Brillouin zone, therefore, $U_c(k_{\text{cross}})$ becomes nonzero, and, therefore, the oscillatory instability [Eq. (17)] can occur. We write down the instability condition. Neglecting the fifth and sixth terms in Eq. (12) ($e_0 \gg |\sigma_z|$), we present the coupling coefficient $U_c(k)$ in the form $U_c(k) = u \sin^2(k\kappa)$, where u is independent of k ,

$$u = 4(-\sigma_{xz}^2 + \sigma_{xz}\sigma_x q_z - \sigma_{xz} q_x e_0 + \sigma_x q_x q_z e_0). \quad (21)$$

We find the crossing point $(k_{\text{cross}}, \Omega_{\text{cross}})$ and write the instability condition [Eq. (17)] in the following form:

$$u < 0, \quad (22)$$

$$|u| > \gamma^2 \frac{\kappa^2 + 2\kappa + 2}{\kappa^2 + 3\kappa + 3} (e_1 + e_0 q_z) \times \left[1 - \left(1 - \frac{\kappa^3 \exp(\kappa) (e_1 + e_0 q_z)}{2(\kappa^2 + 3\kappa + 3)} \right)^2 \right]^{-1}.$$

If condition (22) is not satisfied before the interparticle distance becomes too small so $\Omega_v^2(k)$ becomes negative near the boundary of the first Brillouin zone, the nonoscillatory instability appears first [condition (16) becomes satisfied]: the particles are pushed out of the string due to mutual repulsion exceeding the vertical confinement. The corresponding value of the parameter κ is given by

$$e_1 + e_0 q_z = 4 \frac{\kappa + 1}{\kappa^3} \exp(-\kappa). \quad (23)$$

Numerical example. The physics described above in the present section was observed in the experiment of Ref. 5 performed at the pressure of 2.8 Pa: while injecting new dust particles into the 2D plasma crystal, the melting (oscillatory instability) occurred at some value of the interparticle distance. It was possible to stop the melting by increasing the pressure (up to 5–10 Pa). If the pressure was sufficiently high, the system never melted. In the latter case, when the number of the particles exceeded a certain threshold, the monolayer transformed into a bilayer system.

We substitute into our model the parameters of the experiment of Ref. 5. For the pressure of 2.8 Pa, the following measurements were made. It was found by analyzing the horizontal trajectories of two interacting particles that the dust-dust interaction can be approximately described by the screened Coulomb potential with the absolute value of the charge $Q = 15\,500e$ (where e is the absolute value of the electron charge) and the screening length $\lambda = 0.5$ mm. The resonance vertical frequency of a single particle was measured to be $\omega_v/2\pi \approx 15.5$ Hz. The dust mass was $M \approx 5.5 \times 10^{-10}$ g. Thus we find $e_1 + e_0 q_z = \omega_v^2 \lambda^3 M / Q^2 \approx 11.8$. Solving Eq. (20),

we find the parameter κ at which the intersection of the modes occurs at the boundary of the first Brillouin zone: $\kappa \approx 0.96$. Solving Eq. (23), we find the parameter κ at which the vertical mode becomes unstable due to mutual repulsion of dust particles: $\kappa \approx 0.66$. Therefore, in our model, the melting can occur at $0.66 < \kappa < 0.96$. The pressure of 2.8 Pa corresponds to $\gamma = (4\pi/3)n_n m_n a^2 v_{Tn} \lambda^{3/2} / (Q\sqrt{M}) \approx 0.095$, where n_n is the neutral density, m_n is the neutral mass (in the experiment, argon was used), a is the dust radius (in the experiment, $a \approx 4.45 \mu\text{m}$), $v_{Tn} = \sqrt{8T_n/\pi m_n}$ is the mean neutral speed (the neutral temperature T_n is assumed to be the room temperature $T_n = 300 \text{ K}$) (see Ref. 19). The expression in the right-hand side of Eq. (22) behaves in the range $0.66 < \kappa < 0.96$ as follows: at $\kappa \approx 0.96$, the expression takes the infinitely large value; with decreasing κ , the value of the expression decreases; at $\kappa \approx 0.77$, the expression takes the minimum value of ≈ 0.074 ; with further decreasing κ , the value of the expression increases; finally, at $\kappa \approx 0.66$, the expression takes the value of ≈ 0.087 . Thus, in our model, the melting at the pressure of 2.8 Pa means that, at some κ from the range $0.66 < \kappa < 0.96$, the parameter u is negative, and its absolute value exceeds at least 0.074.

We discuss what terms in Eq. (21) could give a significant contribution to the parameter u of -0.074 . For estimates, we consider the simplest model where the dust-dust interaction is the sum of the screened Coulomb potential and the nonscreened dipole field, i.e.,

$$\phi_n(\mathbf{r}) = \frac{(-Q_n)}{|\mathbf{r} - \mathbf{r}_n|} \exp\left(-\frac{|\mathbf{r} - \mathbf{r}_n|}{\lambda}\right) + \frac{(\mathbf{r} - \mathbf{r}_n) \cdot \mathbf{P}_n}{|\mathbf{r} - \mathbf{r}_n|^3} \quad (24)$$

where the dipole moment \mathbf{P}_n is assumed to be directed downward and proportional to the momentary value of the particle charge. In this model, the parameters σ_x , σ_{xx} , and σ_{zz} are exactly the same as for the pure screened Coulomb interaction [$\sigma_x = -(\kappa + 1)\exp(-\kappa)/\kappa^2$, σ_{xx} and σ_{zz} are given by respectively Eqs. (18) and (19)], while $\sigma_z = -p/\kappa^3$ and $\sigma_{xz} = 3p/\kappa^4$, where p is the absolute value of the dipole moment \mathbf{P}_n in units of $Q\lambda$. We perform estimates assuming that the interparticle distance is as close as possible (i.e., $\kappa \approx 0.66$), so that the coupling is expected to be the strongest. The first term in Eq. (21) gives the value of u of -0.074 for $p \approx 9 \times 10^{-3}$. For this p , the second term in Eq. (21) is equal to the first term at $q_z \approx 0.07$. We find the parameter e_0 present in the last two terms as follows: $QE = Mg$, which gives $e_0 = Mg\lambda^2/Q^2 \approx 24$. Assuming the parameters p and q_z are as found above, we find that at $q_x \approx 6 \times 10^{-3}$ all the four terms in Eq. (21) are equal to each other. Thus, each of the four terms in Eq. (21) can be sufficient to trigger the resonance oscillatory instability in the laboratory experiments.

F. Nonoscillatory instability [Eq. (16)]

In the case of no coupling, the nonoscillatory instability appears when any of the functions $\Omega_h^2(k)$, $\Omega_v^2(k)$ is negative at some k [see Eqs. (15) and (16)]. When the coupling is present, the nonoscillatory instability is possible even in the case where both functions $\Omega_h^2(k)$ and $\Omega_v^2(k)$ are positive for any k [see Eq. (16)]. In this section, we investigate the instability condition in the latter case. We assume the following:

(i) the horizontal mode is given by $\Omega_h^2(k) = 4\sigma_{xx} \sin^2(k\kappa/2)$ [i.e., the last term in Eq. (10) can be neglected], where $\sigma_{xx} > 0$, (ii) the vertical mode is given by $\Omega_v^2(k) = e_1 + e_0 q_z + 4\sigma_{zz} \sin^2(k\kappa/2)$ [i.e., the last term in Eq. (11) can be neglected], (iii) $\Omega_v^2(k) > 0$ for any k (i.e., $e_1 + e_0 q_z > 0$ and $e_1 + e_0 q_z + 4\sigma_{zz} > 0$), (iv) the coupling coefficient is $U_c(k) = u \sin^2(k\kappa)$, where u is independent of k (i.e., $e_0 \gg |\sigma_z|$). In this case, it can be easily shown that the expression $\Omega_v^2(k)\Omega_h^2(k)/\sin^2(k\kappa)$ takes the minimal value at $k \rightarrow 0$. Thus, the instability condition takes the form

$$u > (e_1 + e_0 q_z)\sigma_{xx}. \quad (25)$$

Condition (25) does not depend on γ , which suggests that this is a ‘‘configurational’’ instability.

III. CONCLUSIONS

Using the 1D particle string model, we have shown that the coefficient of coupling between the horizontal (longitudinal) and vertical modes is the sum of six terms, each caused by a different physical mechanism. The first four are related respectively to: (1) only anisotropy of the dust-dust interaction; (2) anisotropy of the dust-dust interaction and vertical dust charge variations; (3) anisotropy of the dust-dust interaction and horizontal dust charge variations; (4) vertical and horizontal dust charge variations. In the laboratory experiments, all these four terms can be comparable with each other, while two remaining terms are negligible if the force of the electric field of the sheath is much greater than the vertical component of the dust-dust interaction in the equilibrium state.

The coupling can trigger the resonance oscillatory instability. In most experiments, the coupling is assumed to be weak, and, therefore, the instability condition actually means (i) intersection of the modes, (ii) the negative sign of the coupling coefficient, and (iii) the neutral pressure is less than some threshold proportional to the square root of the absolute value of the coupling coefficient.

If the coupling is positive and sufficiently strong, it can trigger a nonoscillatory instability at small wave numbers. The corresponding instability condition does not contain the neutral pressure.

ACKNOWLEDGMENTS

R.K. acknowledges the Deutscher Akademischer Austauschdienst (DAAD) for financial and organizational support (scholarship no. A/04/00273). In addition, R.K. wishes to acknowledge the Dynasty Foundation for partial financial support within the framework of the postgraduate students fellowship program.

¹A. Homann, A. Melzer, S. Peters, R. Madani, and A. Piel, Phys. Lett. A **242**, 173 (1998).

²S. Nunomura, D. Samsonov, and J. Goree, Phys. Rev. Lett. **84**, 5141 (2000).

³S. Nunomura, J. Goree, S. Hu, X. Wang, and A. Bhattacharjee, Phys. Rev. E **65**, 066402 (2002).

⁴S. Nunomura, J. Goree, S. Hu, X. Wang, A. Bhattacharjee, and K. Avinash, Phys. Rev. Lett. **89**, 035001 (2002).

⁵A. V. Ivlev, U. Konopka, G. Morfill, and G. Joyce, Phys. Rev. E **68**, 026405 (2003).

- ⁶A. Homann, A. Melzer, S. Peters, and A. Piel, *Phys. Rev. E* **56**, 7138 (1997).
- ⁷T. Misawa, N. Ohno, K. Asano, M. Sawai, S. Takamura, and P. K. Kaw, *Phys. Rev. Lett.* **86**, 1219 (2001).
- ⁸F. Melandsø and J. Goree, *Phys. Rev. E* **52**, 5312 (1995).
- ⁹S. A. Maiorov, S. V. Vladimirov, and N. F. Cramer, *Phys. Rev. E* **63**, 017401 (2000).
- ¹⁰O. Ishihara and S. V. Vladimirov, *Phys. Plasmas* **4**, 69 (1997).
- ¹¹S. Benkadda, V. N. Tsytovich, and S. V. Vladimirov, *Phys. Rev. E* **60**, 4708 (1999).
- ¹²M. Lampe, G. Joyce, G. Ganguli, and V. Gavrishchaka, *Phys. Plasmas* **7**, 3851 (2000).
- ¹³K. Takahashi, T. Oishi, K. Shimomai, Y. Hayashi, and S. Nishino, *Phys. Rev. E* **58**, 7805 (1998).
- ¹⁴A. Melzer, V. A. Schweigert, and A. Piel, *Phys. Rev. Lett.* **83**, 3194 (1999).
- ¹⁵V. N. Tsytovich, G. E. Morfill, and H. Thomas, *Plasma Phys. Rep.* **28**, 623 (2002).
- ¹⁶V. E. Fortov, A. G. Khrapak, S. A. Khrapak, V. I. Molotkov, and O. F. Petrov, *Phys. Usp.* **47**, 447 (2004).
- ¹⁷A. V. Ivlev and G. Morfill, *Phys. Rev. E* **63**, 016409 (2000).
- ¹⁸V. V. Yaroshenko, A. V. Ivlev, and G. E. Morfill, *Phys. Rev. E* **71**, 046405 (2005).
- ¹⁹P. Epstein, *Phys. Rev.* **23**, 710 (1924).

Dust clusters with non-Hamiltonian particle dynamics

R. Kompaneets^{a)}

Max-Planck-Institut für Extraterrestrische Physik, Giessenbachstraße 85748 Garching, Germany
Moscow Institute of Physics and Technology, Institutsky Pereulok 9, Dolgoprudny,
141700 Moskovskaya Oblast, Russia

S. V. Vladimirov

School of Physics, The University of Sydney, New South Wales 2006, Australia

A. V. Ivlev

Max-Planck-Institut für Extraterrestrische Physik, Giessenbachstraße 85748 Garching, Germany

V. Tsytovich

General Physics Institute of the Russian Academy of Sciences, Vavilova 38, 117942 Moscow, Russia

G. Morfill

Max-Planck-Institut für Extraterrestrische Physik, Giessenbachstraße 85748 Garching, Germany

(Received 30 January 2006; accepted 17 May 2006; published online 13 July 2006)

The modes of clusters formed by two or three charged dust particles in a plasma are analyzed. The non-Hamiltonian dynamics of the particles is taken into account, which includes (i) nonreciprocal interaction forces due to wake effects and (ii) spatial variations of the particle charge and shielding parameters. It is shown that these effects can trigger an oscillatory instability under realistic experimental conditions. An experiment is suggested to observe this instability. © 2006 American Institute of Physics. [DOI: 10.1063/1.2212396]

I. INTRODUCTION

Systems of charged dust particles in an inhomogeneous plasma with ion flow (e.g., in the plasma sheath) are characterized by nonreciprocal interaction forces (i.e., $\text{actio} \neq \text{reactio}$) due to the so-called wake fields¹⁻¹⁰) as well as by spatial variations of the particle charge¹¹⁻¹⁵ and shielding parameters. Such systems cannot be described by a Hamiltonian and, hence, energy is not conserved in such systems. The physical reason for the energy nonconservation is that such systems are not closed systems because of the presence of the plasma. This makes a complex (dusty) plasma a convenient model to study non-Hamiltonian dynamical systems which are of fundamental physical interest (see, e.g., Refs. 16 and 17, and references herein) and have a long history in mechanics.¹⁸

One of the properties different from those of Hamiltonian systems was revealed in the experiment of Ref. 19 where the melting of particle monolayer was observed. The dust crystal melted when the neutral friction was not sufficient to suppress the oscillatory instability of coupled in-plane longitudinal and out-of-plane dust-lattice modes.²⁰⁻²² Such oscillatory instability would be impossible for a Hamiltonian dynamical system because of the energy conservation.

The question arises whether the same physics can be observed in a system of a few dust particles. In the present paper, we show that an oscillatory instability due to the non-Hamiltonian particle dynamics is possible for 2- and 3-particle clusters and could be observed in experiments and used for plasma diagnostics.

The paper is organized in the following way: The model

description and the equations of motion are followed by the mode analysis performed in the case of reciprocal interaction forces and no variations of the particle charge and shielding parameters (i.e., in the case of Hamiltonian particle dynamics). Then, the role of charge/shielding variations and the nonreciprocity of the interaction forces is shown: the mode frequencies and instability conditions are obtained in analytical form and the instability mechanism is explained. A numerical example is followed by conclusions where an experiment is suggested.

II. THEORY

A. Model description

We consider $N=2$ (and, separately, $N=3$) dust particles with masses m and charges $-Q(z) < 0$ dependent on the z coordinate (the z axis is directed downward). In equilibrium, the particle positions are in the horizontal plane $z=0$. We denote $Q(0)=Q_0$. In equilibrium, the interparticle distance is L (for $N=3$, the particle positions form an equilateral triangle with side L).

The forces acting on the particles are gravity, the electric field of the sheath, the electrostatic dust-dust interaction, and the neutral friction.

The electric field of the sheath is the sum of the vertical field $E=E(z)$ directed downward [we denote $E(0)=E_0$] and the field given by the electrostatic potential

$$\Phi(r, z) = -b(z) \cdot r^2 \quad (1)$$

responsible for the horizontal confinement of the particles. Here r is the distance from the z axis. We denote $b(0)=b_0$ and introduce b'_z and b''_{zz} as the corresponding derivatives of the function $b(z)$ evaluated at $z=0$.

^{a)}Electronic mail: komp@mpe.mpg.de

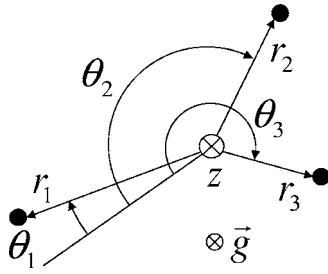


FIG. 1. Sketch of the particle coordinates.

Concerning the electrostatic dust-dust interaction, we employ the following model: each particle induces an electrostatic potential given by

$$\phi = -Q(z) \cdot f(\Delta_h, \Delta_v, z), \quad (2)$$

where Δ_h is the horizontal distance from the particle, Δ_v is the vertical distance from the particle in the z direction, and z is the z coordinate of the particle. We introduce $f'_h, f'_v, f'_z, f''_{hh}$, etc. as the corresponding derivatives of the function $f(\Delta_h, \Delta_v, z)$ evaluated at $\Delta_h=L, \Delta_v=0, z=0$.

The neutral friction is $\mathbf{F}_{fr} = -C_{fr}\mathbf{v}$, where \mathbf{v} is the particle velocity.

Note that the ion drag force¹² is not explicitly included in our model. Instead of this, we can assume that $E(z)$ is the “effective” electric field so that the ion drag force is already included in $Q(z)E(z)$.

B. Force balance in equilibrium

In equilibrium, the interaction force exerted on one particle by another has the horizontal component $-Q_0^2 f'_h$ directed from the latter particle and the vertical component $-Q_0^2 f'_v$ directed downward [see Eq. (2)].

The horizontal force exerted on each particle by all other particles is balanced by the horizontal confinement potential $\Phi(r, z)$. The equation for the latter balance allows us to express b_0 through the given interparticle distance L :

$$b_0 = -\frac{NQ_0 f'_h}{2L}, \quad (3)$$

where, as it was mentioned above, $N=2, 3$.

The vertical forces acting on each particle are gravity, the vertical component of the electric field of the sheath and the vertical components of the interparticle interaction forces. Note that the z component of the electric field of the sheath is $E(z) - d\Phi(r, z)/dz$ where the latter term is due to the vertical dependence of the horizontal confinement potential $\Phi(r, z)$. Thus, the vertical force balance equation is as follows:

$$mg - Q_0 E_0 - Q_0 b'_z \frac{(N+1)L^2}{12} - (N-1)Q_0^2 f'_v = 0. \quad (4)$$

[For $N=2, 3$, the squared distance of the particles from the z axis can be written as $(N+1)L^2/12$.]

C. Equations of motion

We use cylindrical coordinates (Fig. 1): the distances r_1 ,

r_2 (and r_3 , for $N=3$) of the particles from the z axis, the azimuthal angles θ_1, θ_2 (and θ_3) counted from a fixed radial direction clockwise if viewed from above, and the z coordinates z_1, z_2 (and z_3). For $N=3$, the particles are numbered 1, 2, 3 in the positive θ direction.

In these coordinates, the equations of motion are

$$F_{nr}/m = \ddot{r}_n - r_n(\dot{\theta}_n)^2,$$

$$F_{n\theta}/m = r_n \ddot{\theta}_n + 2\dot{r}_n \dot{\theta}_n, \quad F_{nz}/m = \ddot{z}_n, \quad (5)$$

where $F_{nr}, F_{n\theta}, F_{nz}$ are, respectively, the radial, azimuthal, and z components of the net force on the n th particle. These components are defined with respect to the momentary position of the n th particle.

The net force on the n th particle is given by $\mathbf{F}_n = -Q(z_n)\mathbf{E}_n - C_{fr}\dot{\mathbf{r}}_n$, where \mathbf{E}_n is the sum of the electric field of the sheath and the electric fields induced by all other particles at the point \mathbf{r}_n corresponding to the momentary position of the n th particle. Thus, we obtain

$$\begin{aligned} \mathbf{F}_n = & -Q(z_n)E(z_n)\mathbf{e}_z + Q(z_n) \left. \frac{\partial \Phi}{\partial \mathbf{r}} \right|_{\mathbf{r}=\mathbf{r}_n} \\ & + Q(z_n) \sum_{k \neq n} \left. \frac{\partial \phi_k(\mathbf{r})}{\partial \mathbf{r}} \right|_{\mathbf{r}=\mathbf{r}_n} - C_{fr}\dot{\mathbf{r}}_n, \end{aligned} \quad (6)$$

where \mathbf{e}_z is the unit vector in the z direction, Φ is the horizontal confinement potential given by Eq. (1), and $\phi_k(\mathbf{r})$ is the electrostatic potential induced by the k th particle. Thus, we find $F_{nr}, F_{n\theta}, F_{nz}$:

$$\begin{aligned} F_{nr} = & -2Q(z_n)b(z_n)r_n - Q(z_n) \sum_{k \neq n} Q(z_k) \frac{\partial f_{nk}}{\partial r_n} - C_{fr}\dot{r}_n, \\ F_{n\theta} = & -\frac{Q(z_n)}{r_n} \sum_{k \neq n} Q(z_k) \frac{\partial f_{nk}}{\partial \theta_n} - C_{fr}r_n \dot{\theta}_n, \\ F_{nz} = & mg - Q(z_n)E(z_n) - Q(z_n)r_n^2 \frac{db(z_n)}{dz_n} \\ & - Q(z_n) \sum_{k \neq n} Q(z_k) \frac{\partial f_{nk}}{\partial z_n} - C_{fr}\dot{z}_n, \end{aligned} \quad (7)$$

where f_{nk} is the value of the function f [see Eq. (2)] for $\Delta_h = [r_n^2 + r_k^2 - 2r_n r_k \cos(\theta_n - \theta_k)]^{1/2}$, $\Delta_v = z_n - z_k$, $z = z_k$.

D. Dimensionless parameters

We introduce the dimensionless parameters which are the values of the original parameters in units where (i) $Q_0 = 1$, (ii) $m = 1$, and (iii) distances are in units of some arbitrary length λ (this length λ can be associated, for example, with the length of the dust-dust interaction):

$$\kappa = \frac{L}{\lambda}, \quad e_0 = \frac{E_0 \lambda^2}{Q_0}, \quad \gamma = \frac{C_{fr}}{Q_0} \sqrt{\frac{\lambda^3}{m}},$$

$$e_z = \left. \frac{dE(z)}{dz} \right|_{z=0} \frac{\lambda^3}{Q_0}, \quad q_z = \left. \frac{dQ(z)}{dz} \right|_{z=0} \frac{\lambda}{Q_0}. \quad (8)$$

We also introduce the dimensionless parameters characterizing (i) the interaction potential:

$$\sigma_h = f'_h \lambda^2, \quad \sigma_v = f'_v \lambda^2, \quad \sigma_{vz} = f''_{vz} \lambda^3, \dots, \quad (9)$$

and (ii) the z dependence of the horizontal confinement potential:

$$\beta_z = \frac{b'_z \lambda}{b_0}, \quad \beta_{zz} = \frac{b''_{zz} \lambda^2}{b_0}. \quad (10)$$

E. Linearized equations of motion

The linearized equations take the form

$$\frac{d^2}{dt^2} \mathcal{L} + \gamma \frac{d}{dt} \mathcal{L} + \mathcal{M} \mathcal{L} = 0, \quad (11)$$

where t is the time normalized by $\sqrt{m \lambda^3 / Q_0}$,

$$\mathcal{L} = (l_{1r}, l_{1\theta}, l_{1z}, \dots, l_{Nr}, l_{N\theta}, l_{Nz})^T, \quad (12)$$

$l_{nr}, l_{n\theta}, l_{nz}$ are the dimensionless (i.e., normalized by λ) displacements of the n th particle in the r, θ , and z directions, respectively, and

$$\mathcal{M} = \begin{pmatrix} \mathcal{D} & \mathcal{F} \\ \mathcal{F} & \mathcal{D} \end{pmatrix}, \quad \mathcal{D} = \begin{pmatrix} (\sigma_{hh} \kappa - 2\sigma_h) / \kappa & 0 & \sigma_{vh} - \beta_z \sigma_h \\ 0 & -\sigma_h / \kappa & 0 \\ \sigma_{vh} - \beta_z \sigma_h & 0 & e_z + e_0 q_z + \sigma_{vv} + q_z \sigma_v - (\beta_z q_z + \beta_{zz}) \sigma_h \kappa / 4 \end{pmatrix},$$

$$\mathcal{F} = \begin{pmatrix} \sigma_{hh} & 0 & q_z \sigma_h + \sigma_{hz} - \sigma_{vh} \\ 0 & \sigma_h / \kappa & 0 \\ \sigma_{vh} & 0 & -\sigma_{vv} + q_z \sigma_v + \sigma_{vz} \end{pmatrix} (N=2), \quad \mathcal{M} = \begin{pmatrix} \mathcal{D} & \mathcal{F}_+ & \mathcal{F}_- \\ \mathcal{F}_- & \mathcal{D} & \mathcal{F}_+ \\ \mathcal{F}_+ & \mathcal{F}_- & \mathcal{D} \end{pmatrix},$$

$$\mathcal{D} = \begin{pmatrix} (3\sigma_{hh} \kappa - 5\sigma_h) / 2\kappa & 0 & (\sigma_{vh} - \beta_z \sigma_h) \sqrt{3} \\ 0 & (\sigma_{hh} \kappa - 3\sigma_h) / 2\kappa & 0 \\ (\sigma_{vh} - \beta_z \sigma_h) \sqrt{3} & 0 & e_z + e_0 q_z + 2\sigma_{vv} + 2q_z \sigma_v - (\beta_z q_z + \beta_{zz}) \sigma_h \kappa / 2 \end{pmatrix},$$

$$\mathcal{F}_{\pm} = \begin{pmatrix} (3\sigma_{hh} \kappa - \sigma_h) / 4\kappa & \pm (\sigma_{hh} \kappa + \sigma_h) \sqrt{3} / 4\kappa & (\sigma_{hz} + q_z \sigma_h - \sigma_{vh}) \sqrt{3} / 2 \\ \mp (\sigma_{hh} \kappa + \sigma_h) \sqrt{3} / 4\kappa & (-\sigma_{hh} \kappa + 3\sigma_h) / 4\kappa & \pm (\sigma_{vh} - \sigma_{hz} - q_z \sigma_h) / 2 \\ \sigma_{vh} \sqrt{3} / 2 & \pm \sigma_{vh} / 2 & -\sigma_{vv} + q_z \sigma_v + \sigma_{vz} \end{pmatrix} (N=3). \quad (13)$$

All the solutions of Eq. (11) can be written as follows:

$$\mathcal{L}(t) = \text{Re} \sum_{j=1}^{3N} [C_{j,+} \exp(-i\omega_{j,+} t) + C_{j,-} \exp(-i\omega_{j,-} t)] \mathcal{L}_j, \quad (14)$$

where $C_{j,\pm}$ are arbitrary complex constants,

$$\omega_{j,\pm}^2 + i\gamma\omega_{j,\pm} = \Omega_j^2, \quad (15)$$

Ω_j^2 are the eigenvalues of the matrix \mathcal{M} , and \mathcal{L}_j are the corresponding eigenvectors of the matrix \mathcal{M} . Note that the Ω_j^2 are the dimensionless squared mode frequencies in the absence of friction.

F. The case of Hamiltonian dynamics

In this subsection, we consider the case where:

- The interaction forces are reciprocal ($\sigma_v = \sigma_{vh} = \sigma_{vz} = 0$);

- The particle charge and shielding are independent of the particle position ($q_z = \sigma_{hz} = 0$);
- And, for simplicity, the horizontal confinement potential is independent of the height ($\beta_z = \beta_{zz} = 0$).

Note that the presence/absence of the vertical dependence of the horizontal confinement potential has nothing to do with the system's dynamics being Hamiltonian or not.

For $N=2$, we have the following modes ($\Omega_j^2, \mathcal{L}_j$) (we will omit the subscripts in the Ω_j^2):

- The “horizontal rotation” mode: $\Omega^2 = 0$;
- The two “horizontal sloshing” modes (a whole cluster horizontal shift): $\Omega^2 = -2\sigma_h / \kappa$;
- The “breathing” mode [Fig. 2(a)]: $\Omega^2 = 2(\sigma_{hh} - \sigma_h / \kappa)$;
- The “vertical sloshing” mode (a whole cluster vertical shift): $\Omega^2 = e_z$;
- The “vertical shear” mode [Fig. 2(b)]: $\Omega^2 = e_z + 2\sigma_{vv}$.

For $N=3$, we have

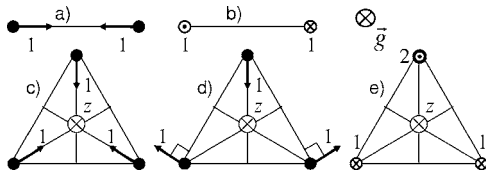


FIG. 2. Modes of $N=2$ (a), (b) and $N=3$ (c), (d), (e) clusters in the case where (i) the interaction forces are reciprocal, (ii) the particle charge and shielding are independent of the particle position, and (iii) the horizontal confinement potential is independent of the height. The numbers represent the relative magnitudes of the particle displacements. Trivial modes corresponding to the horizontal rotation and whole cluster vertical and horizontal shifts are not shown.

- The “horizontal rotation” mode: $\Omega^2=0$;
- The two “horizontal sloshing” modes (a whole cluster horizontal shift): $\Omega^2=-3\sigma_h/\kappa$;
- The “breathing” mode [Fig. 2(c)]: $\Omega^2=3(\sigma_{hh}-\sigma_h/\kappa)$;
- The two “kink” modes [Fig. 2(d)]: $\Omega^2=3(\sigma_{hh}-\sigma_h/\kappa)/2$;
- The “vertical sloshing” mode (a whole cluster vertical shift): $\Omega^2=e_z$;
- The two “vertical shear” modes [Fig. 2(e)]: $\Omega^2=e_z+3\sigma_{vv}$.

G. The general case of non-Hamiltonian dynamics

Now, we consider the general case, i.e., the case where (i) the interaction forces are nonreciprocal, (ii) the particle charge and shielding depend on the particle position, and (iii) the horizontal confinement potential depends on the height. In this case, the horizontal displacements of the particles cause vertical force variations and, simultaneously, the vertical displacements cause horizontal force variations—a feedback takes place. As a result, some horizontal modes become coupled with some vertical modes and, hence, some eigenfrequencies correspond to the simultaneous in- and out-of-plane motion.

1. Frequencies of the coupled “breathing” and “vertical sloshing” modes

As we will see, the coupled “breathing” and “vertical sloshing” modes are of the most interest for realistic experimental conditions. The corresponding particle motion simultaneously satisfies the following relations:

$$\begin{aligned} l_{1r} &= l_{2r}(=l_{3r}), & l_{1\theta} &= l_{2\theta}(=l_{3\theta}) = 0, \\ l_{1z} &= l_{2z}(=l_{3z}). \end{aligned} \quad (16)$$

This gives the following equation for the Ω_j^2 :

$$(\Omega^2 - A)(\Omega^2 - B) = C, \quad (17)$$

where the subscripts in the Ω_j^2 are omitted,

$$A = N(\sigma_{hh} - \sigma_h/\kappa), \quad (18)$$

$$\begin{aligned} B &= e_z + e_0 q_z + 2(N-1)q_z \sigma_v + (N-1)\sigma_{vz} \\ &\quad - (N-1)(\beta_z q_z + \beta_{zz})\sigma_h \kappa/4, \end{aligned} \quad (19)$$

$$C = (2N-3)(2\sigma_{vh} - \sigma_h \beta_z)(\sigma_{hz} + q_z \sigma_h - \beta_z \sigma_h). \quad (20)$$

The parameters A and B are, respectively, the squared “horizontal” and “vertical” frequencies in the following sense. If we assume that the particles can move only radially (i.e., we use $l_{1z}=l_{2z}=l_{3z}=0$ instead of considering the vertical forces), the parameter A will be the squared dimensionless frequency of these radial oscillations (in the absence of friction). Analogously, if we assume that the particles can move only vertically (i.e., we use $l_{1r}=l_{2r}=l_{3r}=0$), the squared dimensionless frequency of these vertical oscillations will be B . The coupling coefficient C characterizes the coupling between the radial and vertical motion.

2. Instability condition

We perform the stability analysis of Eq. (17) for arbitrary real parameters A , B , C , and $\gamma > 0$. We rewrite Eq. (17) in the form

$$(\omega^2 + i\gamma\omega - A)(\omega^2 + i\gamma\omega - B) = C \quad (21)$$

[see Eq. (15)]. All the four solutions ω of Eq. (21) can be easily found analytically. (We have a quadratic equation with respect to $\omega^2 + i\gamma\omega$. After solving it, we have to solve a quadratic equation with respect to ω .) The analysis of the analytic expression for all the four solutions gives the following instability conditions:

- We have an oscillatory instability [i.e., a solution with $\text{Im}(\omega) > 0$ and $\text{Re}(\omega) \neq 0$] if

$$(A - B)^2 + 4C < 0 \quad (22)$$

and

$$|(A - B)^2 + 4C| > 2\gamma^2(A + B). \quad (23)$$

- We have a nonoscillatory instability [i.e., a solution with $\text{Im}(\omega) > 0$ and $\text{Re}(\omega) = 0$] if

$$(A - B)^2 + 4C \geq 0 \quad (24)$$

and any of the following is satisfied:

$$A + B < 0 \quad (25)$$

or

$$AB < C. \quad (26)$$

3. The case of weak coupling

We assume that the parameters A , B , C , and γ are some functions of the controlling parameters. These controlling parameters can be the neutral pressure, the discharge power, the particle size/mass, parameter(s) responsible for the horizontal confinement potential (e.g., if the horizontal confinement potential is induced by a conductive ring placed on the lower electrode, then the radius and thickness of this ring can be considered as controlling parameters). We assume that, for some range of the controlling parameters, the parameters A and B are always positive. Then, for this range of the controlling parameters, an oscillatory instability occurs when

$$(A - B)^2 + 4C < -2\gamma^2(A + B) \quad (27)$$

and a nonoscillatory instability occurs when

$$AB < C \quad (28)$$

[see Eqs. (22)–(26)].

We assume that, for the considered range of the controlling parameters, the absolute value of the mode coupling coefficient C is always small and the parameters A and B are finite (i.e., the coupling between the modes is weak). In this case, a nonoscillatory instability is impossible [see Eq. (28)]. Concerning oscillatory instability, the left-hand side of Eq. (27) can be negative only in the vicinity of point(s)/surface(s) (in the space of the controlling parameters) given by equation $A=B$. If, for some point satisfying $A=B$, the following is satisfied:

$$C < 0, \quad |C| > \gamma^2 A, \quad (29)$$

then an oscillatory instability occurs in the vicinity of this point [see Eq. (27)]. Note that, in the absence of friction ($\gamma=0$),

- the only condition for the existence of oscillatory instability near the resonance $A=B$ is the negative sign of the mode coupling coefficient C ;
- When the mode coupling coefficient C is negative and infinitely small, the increment of the instability is infinitely small as well.

4. Parameter signs relevant to the laboratory experiments

We specify what signs of the parameters are relevant to the laboratory experiments (see, e.g., measurements of Ref. 23): (i) $\sigma_h < 0$ (the horizontal component of the force exerted on one particle by another is repulsive), (ii) $\sigma_{hh} > 0$ (this horizontal repulsion force decreases with the interparticle distance at horizontal displacements), (iii) $\sigma_v < 0$ [the vertical component of the force exerted on one particle by another is directed downward (an excess of the positive charge, i.e., wake, is accumulated “below” the latter particle due to ion focusing)], (iv) $\sigma_{vh} > 0$ (the absolute value of this vertical component decreases with the interparticle distance at horizontal displacements), (v) $\sigma_{vv} < 0$ (as for spherically symmetric repulsion), (vi) $\sigma_{hz} < 0$ (the ratio of the horizontal repulsion force exerted on one particle by another to the squared particle charge increases when both particles are simultaneously shifted in the downward direction, i.e., particle charge shielding becomes weaker as the lower electrode approached), (vii) $\beta_z > 0$ (the horizontal confinement becomes stronger as the lower electrode approached, which is typical when the horizontal confinement potential is induced by a conductive ring placed on the lower electrode or by a cavity machined into the lower electrode), and (viii) $q_z > 0$ (the negative particle charge increases as the lower electrode approached).

5. Physics of the instability

For simplicity of explanation of the instability mechanism, we assume that the signs of the parameters are as specified in the previous subsection.

When the particles are equally radially displaced from their equilibrium positions to each other, the vertical force

balance becomes disturbed because of the variations of the vertical forces exerted on each particle by (i) other particle(s) [i.e., wakes of the other particle(s)] and (ii) the vertical electric field induced due to the vertical dependence of the horizontal confinement potential $\Phi(r, z)$. Hence, there appears a net vertical force on each particle. This force is directed *downward* when the particles are shifted *to each other*. On the other hand, when the particles are equally displaced from their equilibrium positions in the *downward* direction, then, according to the condition $C < 0$ in the instability condition (29), there should appear a net horizontal *repulsive* force on each particle. This implies that increased mutual interparticle repulsion (due to both increased negative particle charge and weakened shielding) should be stronger than increased horizontal confinement. If it is satisfied and the resonance between the “horizontal” and “vertical” frequencies takes place ($A=B$), then the dynamics of particle motion satisfying Eq. (16) is equivalent to the dynamics of a two-dimensional harmonic oscillator in the field of a force whose components are such linear combinations of the displacement components that the lines of this force are closed elliptical lines. This implies two modes corresponding respectively to damped and growing rotation-like motions in opposite directions around the equilibrium point. The condition $|C| > \gamma^2 A$ in Eq. (29) means that the friction should be not sufficient to suppress this growth.

6. Other modes

The analysis of all other modes is given in the Appendix. The main conclusion of this analysis is as follows:

- If the parameter signs are as specified in Sec. II G 4;
- $\sigma_{hh}\kappa + \sigma_h > 0$ (i.e., the product of the horizontal repulsion force and the interparticle distance decreases with the interparticle distance at horizontal displacements);
- the coupling between the modes is weak;

then the coupling between these modes cannot trigger an instability (even in the absence of friction).

H. Numerical example

We employ the following model: the particle potential is the sum of the screened Coulomb potential [with screening length $\lambda_s(z)$ dependent on the particle z coordinate] and the dipole field which is the simplest model of the wake field, i.e.,

$$\phi_n = -\frac{Q(z_n)}{|\mathbf{r} - \mathbf{r}_n|} \exp\left[-\frac{|\mathbf{r} - \mathbf{r}_n|}{\lambda_s(z_n)}\right] + \frac{(\mathbf{r} - \mathbf{r}_n) \cdot \mathbf{P}(z_n)}{|\mathbf{r} - \mathbf{r}_n|^3}. \quad (30)$$

The particle-wake dipole moment $\mathbf{P}(z)$ is assumed to be directed downward (an excess of the positive charge is accumulated “below” the negatively charged particle due to ion focusing).

This model is reasonable since the experiments of Refs. 23 and 25 show that, for plasma conditions considered below, the horizontal forces between the particles levitated in the same horizontal plane are described by the screened Coulomb potential. Also, the only parameters responsible for the

effect of nonreciprocal interaction forces and present in the linearized equations of motion are σ_v , σ_{vh} , σ_{vz} [see Eq. (13)]. Of these parameters, only σ_{vh} is present in the expressions for the mode coupling coefficients [see Eqs. (20), (A6), (A13), and (A14)]. Hence, the dipole moment $\mathbf{P}(0)$ can be treated as the “effective” dipole moment which gives the same value of the parameter σ_{vh} (for given interparticle distance) as the real wake field and, hence, gives the same contributions to the mode coupling coefficients as the real wake field.

We choose the length λ used to normalize distances in Eq. (8) to be equal to $\lambda_s(0)$. Thus, we obtain

$$\begin{aligned}\sigma_h &= -\frac{\kappa+1}{\kappa^2}e^{-\kappa}, & \sigma_v &= -\frac{p}{\kappa^3}, \\ \sigma_{hh} &= \frac{(\kappa^2+2\kappa+2)}{\kappa^3}e^{-\kappa}, & \sigma_{vv} &= -\frac{\kappa+1}{\kappa^3}e^{-\kappa}, \\ \sigma_{vh} &= \frac{3p}{\kappa^4}, & \sigma_{hz} &= -\lambda_{s,z}e^{-\kappa}, & \sigma_{vz} &= \frac{pq_z - p_z}{\kappa^3},\end{aligned}\quad (31)$$

where

$$\begin{aligned}p &= \frac{|\mathbf{P}(0)|}{Q_0\lambda_s(0)}, & \lambda_{s,z} &= \left. \frac{d\lambda_s(z)}{dz} \right|_{z=0}, \\ p_z &= \left. \frac{1}{Q_0} \frac{d|\mathbf{P}(z)|}{dz} \right|_{z=0}.\end{aligned}\quad (32)$$

We use the parameters of the experiment of Ref. 19:

- $Q_0=15500e$ (where e is the elementary charge),
- $\lambda_s(0)=0.5$ mm,
- neutral (argon) pressure $P_n=2.8$ Pa,
- neutral temperature $T_n=300$ K,
- particle radius $a=4.45$ μm ,
- $m=5.5 \times 10^{-10}$ g,
- vertical frequency of a single particle $\omega_v/2\pi=15.5$ Hz.

We find

$$\gamma = \frac{4\pi n_n m_n a^2 v_{Tn}}{3 Q_0} \sqrt{\frac{\lambda^3}{m}} \approx 0.1 \quad (33)$$

(the Epstein neutral friction²⁴), where $n_n=P_n/kT_n$ is the neutral density, m_n is the neutral mass (the gas was argon, as mentioned above), $v_{Tn}=\sqrt{8kT_n/\pi m_n}$, k is the Boltzmann constant.

Since the vertical forces due to (i) wake effects and (ii) the vertical electric field induced due to the vertical dependence of the horizontal confinement potential $\Phi(r,z)$ are small with respect to gravity and the electric field of the sheath, we neglect

- all forces except mg and Q_0E_0 in the vertical force balance equation for equilibrium [Eq. (4)];
- the difference between the equilibrium vertical positions of a single particle and a cluster, as well as the corresponding difference in the particle charge and other parameters;

- all terms except $e_z+e_0q_z$ in the expression for the squared “vertical” frequency B [Eq. (19)].

Thus, we find

$$e_0 = \frac{mg\lambda^2}{Q_0^2} \approx 24, \quad e_z + e_0q_z = \frac{\omega_v^2\lambda^3 m}{Q_0^2} \approx 12. \quad (34)$$

Solving equation $A=B$ [where A is given by Eq. (18), $B=e_z+e_0q_z$ as mentioned above, σ_h and σ_{hh} are given by Eq. (31)], we find that the resonance $A=B$ occurs at $\kappa \approx 0.77$ and $\kappa \approx 0.88$ for $N=2$ and $N=3$, respectively. Thus, an oscillatory instability of the coupled “breathing” and “vertical sloshing” modes is possible only in the vicinity of these values of κ . This instability occurs if

$$(17p + 1.4\beta_z)[0.5\lambda_{s,z} + 1.4(q_z - \beta_z)] \geq 0.1(N=2), \quad (35)$$

$$3(10p + \beta_z)[0.4\lambda_{s,z} + (q_z - \beta_z)] \geq 0.1(N=3), \quad (36)$$

according to the instability condition (29), the expression for the mode coupling coefficient (20) and Eq. (31).

The measurements of Ref. 23 performed under the same conditions give the parameters $\lambda_{s,z}$ and q_z to be positive and ~ 0.2 . Concerning the parameter β_z , the horizontal confinement potential in the experiment of Ref. 23 was induced by a copper ring placed on the lower electrode, leading to the parameter β_z being positive and ~ 0.2 . For p , we can expect $p \sim 0.1$ (see, e.g., Fig. 2 of Ref. 8). Thus, the conditions concerned approximately correspond to the instability threshold and, therefore, the instability could be observed under similar conditions or, probably, under a smaller neutral pressure like in the experiment of Ref. 26 on 3-, 4-, and 7-particle clusters.

In Fig. 3, all mode frequencies are shown as functions of the interparticle distance for the parameters concerned. The Ω_j^2 are calculated directly from the matrix \mathcal{M} [Eq. (13)] without neglecting any terms. We can see that, when the interparticle distance is large enough, the frequency of the “vertical sloshing” mode is much larger than that of the “breathing” mode. With decreasing the interparticle distance (i.e., with increasing the horizontal confinement), the latter frequency increases so that at some distance the resonance takes place. An oscillatory instability is possible in the vicinity of this distance. At some distance less than the mentioned resonance distance, the “vertical shear” mode becomes unstable and the particles are pushed out of the plane due to mutual repulsion.

III. CONCLUSIONS

To conclude, we have shown that, under realistic experimental conditions, the non-Hamiltonian dynamics of dust particles can give rise to an oscillatory instability of 2- and 3-particle clusters when the interparticle distance is close to the resonance value at which the frequencies of the “breathing” and “vertical sloshing” modes coincide. In addition to the mentioned resonance condition, the negative sign of the mode coupling coefficient and the smallness of the neutral friction are required for this instability.

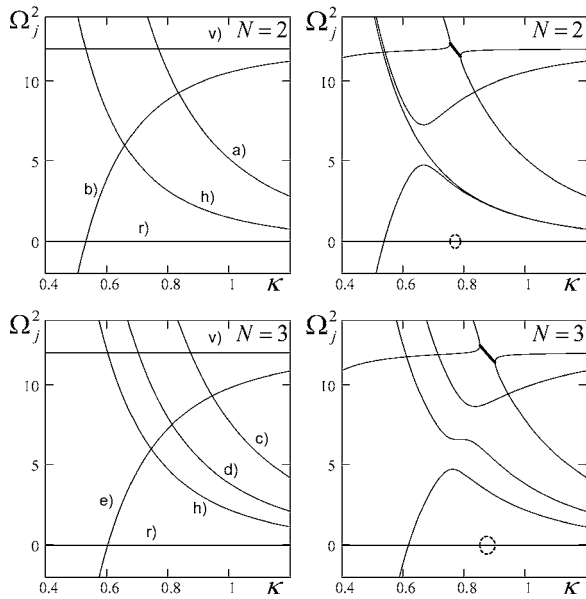


FIG. 3. Squared mode frequencies (in the absence of friction) Ω_j^2 as functions of the interparticle distance κ ; the case where the interaction potential is the sum of the screened Coulomb potential and the potential of a dipole field which is taken as a model of the wake field. The units are such that the particle mass, the absolute value of the particle charge, and the screening length are equal to unity. Calculations are performed for $e_0=24$, $e_z+e_0q_z=12$, which corresponds to the experiment of Ivlev *et al.* (Ref. 19). The left figures correspond to the case where (i) the interaction forces are reciprocal [i.e., no dipole field ($p=0$)], (ii) the particle charge and the screening length are independent of the particle position ($q_z=\lambda_{s,z}=0$), (iii) the horizontal confinement potential is independent of the height ($\beta_z=\beta_{zz}=0$). The modes are denoted in accordance with Fig. 2. The modes corresponding to the horizontal rotation and whole cluster vertical and horizontal shifts are denoted by (r), (v), (h), respectively. In the right figures, the role of the non-reciprocity of interaction forces, charge/shielding variations, and the vertical dependence of the horizontal confinement potential is shown for typical values of the corresponding parameters ($p=0.1$, $\lambda_{s,z}=q_z=\beta_z=0.2$, the parameters β_{zz} and p_z are practically unimportant and are taken to be $\beta_{zz}=0$, $p_z=pq_z$). The nonzero imaginary parts of the Ω_j^2 are shown by the dashed lines. The real parts corresponding to these nonzero imaginary parts are shown by the thick lines. It can be seen that an oscillatory instability appears near the interparticle distance corresponding to the crossing point of the curves of the “breathing” (a), (c) and “vertical sloshing” (v) modes. Note that the “vertical shear” mode (b),(e) is still stable at this interparticle distance.

An experiment can be suggested to observe this instability, where the interparticle distance could be varied by changing the horizontal confinement potential. The instability could be identified as a significant increase of particle oscillation amplitudes (i.e., excitation of nonlinear oscillations) at some value of the interparticle distance. This would be a clear demonstration of the non-Hamiltonian dynamics of dust particles in a plasma. In addition, this instability can be used for plasma diagnostics in the sheath where the dust particles are usually levitated in the laboratory experiments. For example, in the case of the screened Coulomb interaction in the horizontal plane, the measured resonance interparticle distance L_r , the vertical and horizontal frequencies of a single particle ($\omega_v/2\pi$ and $\omega_h/2\pi$, respectively), and the particle mass m give the particle charge Q and the screening length λ_s by solving the following system of two equations:

$$N \frac{\kappa_r^2 + 3\kappa_r + 3}{\kappa_r^3} \exp(-\kappa_r) = \frac{\omega_v^2 \lambda_s^3 m}{Q^2}, \quad (37)$$

$$N \frac{\kappa_r + 1}{\kappa_r^3} \exp(-\kappa_r) = \frac{\omega_h^2 \lambda_s^3 m}{Q^2}, \quad (38)$$

where $\kappa_r=L_r/\lambda_s$, N is the number of particles in the cluster considered ($N=2$ or $N=3$).

ACKNOWLEDGMENTS

R.K. acknowledges the Deutscher Akademischer Austauschdienst (DAAD) for financial and organizational support (Scholarship No. A/04/00273). The work of S.V.V. was partially supported by the Australian Research Council and the Max Planck Society (MPG, Germany).

APPENDIX

In this Appendix we perform the analysis of all modes in the general case of non-Hamiltonian dynamics.

1. $N=2$ cluster

For $N=2$, we have the following modes.

- The “horizontal rotation” mode: $\Omega^2=0$.
- The two coupled “breathing” and “vertical sloshing” modes considered in the main text of the present paper.
- The “horizontal transverse sloshing” mode. The corresponding motion simultaneously satisfies the following relations:

$$l_{1r}=l_{2r}=0, \quad l_{1\theta}=-l_{2\theta}, \quad l_{1z}=l_{2z}=0. \quad (A1)$$

The frequency is given by $\Omega^2=-2\sigma_h/\kappa$.

- The two coupled “horizontal longitudinal sloshing” and “vertical shear” modes. The corresponding motion simultaneously satisfies the following relations:

$$l_{1r}=-l_{2r}, \quad l_{1\theta}=l_{2\theta}=0, \quad l_{1z}=-l_{2z}. \quad (A2)$$

The frequencies are given by

$$(\Omega^2 - \tilde{A})(\Omega^2 - \tilde{B}) = \tilde{C}, \quad (A3)$$

where

$$\tilde{A} = -2\sigma_h/\kappa, \quad (A4)$$

$$\tilde{B} = e_z + e_0q_z + 2\sigma_{vv} - \sigma_{vz} - (\beta_z q_z + \beta_{zz})\sigma_h \kappa/4, \quad (A5)$$

and the mode coupling coefficient \tilde{C} is given by

$$\tilde{C} = (-2\sigma_{vh} + \sigma_h \beta_z + \sigma_{hz} + q_z \sigma_h)\sigma_h \beta_z. \quad (A6)$$

Equation (A3) has the same form as Eq. (17) and, hence, we can directly apply the results of the stability analysis of Eq. (17). In particular, in the case of small $|\tilde{C}|$ (weak coupling between the modes) and finite $\tilde{A}, \tilde{B} > 0$, an oscillatory instability occurs near the resonance $\tilde{A}=\tilde{B}$ if

$$\tilde{C} < 0, \quad |\tilde{C}| > \gamma^2 \tilde{A} \quad (\text{A7})$$

[see Eq. (29)]. For the parameter signs relevant to the laboratory experiments (see Sec. II G 4), the parameter \tilde{C} is always positive and, hence, the instability condition (A7) cannot be satisfied.

2. $N=3$ cluster

For $N=3$, we have the following modes.

- The “horizontal rotation” mode: $\Omega^2=0$.
- The two coupled “breathing” and “vertical sloshing” modes considered in the main text of the present paper.
- The coupled “vertical shear,” “horizontal sloshing,” and “kink” modes. Each mode is doubly degenerated and, hence, the matter concerns six modes. The corresponding equation for the frequencies can be obtained by considering particle motion which simultaneously satisfies the following relations:

$$l_{1r} = -2l_{2r} = -2l_{3r}, \quad l_{1\theta} = 0, \quad l_{2\theta} = -l_{3\theta},$$

$$l_{1z} = -2l_{2z} = -2l_{3z}. \quad (\text{A8})$$

(Of course, the subscripts 1, 2, 3 can be rearranged.) This gives

$$(\Omega^2 - W_{\text{hsl}})[(\Omega^2 - W_{\text{kink}})(\Omega^2 - W_{\text{vsh}}) - C_1] = C_2, \quad (\text{A9})$$

where

$$W_{\text{hsl}} = -3\sigma_h/\kappa, \quad (\text{A10})$$

$$W_{\text{vsh}} = e_z + e_0 q_z + 3\sigma_{vv} + q_z \sigma_v - \sigma_{vz} - (\beta_z q_z + \beta_{zz})\sigma_h \kappa/2, \quad (\text{A11})$$

$$W_{\text{kink}} = 3(\sigma_{hh} - \sigma_h/\kappa)/2, \quad (\text{A12})$$

$$C_1 = \frac{3}{2}[\sigma_{vh}^2 - 4\sigma_h \beta_z \sigma_{vh} + 2\sigma_h^2 \beta_z^2 + (\sigma_{hz} + q_z \sigma_h)\sigma_h \beta_z], \quad (\text{A13})$$

$$C_2 = \frac{9}{4}\beta_z \sigma_h (\sigma_{hh} + \sigma_h/\kappa)[2\sigma_{vh} - \sigma_{hz} - (\beta_z + q_z)\sigma_h]. \quad (\text{A14})$$

In contrast to Eq. (17), Eq. (A9) is cubic with respect to Ω^2 and, hence, it is difficult to find the solutions analytically and analyze them. However, the stability analysis can be easily performed in the case of weak coupling of the modes.

We assume that $|C_1|$ and $|C_2|$ are small (i.e., the coupling between the modes is weak) and that W_{hsl} , W_{vsh} , and W_{kink} are finite and positive. In this case, an instability is possible only when two of three parameters W_{hsl} , W_{vsh} , W_{kink} are sufficiently close to each other (i.e., a resonance takes place). [Otherwise, Eq. (A9) has three real solutions Ω^2 slightly different from W_{hsl} , W_{vsh} , W_{kink} , respectively.] We consider all three possible resonances separately.

Resonance $W_{\text{hsl}}=W_{\text{vsh}}$: We consider the case where W_{hsl} and W_{vsh} are close to each other and significantly different

from W_{kink} . In this case, the first solution of Eq. (A9) is real and approximately equal to W_{kink} . Since the two remaining solutions are close to W_{hsl} , we replace $\Omega^2 - W_{\text{kink}}$ by $W_{\text{hsl}} - W_{\text{kink}}$ in Eq. (A9) to find these solutions. Thus, we obtain

$$(\Omega^2 - W_{\text{hsl}})\left(\Omega^2 - W_{\text{vsh}} - \frac{C_1}{W_{\text{hsl}} - W_{\text{kink}}}\right) = \frac{C_2}{W_{\text{hsl}} - W_{\text{kink}}}. \quad (\text{A15})$$

Equation (A15) has the same form as Eq. (17) and, hence, the instability condition has the same form as Eq. (29):

$$C_{\text{hsl,vsh}} < 0, \quad |C_{\text{hsl,vsh}}| > \gamma^2 W_{\text{hsl}}, \quad (\text{A16})$$

where $C_{\text{hsl,vsh}} = C_2/(W_{\text{hsl}} - W_{\text{kink}})$. Using Eqs. (A10), (A12), and (A14), we obtain

$$C_{\text{hsl,vsh}} = \frac{3}{2}(-2\sigma_{vh} + \sigma_h \beta_z + \sigma_{hz} + q_z \sigma_h)\sigma_h \beta_z. \quad (\text{A17})$$

For the parameter signs relevant to the laboratory experiments (see Sec. II G 4), the parameter $C_{\text{hsl,vsh}}$ is always positive and, hence, instability condition (A16) cannot be satisfied.

Resonance $W_{\text{kink}}=W_{\text{vsh}}$: We consider the case where W_{kink} and W_{vsh} are close to each other and significantly different from W_{hsl} . In this case, the first solution of Eq. (A9) is real and approximately equal to W_{hsl} . Since the two remaining solutions are close to W_{kink} , we replace $\Omega^2 - W_{\text{hsl}}$ by $W_{\text{kink}} - W_{\text{hsl}}$ in Eq. (A9) to find these solutions. Thus, we obtain

$$(\Omega^2 - W_{\text{kink}})(\Omega^2 - W_{\text{vsh}}) = C_1 + \frac{C_2}{W_{\text{kink}} - W_{\text{hsl}}}. \quad (\text{A18})$$

Equation (A18) has the same form as Eq. (17) and, hence, the instability condition has the same form as Eq. (29):

$$C_{\text{kink,vsh}} < 0, \quad |C_{\text{kink,vsh}}| > \gamma^2 W_{\text{kink}}, \quad (\text{A19})$$

where $C_{\text{kink,vsh}} = C_1 + C_2/(W_{\text{kink}} - W_{\text{hsl}})$. Using Eqs. (A10) and (A12)–(A14), we obtain

$$C_{\text{kink,vsh}} = \frac{3}{2}(\sigma_{vh} - \sigma_h \beta_z)^2. \quad (\text{A20})$$

Thus, $C_{\text{kink,vsh}}$ is always positive and, hence, the instability condition (A19) cannot be satisfied.

Resonance $W_{\text{hsl}}=W_{\text{kink}}$: Using the same technique, we obtain the instability condition

$$C_{\text{hsl,kink}} < 0, \quad |C_{\text{hsl,kink}}| > \gamma^2 W_{\text{hsl}}, \quad (\text{A21})$$

where $C_{\text{hsl,kink}} = C_2/(W_{\text{kink}} - W_{\text{vsh}})$. Note that the equation $W_{\text{hsl}} = W_{\text{kink}}$ is equivalent to $\sigma_{hh}\kappa + \sigma_h = 0$ [see Eqs. (A10) and (A12)]. Hence, the resonance $W_{\text{hsl}} = W_{\text{kink}}$ is impossible as long as $\sigma_{hh}\kappa + \sigma_h > 0$ (i.e., the product of the horizontal repulsion force and the interparticle distance decreases with the interparticle distance).

¹S. V. Vladimirov and M. Nambu, Phys. Rev. E **52**, R2172 (1995).

²F. Melandsø and J. Goree, Phys. Rev. E **52**, 5312 (1995).

³S. V. Vladimirov and O. Ishihara, Phys. Plasmas **3**, 444 (1996).

⁴O. Ishihara and S. V. Vladimirov, Phys. Plasmas **4**, 69 (1997).

⁵K. Takahashi, T. Oishi, K. Shimomai, Y. Hayashi, and S. Nishino, Phys. Rev. E **58**, 7805 (1998).

- ⁶S. Benkadda, V. N. Tsytovich, and S. V. Vladimirov, *Phys. Rev. E* **60**, 4708 (1999).
- ⁷G. Lapenta, *Phys. Rev. E* **62**, 1175 (2000).
- ⁸M. Lampe, G. Joyce, G. Ganguli, and V. Gavrishchaka, *Phys. Plasmas* **7**, 3851 (2000).
- ⁹S. A. Maiorov, S. V. Vladimirov, and N. F. Cramer, *Phys. Rev. E* **63**, 017401 (2001).
- ¹⁰G. A. Hebner, M. E. Riley, and B. M. Marder, *Phys. Rev. E* **68**, 016403 (2003).
- ¹¹S. V. Vladimirov and K. Ostrikov, *Phys. Rep.* **393**, 175 (2004).
- ¹²V. E. Fortov, A. G. Khrapak, S. A. Khrapak, V. I. Molotkov, and O. F. Petrov, *Phys. Usp.* **47**, 447 (2004).
- ¹³A. V. Ivlev, S. K. Zhdanov, B. A. Klumov, V. N. Tsytovich, U. de Angelis, and G. E. Morfill, *Phys. Rev. E* **70**, 066401 (2004).
- ¹⁴S. V. Vladimirov, K. Ostrikov, and A. A. Samarian, *Physics and Applications of Complex Plasmas* (Imperial College, London, 2005).
- ¹⁵S. K. Zhdanov, A. V. Ivlev, and G. E. Morfill, *Phys. Plasmas* **12**, 072312 (2005).
- ¹⁶M. E. Tuckerman, C. J. Mundy, and G. J. Martyna, *Europhys. Lett.* **45**, 149 (1999).
- ¹⁷M. E. Tuckerman, Yi Liu, G. Ciccotti, and G. J. Martyna, *J. Chem. Phys.* **115**, 1678 (2001).
- ¹⁸K. F. Gauss, *J. Reine Angew. Math.* **IV**, 232 (1829).
- ¹⁹A. V. Ivlev, U. Konopka, G. Morfill, and G. Joyce, *Phys. Rev. E* **68**, 026405 (2003).
- ²⁰A. V. Ivlev and G. Morfill, *Phys. Rev. E* **63**, 016409 (2001).
- ²¹V. V. Yaroshenko, A. V. Ivlev, and G. E. Morfill, *Phys. Rev. E* **71**, 046405 (2005).
- ²²R. Kompaneets, A. V. Ivlev, V. Tsytovich, and G. Morfill, *Phys. Plasmas* **12**, 062107 (2005).
- ²³U. Konopka, Ph.D. thesis, Ruhr-Universität Bochum (2000).
- ²⁴P. Epstein, *Phys. Rev.* **23**, 710 (1924).
- ²⁵U. Konopka, G. E. Morfill, and L. Ratke, *Phys. Rev. Lett.* **84**, 891 (2000).
- ²⁶A. Melzer, M. Klindworth, and A. Piel, *Phys. Rev. Lett.* **87**, 115002 (2001).